2008-10-14

The Molecular Mechanisms Underlying the Polarized Distribution of Drosophila Dscam in Neurons: A Dissertation

Shun-Jen Yang
University of Massachusetts Medical School

THE MOLECULAR MECHANISMS UNDERLYING THE POLARIZED DISTRIBUTION OF *DROSOPHILA* DSCAM IN NEURONS

A Dissertation Presented

By

Shun-Jen Yang

Submitted to the Faculty of

the University of Massachusetts Graduate School of Biomedical Sciences, Worcester

Submitted in partial fulfillment of the requirements for the degree of

DOCTOR OF PHILOSOPHY

Oct 14th, 2008

THE MOLECULAR MECHANISMS UNDERLYING THE DIFFERENTIAL DISTRIBUTION OF *DROSOPHILA* DSCAM IN NURONS

A Dissertation Presented
By

Shun-Jen Yang

This signatures of the Dissertation Defense Committee signifies completion and approval as to style and content of Dissertation

Tzumin Lee, M.D., Ph.D., Thesis Advisor

Mark Alkema, Ph.D., Member of Committee

Marc R. Freeman, Ph.D., Member of Committee

Paul Garrity, Ph.D., Member of Committee

Elizabeth Luna, Ph.D., Member of Committee

The signature of the Chair of the Committee signifies that the written dissertation meets the requirements of the Dissertation Committee

Vivian Budnik, Ph.D., Chair of Committee

The signature of the Dean of the Graduate School of Biomedical Sciences signifies that the student has met all graduation requirements of the school

Anthony Carruthers, Ph.D.,
Dean of the Graduate School of Biomedical Sciences

Program in Neuroscience

October 14th, 2008

Dedication

Dedicated to my beloved family:

Hsueh-chin (mother) & Cheng-Li (father) & Chia-ching (sister) Yang,

Mei-Jung Yeh (grandmother) & Hui-chu (aunt) Yang and Yo-Ning Chen (my wife).

Acknowledgements

I would like to express my deep gratitude to my advisor Dr. Tzumin Lee, not only for his mentoring, guidance and support throughout my Ph.D. studies, but also for his sharing of his knowledge and passion for science. I would also like to thank my committee members Dr. Mark Alkema, Dr. Vivian Budnik, Dr. Akira Chiba, Dr. Marc Freeman, Dr. Paul Garrity, Dr. Byron Kemper, Dr. Elizabeth Luna, Dr. Phillip Newmark and Dr. Benjamin Williams for their invaluable advice and encouragement on my research. I am grateful for the all the members of the Neurobiology Department at the University of Massachusetts Medical School, who create an exciting and cooperative environment for students like me to enjoy doing research and discussing science with one another. I also thank the members of the Cell and Developmental Biology Department of the University of Illinois at Urbana-Champaign, who supported me during the first three years of my graduate study and showed me a good time in Illinois. Thanks to the current and former Lee lab members for all the great help and support on my various projects.

I would also like to acknowledge the following people with their corresponding contributions to each chapter.

Chapter II (Dynein/dynactin and Dscam[TM1] project):

Dr. Jian Wang is the first person who observed the differential distribution patterns of Dscam[TM1] and Dscam[TM2] in *Drosophila* MB and PN neurons. I joined him in examining Dscam's functions governed by protein distribution. Jia-Min Bai worked with me on the genetic screen and taught me background knowledge of *Drosophila* genetics. I

also thank Dr. Hung-Hsiang Yu for *UAS-mCD8::RFP*, Dr. Andreas Prokop for *UAS-Rdl-HA* and *UAS-Act5C-GFP*, Dr. Marcus Allen for *UAS- GI^{Δ}*, Melissa Rolls for *UAS-Apc2-GFP* and *UAS-homer-GFP*, and the Bloomington Stock Center for mutant flies. I would also like to thank Dr. Benjamin Leung, Kimberley Kerr, Dr. Lily Jan, Dr. Yuh Nung Jan and members of the Jan Lab (University of California, San Francisco) for critical reading of this manuscript. The 1D4 antibody was obtained from the Developmental Studies Hybridoma Bank.

Chapter III (targeting motifs projects)

I would like to acknowledge Dr. Jian Wang, Dr. Xiaojun Ma, and Dr. Po-Ju Chu who generated different deletion and chimeric constructs of Dscam[TM1] and Dscam[TM2]. With their efforts, I was able to start the project immediately after I joined the lab and continue this line of research.

Chapter IV (Dscam[TM1] and Dscam[TM2] project):

I would like to thank Lei Shi and Dr. Hung-Hsiang Yu for generating very critical microRNAs against various Dscam isoforms. We worked together to dissect out the molecular functions of Dscam[TM1] and Dscam[TM2]. Thanks for their continuous input and discussions during the progression and publication of this work.

Chapter V (Dscam endodomain project):

Foremost, I would like to thank Dr. Hung-Hsiang Yu for his very significant contributions during progression and publication of this project. Hung-Hsiang gave me a

great deal of guidance throughout the experiments in Chapter V. I would also like to acknowledge Jian Wang for his initial work on identifying Dscam's endodomain diversity. I am grateful to Ya-ling Huang who helped to generate microRNA constructs. In addition, I thank Dr. Thomas Kidd and Gracie Andrews for the *abelson* mutants and personal communications.

Abstract

Neurons exhibit highly polarized structures, including two morphologically and functionally distinct domains, axons and dendrites. Dendrites and axons receive versus send information, and proper execution of each requires different sets of molecules. Differential distribution of membrane proteins in distinct neuronal compartments plays essential roles in neuronal functions. The major goal of my doctoral thesis was to study the molecular mechanisms that govern the differential distribution of membrane proteins in neurons, using the *Drosophila* larval mushroom body (MB) as a model system.

My work was initiated by an observation of differential distribution of distinct Dscam isoforms in neurons. Dscam stands for Down Syndrome Cell Adhesion Molecule, which is a *Drosophila* homolog of human DSCAM. According to genomic analysis, *Drosophila* Dscam gene can generate more than 38,000 isoforms through alternative splicing in its exons 4, 6, 9 and 17. All Dscam isoforms share similar domain structures, with 10 immunoglobulin domains and 6 fibronectin type III repeats in the ectodomain, a single transmembrane domain and a cytoplasmic endodomain. There are two alternative exons in exon 17 (17.1 and 17.2), which encodes Dscam's transmembrane domain. Interestingly, in ectopic expression, Dscam isoforms carrying exon 17.1 (Dscam[TM1]) can be preferentially localized to dendrites and cell bodies, while Dscam isoforms carrying exon 17.2 (Dscam[TM2]) are distributed throughout the entire neuron including axons and dendrites.

To unravel the mechanisms involved in the differential distribution of Dscam[TM1] versus Dscam[TM2], I conducted a mosaic genetic screening to identify the

possible factors affecting dendritic distribution of Dscam[TM1], established an *in vivo* TARGET system to better distinguish the differential distribution of Dscam, identified the axonal and dendritic targeting motifs of Dscam molecules and further showed that Dscam's differential roles in dendrites versus axons are correlated with its localization.

Several mutants affecting dendritic distribution of Dscam[TM1] have been identified using a MARCM genetic screen. Three of these mutants (Dlis1, Dmn and p24) are components of the dynein/dynactin complex. Silencing of other dynein/dynactin subunits and blocking dynein function with a dominant-negative Glued mutant also resulted in mislocalization of Dscam[TM1] from dendrites to axons. However, microtubule polarity in the mutant axons was maintained. Taken together, this was the first demonstration that the dynein/dynactin complex is involved in the polarized distribution of membrane proteins in neurons. To further examine how dynein/dynactin is involved in the dendritic distribution of Dscam[TM1], I compromised dynenin/dynactin function with dominant-negative Glued and transiently induced Dscam[TM1] expression. The results suggested that dynein/dynactin may not be directly involved in the targeting of newly synthesized Dscam[TM1] to dendrites. Instead, it plays a role in maintaining dendritic restriction of Dscam[TM1]. Notably, dynein/dynactin dysfunction did not alter distribution of another dendritic transmembrane protein Rdl (*Resistant to Dieldrin*), supporting involvement of diverse mechanisms in distributing distinct molecules to the dendritic membrane.

To identify the targeting motifs of Dscam, I incorporated the TARGET (Temporal and regional gene expression targeting) system into mushroom body (MB) neurons, and this allowed the demonstration of the differential distribution of Dscam[TM1] and

Dscam[TM2] with more clarity than conventional overexpression techniques. Using the TARGET system, I identified an axonal targeting motif located in the cytoplasmic juxtamemebrane domain of Dscam[TM2]. This axonal targeting motif is dominant over the dendritic targeting motif located in Dscam's ectodomain. Scanning alanine mutagenesis demonstrated that two amino acids in the axonal targeting motif were essential for Dscam's axonal distribution. Interestingly, swapping the cytoplasmic juxtamembrane portions between TM1 and TM2 not only reversed TM1's and TM2's differential distribution patterns but also their functional properties in dendrites versus axons.

My thesis research also involved studying endodomain diversity of Dscam isoforms. Besides the diversity originally found in the ectodomain and transmembrane domain of Dscam, my colleagues and I further demonstrated the existence of four additional endodomain variants. These four variants are generated by skipping or retaining exon 19 or exon 23 through independent alternative splicing. Interestingly, different Dscam endodomain isoforms are expressed at different developmental stages and in different areas of the nervous system. Through isoform-specific RNA interference, we showed the differential involvement of distinct Dscam endodomains in specific neuronal morphogenetic processes. Analysis of the primary sequence of the Dscam endodomain indicated that endodomain variants may confer activation of different signaling pathways and functional roles in neuronal morphogenesis.

In Summary, my thesis work identified and characterized several previously unknown mechanisms related to the differential distribution of membrane proteins in neurons. I showed that there may be a dynein/dynactin-independent mechanism for

selective transport of dendritic membrane proteins to dendrites. Second, dynein/dynactin plays a maintenance role in dendritic restriction of Dscam[TM1]. Third, different membrane proteins may require distinct combinations of mechanisms to be properly targeted and maintained in certain neuronal compartments. Further analysis of the mutants indentified from my genetic screen will definitely help to resolve the missing pieces of the puzzle. These findings provide novel mechanistic insight into the differential distribution of membrane proteins in polarized neurons.

Table of contents

List of figures

List of abbreviations

CNS central nervous system

DN dominant-negative

DSCAM Down Syndrome cell adhesion molecule

Dscam Drosophila Down Syndrome cell adhesion molecule

GFP green fluorescent protein

LH lateral horn

mAb monoclonal antibody

MARCM mosaic analysis with a repressible cell marker

MB mushroom body

Nb neuroblast

ORN olfactory receptor neuron

PN projection neuron

Rdl resistant to Dieldrin

RFP red fluorescent protein

TARGET temporal and regional gene expression targeting

TM1 transmembrane domain encoded by exon 17.1

TM2 transmembrane domain encoded by exon 17.2

UAS upstream activating sequence

vPN ventral projection neuron

WL wandering larvae

WT wild-type

Chapter 1

Introduction

Neuroscience is a field devoted to the scientific study of the nervous system. The complexity and diversity in the nervous system depends on the interconnections between neurons. Since the time of Cajal, it has been understood that each neuron is highly polarized and is comprised of a cell body called the soma, multiple dendrites and a single long axon. Dendrites bring information to the cell body, and axons take information away from the cell body. Dendrites and axons require distinct sets of cell surface molecules to perform distinct electrophysiological functions. Doubtlessly, proper sorting, targeting and maintenance of these cell surface molecules into different compartments are essential for all basic neuronal activities. The major goal of this thesis is to elucidate the molecular mechanisms underlying polarized distribution of cell surface proteins in neurons.

Neuronal Polarity

The concept of neuronal polarity can be traced back to 140 years ago when Otto Dieters described the morphology of neurons. It took another thirty years to appreciate the significance of these morphological features with the proposition by Santiago Ramón y Cajal. “The law of dynamic polarization”, proposed by Cajal, stated that neurons are polarized, receive information on their cell bodies and dendrites, and conduct information to distant locations through axons (Cajal, 1989). Although many exceptions have been found to this rule, it remains a basic principle regarding the functioning of neuronal connections.

Apart from the differences in gross morphology, how do dendrites and axons differ? One of the clear molecular differences was found to exist between the dendritic and axonal cytoskeletons. The polarity orientation of microtubules in the dendrites and axons of cultured rat hippocampal neurons are different (Baas et al., 1988; Black and

Baas, 1989). Microtubules in axons are uniformly oriented with the plus-end pointed away from the cell body toward the tips of axons; in contrast, microtubules in dendrites are arranged with mixed polarity. This organization of microtubules has also been suggested in *Drosophila* axons and dendrites (Stone et al., 2008; Zheng et al., 2008). Furthermore, some microtubule-associated proteins (MAPs) were found exclusively in dendrites (e.g. MAP2) or axons (e.g. Tau) (Kosik and Finch, 1987). These studies revealed that microtubules in dendrites and axons vary in both organization and composition.

The polarized distribution of molecules is essential to neuronal function

Dendrites and axons differ not only in morphology and structure but also in function. Proper cellular morphology and function depends on the polarized distribution of organelles and proteins in distinct subcellular compartments. For example, in mammalian and fly neurons, Golgi outposts localize to dendrites and influence dendritic branching. Mislocalization of Golgi outposts in neurons parallels change in branch distribution (Ye et al., 2007; Zheng et al., 2008).

Distinct protein composition exists not only in the cytoplasm, but also on the plasma membrane. The polarized distribution of many cell surface proteins including ion channels, receptors and cell adhesion molecules has been shown to be essential for all basic neuronal functions and activities (Craig et al., 1994; Endoh, 2004). For instance, dendritic voltage-gated channels have been proposed to play a critical role in regulating the propagation of synaptic signals and action potentials in dendrites (Stuart et al., 1997). Dendritic voltage-gated potassium channels (e.g. Kv2.1 and Kv2.2) which undergo slower inactivation than axonal voltage-gated potassium channels (e.g. Kv1.3 and Kv1.4)

prevent back-propagation of action potentials into the dendrites (Wei et al., 1990; Hoffman et al., 1997). In addition, certain metabotropic glutamate receptors, including mGluR1a and mGluR2, also show polarized distribution (Stowell and Craig, 1999), and potentially underlie differential glutamate effects in different compartments of neurons (Nakanishi, 1992; Endoh, 2004).

The mechanisms involved in the polarized distribution of cell surface proteins

Neuroscientists have long been interested in how different neuronal membrane proteins are segregated and correctly maintained. To dissect out this fundamental problem, studies in cultured rat hippocampal neurons and epithelial cells such as Madin-Darby canine kidney (MDCK) cells have provided significant insight into the highly conserved mechanisms that establish and maintain polarity (reviewed in Horton and Ehlers, 2003). For example, neurons recognize the same targeting motifs for somatodendritic targeting that epithelial cells use for basolateral targeting (West et al., 1997; Stowell and Craig, 1999). Indeed, it is believed that the basolateral and apical compartments of epithelial cells may correspond to the somatodendritic and axonal compartments of neurons, respectively (Dotti and Simons, 1990; Matter and Mellman, 1994).

This polarized distribution is thought to begin with the sorting of membrane proteins into distinct populations of carrier vesicles (Keller et al., 2001). These vesicles are transported out toward the dendrites or axons by ‘smart’ motor proteins, which can recognize sorting signals on membrane proteins and distinguish different microtubules that lead to different destinations. Once at the plasma membrane, distinct mechanisms work to achieve selective fusion and retention of these proteins (Goldstein and Yang,

2000; Tang, 2001; Dotti and Poo, 2003). In addition, a diffusion barrier is formed between certain subcellular compartments to prevent free lateral diffusion of membrane proteins in the plane of plasma membrane (Nakada et al., 2003). Although numerous results and discoveries provide us a rough picture of the molecular events underlying polarized distribution processes in neurons, understanding of the mechanistic details remains incomplete. For instance, what molecules are involved in each process? How are different membrane proteins sorted into distinct vesicles? How do molecular motors recognize the intrinsic cues from vesicular cargo and microtubules? One issue complicating further elucidation of these questions is that there is no one universal or predominant mechanism that functions across different membrane proteins and all cell types. Multiple mechanisms can contribute to the polarized distribution of a single membrane protein, and different membrane proteins can adopt different mechanisms to achieve and maintain their polarized distribution patterns. To investigate these important questions, identification of additional intrinsic sorting signals and the protein machinery that recognizes them will assist in a molecular dissection of neuronal polarity and protein targeting.

Polarized distribution of different *Drosophila* Down Syndrome cell adhesion molecule (Dscam) isoforms

Drosophila Down Syndrome cell adhesion molecule (Dscam) is a homolog of human DSCAM. Down syndrome in *humans* is a congenital disorder with intellectual impairment and physical abnormalities, and is caused by the existence of a triple chromosome 21 and related DSCAM over-expression. Notably, Dscam has been shown

to be widely involved in neuronal morphogenesis in the *Drosophila* brain. Either loss or over-expression of the Dscam protein perturbs segregation of axonal branches in the mushroom bodies (MBs), alters target specificity in olfactory receptor neurons (ORNs), impedes axonal growth and extension in mechanosensory neurons and causes self-avoidance defects in dendritic arborization (da) neurons (Schmucker et al., 2000; Wang et al.,2002; Hummel et al., 2003; Chen et al., 2006; Soba et al., 2007; Mathews et al., 2007).

Drosophila Dscam is a cell surface molecule which belongs to the immunoglobulin-fibronectin superfamily. According to genomic and cDNA analysis, the *Dscam* gene encodes potentially 152,064 isoforms through alternative splicing (Figure 1-1A) (Schmucker et al., 2000; Wang et al., 2004). Dscam's extracellular domain contains three variable regions that are encoded by one of 12 exon 4 alternatives, one of 48 exon 6 alternatives and one of 33 exon 9 alternatives, respectively. In addition, its transmembrane domain is encoded by one of two exon 17 alternatives (exon 17.1 and exon 17.2). In Dscam's endodomain, exons 19 and 23 can be independently deleted to generate another four different combinations.

Remarkably, when different GFP-tagged *Dscam* trangenes are individually expressed in the *Drosophila* mushroom body (MB) neurons, we observe two distinct protein distribution patterns. Those Dscam isoforms with their transmembrane domains derived from exon 17.1 (termed Dscam[TM1]) are preferentially localized in the cell bodies and dendrites (Figure 1-1C). In contrast, Dscam isoforms carrying exon 17.2 (termed Dscam[TM2]) are always distributed throughout cell bodies, dendrites, and axons (Figure 1-1D) (Wang et al., 2004; Zhan et al, 2004). Expression at low level with the Dscam promoter, Dscam[TM1]-GFP is preferentially localized to dendrites, while

Dscam[TM2]-GFP is largely restricted to axons. With regards to the endodomain, Dscam isoforms with exon 19 (termed Dscam+19) tend to accumulate more in the cell body regions than Dscam isoforms without exon 19 (termed Dscam-19). These differential distribution patterns can also be observed in other model neurons in *Drosophila*, such as the projection neurons (PNs). These phenomena raised my interest in studying the underlying mechanisms of Dscam's differential distribution in neurons and examining whether the polarized distribution of Dscam is associated with its diverse functions *in vivo*.

The *Drosophila* Mushroom Bodies (MBs) as a model system to study the polarized distribution of Dscam

Previously, we found that a lethal mutation in *Dscam* specifically perturbs segregation of axonal branches in the *Drosophila* mushroom bodies (MBs) (Wang et al., 2002). To examine possible involvement of distinct Dscam isoforms in different neuronal morphogenetic processes and how its polarized distribution was related to these processes, I used the MBs as a model system to explore these questions.

The MBs, prominent structures in the *Drosophila* brain, are the center of olfactory associative learning and memory and are functionally equivalent to the hippocampus in mammals (Heisenberg, 2003). *Drosophila* MBs are paired neuropil structures, one in each hemisphere (Figure 1-2A). Each MB consists of approximately 2,500 small neurons called Kenyon cells (Ito et al, 1997). The cell bodies are located in the dorsal and posterior cortex of the brain. Their dendrites form the ball-shaped protrusion called the calyx located below the cell body region. The dendrites mainly receive olfactory inputs

from projection neurons (PNs) in the antennal lobe (Stocker et al., 1990), which is the *Drosophila* counterpart of the mammalian olfactory bulb. MB neurons extend their axons as a bundle through a stalk-like structure named the peduncle toward the anterior margin of the brain, where the axons project into five lobes: γ, α', β', α and β lobes (Figure 1-2B) (Crittenden et al., 1998; Lee et al., 1999).

The development and projection patterns of individual MB neurons have been well characterized (Figure 1-2C) (Lee et al., 1999). Systematic studies with mosaic expression systems showed that three distinct types of MB neurons are born in a birth order-dependent manner. γ neurons are born first, from late embryonic stage to the mid-3rd instar larval stage, followed by α'/β' neurons which are born between the mid-3rd instar larval stage and end of wandering larval stage. Afterward, the MB neuroblasts (Nbs) exclusively produce α/β neurons. γ neurons have different axonal projection patterns in larval and adult stages. At larval stages, axons of γ neurons bifurcate to form dorsal and medial lobes. During metamorphosis, γ neurons undergo dramatic remodeling. Shortly after puparium formation, larval-specific axons are pruned, followed by reextension of adult-specific axons which project medially into the γ lobes with multiple axonal arbors (Armstrong et al., 1998; Lee et al., 1999). α'/β' and α/β neurons have bifurcated axonal projection patterns--they extend their axons perpendicularly into α'/β' and α/β lobes, respectively. Therefore, distinct subtypes of MB neurons in different developmental stages can be easily identified based on their projection patterns.

Thus, using the *Drosophila* MB as a model system, we can study various aspects of neuronal function and development, such as neuronal remodeling, axon bifurcation, dendritic arborization, axonal growth and targeting, and protein distribution. In addition,

both candidate gene analysis and forward genetic screens have been conducted in the *Drosophila* MB and successfully identified genes involved in various poorly understood neuronal functions (Lee et al., 2000a; Lee et al., 2000b; Wang et al., 2002; Zheng et al., 2003; Zhu et al., 2005; Wang et al., 2006; Zhu et al., 2006). Therefore, as part of my thesis research, I conducted a forward genetic screen in the *Drosophila* MB to identify molecules that are involved in the polarized distribution of *Drosophila* Dscam. I also used the *Drosophila* MB as a model system to study the functions of Dscam during neuronal development.

Approaches: Mosaic analysis with a repressible cell marker (MARCM), temporal and regional gene expression targeting (TARGET) and microRNA-based RNAi

Based on the previous results, a forward genetic screen using MARCM was performed in order to identify novel genes required for polarized distribution of Dscam. MARCM, a positive-labeling genetic mosaic technique, has allowed us to generate homozygous mutant cells from heterozygous precursors via mitotic recombination (Lee et al., 1999; Lee and Luo, 1999). Dscam[TM1]::GFP was been incorporated into my MARCM screen as a reporter concentrated in MB calyx. This screen should allow me to uncover genes that are involved in the dendritic distribution of Dscam[TM1]. Dscam[TM2] could not be a reporter for a similar screen because ectopically overexpressed Dscam[TM2] showed no obvious polarized distribution pattern. Of 1,850 mutant chromosome arms of 2R screened, I found 35 potentially interesting mutations that caused mislocalization of Dscam[TM1] from dendrites to axons. Judging from the phenotypes of mislocalization, I selected nine mutants for further study.

Complementation tests revealed three mutations in *Lis1*, *p24*, and *Dynamitin (Dmn)*, which are all components of dynein/dynactin complex. Detailed phenotypic analysis showed that the dynein/dynactin complex is involved in the dendritic restriction of Dscam[TM1] expression, likely through a scavenger mechanism. (Please see Chapter II for more details.)

By utilizing the TARGET system in which GAL4-dependent expression of UAS-transgenes is acutely controlled by a temperature-sensitive GAL4 repressor, GAL80ts (McGuire et al., 2003), transiently induced and newly synthesized Dscam molecules can be exclusively targeted to different neuronal compartments, using Dscam[TM1]::GFP in dendrites and Dscam[TM2]::GFP in axons. This transient induction system can detect distribution of proteins expressed at extremely low levels, which should better mimic the distribution of endogenous proteins. Through the use of the TARGET system, dendritic and axonal targeting motifs of Dscam were identified. The ectodomain of Dscam carries a dendritic targeting motif, and the cytoplasmic juxtamembrane portion of TM2 contains an axonal targeting motif. The axonal targeting motif is dominant over the dendritic targeting motif in Dscam. (Please see Chapter III for more details.)

To relate the polarized distribution of Dscam to its endogenous functions, microRNA-based RNAi technology was utilized to selectively knock down different subsets of Dscam proteins containing either exon 17.1 or exon 17.2. Target recognition of miRNA involves only 22 contiguous nucleotides, making it more feasible to silence expression of specific subsets of *Dscam* transcripts, which differ only in small alternative exons. We found that endogenous Dscam[TM1] and Dscam[TM2] primarily mediate dendritic elaboration and axonal arborization, respectively. Swapping the cytoplasmic

juxtamembrane portions between TM1 and TM2 reversed not only their polarized distribution patterns but also their distinct functions. Together, we concluded that functional differences between Dscam[TM1] and Dscam[TM2] likely rely on polarized protein targeting. (Please see Chapter IV for more details.)

Following this line of research, differential protein distribution patterns were also observed for Dscam isoforms with various endodomains. According to cDNA analysis, four Dscam endodomains can be generated from independent alternative splicing of exon 19 and exon 23. We found that transgenic Dscam without exon 19 is more efficiently targeted to neurites and more potently suppresses axon bifurcation in *Dscam* mutant neurons than exon 19-containing Dscam. To determine whether distinct Dscam endodomains are utilized to govern different Dscam-dependent neuronal morphogenetic processes, microRNAs against distinct endodomains and isoforms-specific antibodies were generated. Intriguingly, the wiring of adult fly neural circuitry primarily involves Dscam isoforms lacking both exon 19 and exon 23. However, Dscam with exon 19 plays a more dominant role than Dscam without exon 19 in supporting the wiring of embryonic neural circuitry. (Please see Chapter V for more details.)

In Summary, the work addressed in this thesis highlights the molecular mechanisms underlying the differential distribution of various Dscam isoforms and their functions in neuronal morphogenesis, with regard to their distribution. These results lay the foundation for future genetic and molecular studies to elucidate how neurons establish polarized distribution of membrane proteins for diverse neuronal activities.

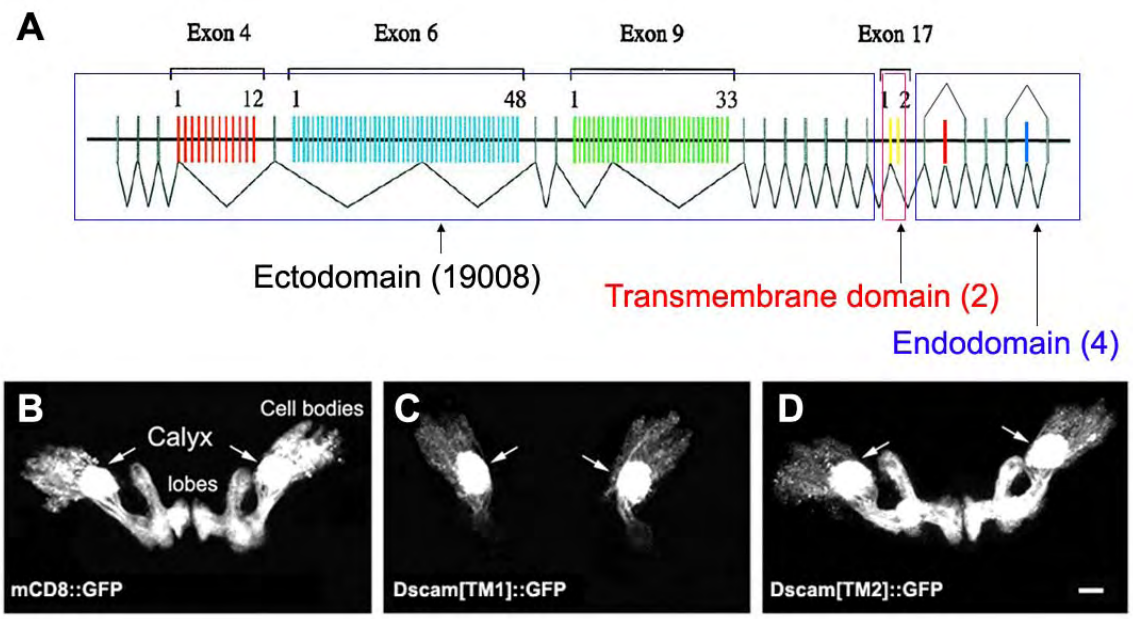

Figure 1-1. Dscam isoforms and transgenic protein distribution.

(A) Dscam potentially encodes 152,064 isoforms via alternative splicing in its exons 4, 6, 9, 17, 19 and 23 (adapted from Schmucker et al., 2000; Wang et al., 2004). (B) GAL4-201Y was used to drive expression of UAS-mCD8-GFP in MB neurons. (C) Ectopically expressed Dscam[TM1]::GFP was preferentially enriched in dendrites of MBs, called the MB calyx. (D) Ectopically expressed Dscam[TM2]::GFP was distributed throughout the entire MB neuron. (adapted from Wang et al., 2004).

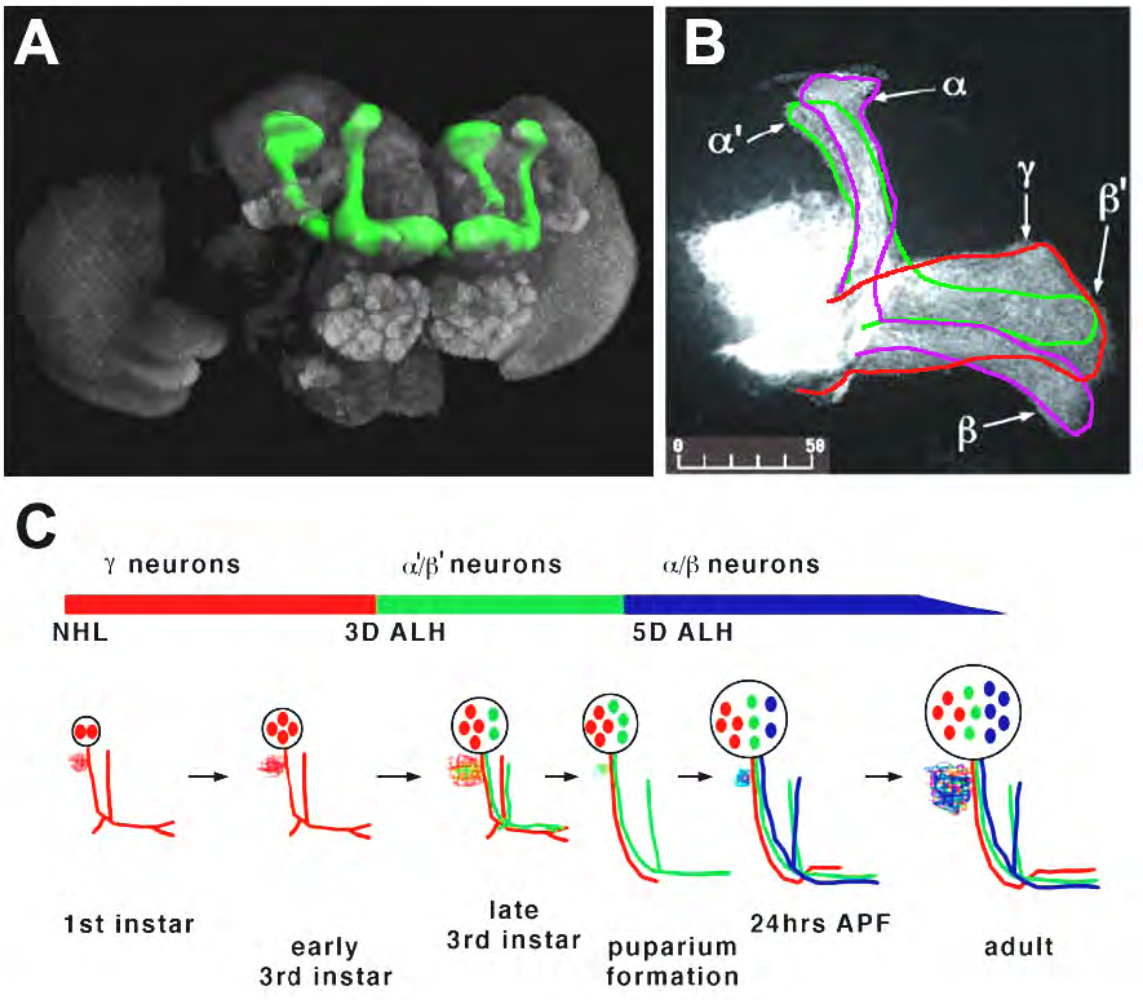

Figure 1-2. The organization and development of *Drosophila* mushroom bodies (MBs).
(A) *Drosophila* MBs in an adult brain are highlighted in green (adapted from Rein K, 2000). (B) Close-up view of the MBs in the right hemisphere under the microscope. Individual axonal lobes are outlined with solid lines: γ in red, α'/β' in green and α/β in purple. (C) Schematic view of MB development. Three types of MB neurons are born in a specific temporal order (adapted from Lee et al., 1999). NHL, newly hatched larvae; ALH, after larval hatching; D, day. Scale bar unit: μm.

Chapter 2

Dynein-dynactin complex is essential for dendritic restriction of TM1-containing *Drosophila* Dscam

The following work is reprinted from the PLoS ONE article of the same name published as:

Jacob Shun-Jen Yang, Jia-Min Bai, and Tzumin Lee.

PLoS ONE, Oct 2008: Vol. 3, Issue 10, e3504

ABSTRACT

Many membrane proteins, including *Drosophila* Dscam, are enriched in dendrites or axons within neurons. However, little is known about how the differential distribution is established and maintained. Here we investigated the mechanisms underlying the dendritic targeting of Dscam[TM1]. Through forward genetic mosaic screens and by silencing specific genes via targeted RNAi, we found that several genes, encoding various components of the dynein-dynactin complex, are required for restricting Dscam[TM1] to the mushroom body dendrites. In contrast, compromising dynein/dynactin function did not affect dendritic targeting of two other dendritic markers, Nod and Rdl. Tracing newly synthesized Dscam[TM1] further revealed that dynein-dynactin is dispensable for the initial dendritic targeting of Dscam[TM1] and apparently plays a role in excluding dendritic Dscam from axons by retrograde transport.

INTRODUCTION

Neurons exhibit highly polarized structures, including two morphologically and functionally distinct domains, axons and dendrites. Dendrites and axons respectively receive or send information, proper execution of which requires different sets of molecules. For example, in the mammalian brain and in cultured neurons, voltage-gated potassium channels of the Kv1 (*Shaker*) family reside in the axons. In contrast, voltage-gated potassium channel Kv2.1 and Kv2.2 are selectively enriched in the somatodendritic region (Lim et al., 2000; Monaghan et al., 2001; Gu et al., 2003). The dendritic potassium channels undergo slower inactivation to prevent back-propagation of action potentials into the dendrites (Wei et al., 1990; Hoffman et al., 1997). Certain

metabotropic glutamate receptors, including mGluR1a and mGluR2, also show polarized distribution (Stowell and Craig, 1999), and potentially underlie differential glutamate effects in different compartments of neurons (Nakanishi, 1992; Endoh, 2004).

One dominant model to explain the differential distribution of neuronal membrane proteins involves directed transport of vesicular cargos along the microtubules that extend into the dendrites and axons (Goldstein and Yang, 2000). Microtubules have polarity; directed transport requires motors to move cargos toward the plus- or minus-end of the microtubules. In axons microtubules are uniformly oriented with minus-ends pointing to the cell body, while microtubules exist with mixed polarity within the somatodendritic region (Bass et al., 1998). This difference in microtubule organization supports the hypothesis that minus-end-directed motors are constantly moving molecules out of axons and may selectively transport their cargos into the dendrites (Burack et al., 2000). Identified minus-end-directed motors include dynein and C-terminal kinesins. Cytoplasmic dynein, which forms a large complex with its activator dynactin, is responsible for the retrograde transport in axons (reviewed in Goldstein and Gunawardena, 2000; Schroer, 2004). Dynein/dynactin complex contains more than twenty subunits. Although the functions of each subunit remain to be determined, it is believed that all the subunits act together to regulate the processivity and cargo-binding selectivity of dynein (King and Schroer, 2000; Schroer, 2004). Various C-terminal kinesins (i.e. *Ncd* in *Drosophila* and *KIFC2* in *mouse*), which carry their motor domain at the C-terminus, also move specifically toward the minus end. But their real function in

vesicular transport is unclear (McDonald et al., 1990; Saito et al., 1997). The role of minus-end-directed motors in dendritic protein targeting remains undocumented.

Besides selective transport, additional mechanisms may contribute to the polarized distribution by differential depletion or stabilization. For example, the steady-state axonal distribution of Nav1.2 and VAMP2 is primarily achieved through their selective removal by endocytosis from the dendritic plasma membrane (Garrido et al., 2001; Sampo et al., 2003). Preferential fusion of vesicular cargos with different plasma membrane domains may mediate some polarized distribution as well. One precedent for fusion selectivity involves targeting of distinct SNAREs to the apical or basolateral domains of epithelial MDCK cells (Low et al., 1996). Other possible mechanisms include existence of diffusion barriers and/or protein stabilization by scaffold proteins. However, most of these studies shed light on the polarized distribution of axonal proteins; and little is known about dendritic protein targeting (Stowell and Craig, 1999; Horton and Ehlers, 2003; Rivera et al., 2003).

Drosophila Down Syndrome cell adhesion molecule (Dscam) is a transmembrane protein, which belongs to the immunoglobulin (Ig) superfamily. Dscam is essential for diverse neuronal morphogenetic processes, including axon guidance, branch segregation, and dendritogenesis (Schmucker et al., 2000; Wang et al., 2002; Matthews et al., 2007; Soba et al., 2007). Notably, *Drosophila Dscam* can encode thousands of isoforms through alternative splicing involving many choices of exon 4, 6, 9 and 17. Distinct Dscam isoforms may be targeted to dendrites or axons, depending on which of the two

transmembrane-domain-encoding exon 17 alternatives, 17.1 or 17.2, is utilized (Wang et al., 2004). Dscam isoforms carrying exon 17.1 (Dscam[TM1]) are largely restricted to dendrites, while Dscam isoforms with exon 17.2 (Dscam[TM2]) are enriched in axons. Further, depleting Dscam[TM1] or Dscam[TM2] blocks morphogenesis of dendrites versus axons (Shi et al., 2007). Understanding how isoforms of Dscam are differentially distributed in neurons promises to shed new light on neuron polarity and its underlying mechanisms.

Here we performed genetic mosaic screens to identify genes required cell-autonomously for the dendritic targeting of Dscam[TM1]. We obtained mutants that exhibit different mislocalization phenotypes. We identified three mutations in the known components of dynein-dynactin complex (*Lis1*, *p24* and *Dynamitin*) that all affect Dscam dendritic targeting. Misdistribution of dendritic Dscam to axons was also observed when we suppressed the expression of other dynein/dynactin components with RNA interference. However, microtubule polarity in the mutant axons was maintained. Transient induction of Dscam[TM1] further revealed that disrupting dynein/dynactin function did not affect the targeting of newly synthesized Dscam[TM1] to the dendrites. Instead, dendritic Dscam later diffused into the axons. These observations indicate that dynein/dynactin plays a role in maintaining dendritic restriction of Dscam[TM1], and further suggest a dynein/dynactin-independent mechanism for the initial targeting of Dscam[TM1] to dendrites. Notably, dynein/dynactin dysfunction did not alter distribution of another dendritic transmembrane protein Rdl (*Resistant to Dieldrin*),

supporting involvement of diverse mechanisms in locating distinct molecules to the dendritic membrane.

MATERIALS AND METHODS

Generation of *UAS-mCD8::RFP*

The monomeric red fluorescence protein (*mRFP*) open reading frame (Campbell et al., 2002) was amplified by PCR and was cloned into the mCD8-comtaining pBS (Lee and Luo, 1999) with BamHI and XbaI as the cloning sites, generating a new ORF with *mRFP* fused in frame to the 3' of mCD8. Then, *mCD8::RFP* was subcloned into *pUAST* (Brand and Perrimon, 1993) with XhoI and XbaI as the cloning sites. *pUAST-mCD8::RFP* transgene was introduced into the fly genome via P element-mediated germline transformation by Genetic Services Inc., MA.

Fly Stocks and Crosses

For creation of MARCM clones, we crossed *UAS-mCD8::RFP; hs-FLP, FRT^{G13}, tubP-GAL80/CyO,Y* to either wildtype or mutagenized *UAS-Dscam[TM1]::GFP, FRT^{G13}, GAL4-201Y/CyO,Y*. *UAS-Nod-β-gal* (Lee et al., 2000b) or *UAS-Rdl-HA* (Sanchez-Soriano et al., 2005) was incorporated on third or X chromosomes, respectively, for examining their distribution in MARCM clones.

For acute induction by TARGET system, we crossed *UAS-Dscam[TM1]::GFP* or *UAS-mCD8::GFP* to *tubP-$GAL80^{ts}$; tubP-$GAL80^{ts}$; GAL4-OK107 . UAS-dominant-negative Glued, P[UAS-$Gl^{\Delta 84}$]*, (Allen et al., 1999) was used to block dynein/dynactin function. To increase copy numbers of *P[UAS- Gl^{Δ}]*, we generated another two insertion

lines on third chromosome (*UAS-Gl*$^{\Delta 008m}$ and *UAS-Gl*$^{\Delta 020m}$) by hopping out *P[UAS-Gl*$^{\Delta 84}$*]* from second chromosome.

Other flies stocks collected for this study include *Dmn*^{k16109}*/CyO* (BL-11159), *l(2)06496 /CyO* (BL-12316), *Lis-1*^{k13209}*/CyO* (BL-11072), *tubP-GAL80*^{ts}*;Tm2/Tm6B* (BL-7019), *noc/CyO; tubP-GAL80*^{ts} (BL-7018), and *RNAi* lines from VDRC stock center (Dietzl et al., 2007), including *CG8446RNAi* (23139), *Lis1RNAi* (6216), *DmnRNAi* (23728), *p25RNAi* (8058), *Dhc64CRNAi* (28054), *Dhc62BRNAi* (48153) and *Dlc90FRNAi* (31750).

MARCM-based Genetic Screens and Analysis of MARCM Clones

Chemical mutagenesis was conducted in the UAS-Dscam[TM1]::GFP, FRT^{G13}, GAL4-201Y male flies using standard procedure (Lewis and Bacher, 1968) with an EMS concentration of 40 mM. Individual male progeny derived from the mutagenized flies were then crossed with mCD8::RFP; hs-FLP, FRT^{G13}, tubP-GAL80 for MARCM analysis of MB clones. To induce mitotic recombination, newly hatched larvae were heat shocked in a 38℃ water bath for one hour and then returned to 25℃. The central nervous systems from wandering third instar larvae were dissected out, fixed and immunostained as previously described (Lee and Luo, 1999). Protein expression was detected by the rabbit anti-GFP Ab (1:300, Molecular Probes) and MB lobes were labeled by the 1D4 mAb (1:80). Immunofluorescent signals were collected by confocal microscopy and then processed using Adobe Photoshop to normalize and exclude the background neurons.

Deficiency Mapping and Complementation Testing

Following screening, the homozygous lethal mutants were mapped initially by crossing to the second chromosome deficiency kit, provided by the Bloomington Drosophila Stock Center. We performed further fine scale mapping with smaller deficiencies to define the minimal regions containing the lethal mutations. Lines mapped to the similar regions were placed in complementation groups by the complementation testing. Eventually, we tested candidate genes in these regions with available lethal mutant lines from Bloomington.

Acute Induction of UAS-transgenes by TARGET system

Larvae carrying two copies of *tubP-GAL80^{ts}* (McGuire et al., 2003) were cultured at the permissive temperature of 18°C since embryogenesis in order to repress GAL4-mediated transcription. Wandering larvae were shifted to 38°C for 30 min, followed by incubation at the non-permissive temperature of 29°C for various periods.

RESULTS

***Drosophila* Dscam[TM1] as a dendritic marker for genetic mosaic analysis of dendritic protein targeting**

We have previously shown that transgenic Dscam carrying the exon 17.1-encoding transmembrane domain (referred to as Dscam[TM1] as opposed to Dscam[TM2] that carries exon 17.2) is selectively targeted to dendrites. When ectopically expressed in the neurons of the *Drosophila* olfactory learning and memory center, the mushroom bodies (MBs), Dscam[TM1]::GFP exists abundantly in the calyx where MB dendrites are located, but could not be detected in the axons which extend

through the peduncle before entering the MB lobes (Figures 2-1B, C and C'). MARCM, a positive-labeling genetic mosaic technique, has allowed us to effectively generate clones of MB neurons that are homozygous for a specific chromosome arm in an otherwise heterozygous organism and simultaneously express a reporter gene in an unlabeled background (Lee and Luo, 1999; Lee et al., 1999). Using mCD8::GFP as a reporter to visualize the morphology of the MBs, we have been screening for genes required for various aspects of MB development through loss-of-function genetic mosaic analysis (Lee et al., 2000a; Wang et al., 2002; Wang et al., 2006; Zheng et al., 2003; Zhu et al., 2005; Zhu et al., 2006). We reasoned that incorporating Dscam[TM1]::GFP into our MARCM screens should allow us to uncover genes, regardless of their possible involvement in other essential cellular events, that are essential for proper dendritic targeting of Dscam[TM1]::GFP. Our goal was to fully elucidate the cellular/molecular mechanisms of dendritic protein targeting.

To adapt the system for genetic mosaic screens on dendritic protein targeting, we incorporated *UAS-mCD8::RFP* and *UAS-Dscam[TM1]::GFP* into MARCM (Figure 2-1A). In combination with *GAL4-201Y*, a MB GAL4 enhancer trap line, we simultaneously expressed Dscam[TM1]::GFP and mCD8::RFP in the MB clones and directly examined Dscam[TM1]::GFP distribution inside the MBs of live mosaic larval brains (Figure 2-1C). While mCD8::RFP outlined the entire clone (Figure 2-1C', red), Dscam[TM1]::GFP was well restricted to the MB calyx in wild-type clones (Figure 2-1C). Using this as readout, we screened 1,850 chemically mutagenized 2R chromosome arms for mutations that affect the dendritic restriction of Dscam[TM1]::GFP. We

recovered 35 mutant lines that exhibited abnormal Dscam[TM1]::GFP protein distribution patterns. We clustered them into four groups according to their phenotypes. Group I consisted of 9 independent lines that showed significant Dscam[TM1]::GFP accumulation in both MB peduncles and lobes (e.g. Figures 2-1D and D'). Group II carried mutations that have mistargeted Dscam[TM1]::GFP gradually disappeared along the MB axon bundles (e.g. Figures 2-1E and E'). In Group III, Dscam[TM1]::GFP becomes restricted to MB cell bodies (e.g. Figures 2-1F and F'), while mutations in group IV disrupted gross MB morphology (e.g. Figures 2-1G and G'). All the recovered lines were lethal as homozygotes, thus it would be impossible to systematically uncover the genes required for dendritic protein targeting as well as organism viability without genetic mosaics. In the following work, we selectively focused on group I mutants that displayed mistargeting of dendritic Dscam more uniformly throughout the MBs.

Analysis of mutants that exhibited aberrant accumulation of Dscam[TM1]::GFP in axons

Detailed analysis of group 1 mutants further revealed subclasses of misdistribution phenotypes. Five of the nine mutants exhibited granular accumulation of Dscam[TM1]::GFP in the MB lobes (e.g. Figures 2-2A-D), three had Dscam[TM1]::GFP selectively accumulated in the peduncle (e.g. Figure 2-2E), and the last one showed broad non-granular distribution of Dscam[TM1]::GFP (e.g. Figure 2-2F). In addition, many of the mutant clones were smaller than controls (e.g. Figure 2-1H). Two of the lines with granular accumulation had reduced calycal volume, suggesting possible defects in dendritic morphogenesis. These phenomena indicated that genes involved in dendritic

protein targeting potentially underlie multiple fundamental cellular functions. Further, the identification of several clusters of misdistribution phenotypes suggested the involvement of multiple mechanisms in restricting Dscam[TM1] to dendrites.

Complementation among the mutations yielded six complementation groups. Mapping against deficiency lines and other known mutations further revealed that mutations in *Lis1*, *p24*, and *Dynamitin (Dmn)* constituted three of the four complementation groups which showed mistargeted Dscam[TM1]::GFP in granules (Figures 2-2A-C, arrows). Both lines that exhibited defective dendritic morphogenesis carried mutations in *Lis1* (Figure 2-2A', arrowhead). *Lis1*, a mutation of which underlies human *lissencephaly*, is a regulatory protein of the microtubule motor dynein, and is highly conserved from human to *Drosophila*. *Drosophila Lis1* has been shown to play an essential role in MB neurogenesis and dendritic elaboration (Reiner et al., 1993; Swan et al., 1999; Liu et al., 2000). However, it has never been shown to be involved in differential distribution of cell surface proteins. *p24 (CG9893)* is a novel molecule that may be integral to the dynactin complex, as implicated from its sequence and structural similarity with vertebrate *DCTN3* (Goldstein and Gunawardena, 2000). *p50/Dmn* is also a dynactin subunit. The dynactin complex regulates the cargo selection and processivity of dynein. Mutations in the dynactin complex can affect the assembly of dynein/dynactin complex and its binding affinity for microtubules (Puls et al., 2003; Schroer, 2004; Clark and Rose, 2005). The recovery of multiple dynein/dynactin components and regulators indicates that proper dynein/dynactin function is essential for the restriction of Dscam[TM1]::GFP to dendrites.

Requirement of dynein-dynactin complex for the restriction of Dscam[TM1]::GFP to dendrites

In order to substantiate the involvement of dynein-dynactin complex, we first confirmed that Lis1, Dmn, and p24 are required for the dendritic restriction of Dscam[TM1]::GFP using reagents independent of our genetic screen. Genes could be effectively silenced in the MBs by RNA interference (RNAi) (Didelot et al., 2006; Shi et al., 2007); and transgenic flies carrying *UAS-RNAi* against various *Drosophila* genes, including *Lis1*, *Dmn*, and many other components of dynein-dynactin complex, are available in the Vienna Drosophila RNAi Center (VDRC) (Dietzl et al., 2007). Encouragingly, silencing *Lis1* or *Dmn*, as opposed to various control genes (such as *CG8446* and *CG18247*), by targeted RNAi effectively mislocalized transgenic Dscam[TM1]::GFP to MB axon lobes (Figures 2-3A-C). These results not only confirmed the roles of *Lis1* and *Dmn*, but also illustrated the utility of RNAi in quickly uncovering more genes in a common pathway. We confirmed the indispensability of *p24* in Dscam localization by examining Dscam[TM1]::GFP distribution in MB clones homozygous for a pre-existing loss-of-function allele of *p24* (data not shown). Analogous mislocalization phenotypes were obtained when Lis1, Dmn, or p24 were depleted by various means, substantiating their involvement, possibly through the dynein-dynactin complex, in excluding dendritic Dscam from axons.

Further, we knocked down additional components of the dynein/dynactin complex (Figure 2-3J), including dynein heavy chains (Dhc64C and Dhc62B), dynein light chain

(Dlc90F), and another dynactin subunit (p25), by targeted RNAi. Aberrant accumulation of dendritic Dscam in the MB axons was detected in all the cases (Figures 2-3D-G), though the detailed mislocalization patterns varied depending on which gene was silenced. For example, targeting RNAi against *Lis1*, *Dmn* or *Dhc64C* caused excessive accumulation of dendritic Dscam near the ends of the axonal lobes (Figures 2-3B-D, arrowheads), while Dscam[TM1] uniformly distributed throughout the axonal lobes following depletion of *Dhc62B*, *Dlc90F* or *p25* (Figures 2-3E- G, arrows). These different phenotypes could be derived from different residual dynein/dynactin function due to partial knockdown or differential redundancy. Alternatively, they might result from crippling distinct aspects of Dscam protein targeting, since it remains unclear as to the individual proteins' full spectra of function (see Discussion). Notably, simultaneously depleting either two of *Dhc62B*, *Dlc90F* or *p25* shifted the misdistribution from the peduncle to the lobes (e.g. Figures 2-3H and I), better recapitulating the terminal accumulation phenotype in other dynein/dynactin mutants. These results indicate that all these molecules act through dynein/dynactin complexes to restrict Dscam[TM1] to dendrites.

In addition, the role of *Glued* was determined through inhibition of its function by a dominant-negative Glued (Gl^{Δ}) (Allen et al., 1999). Glued is the largest subunit of dynactin complex and plays a particular important role in dynein binding and enhancement of dynein processivity. Overexpression of C-terminal-truncated Glued (Gl^{Δ}), known to dominantly block dynein/dynactin function, also resulted in axonal accumulation of dendritic Dscam, especially near the ends of axonal lobes (Figures 2-4A

and B, arrows). These results indicate that normal dynein/dynactin function is essential for dendritic restriction of Dscam[TM1]::GFP. Suppressing any component of dynein/dynactin complex may impede dynein/dynactin function and lead to the accumulation of Dscam[TM1]::GFP in axons.

Blocking dynein/dynactin function does not affect dendritic targeting of two other dendritic markers

To determine how broadly dynein/dynactin is involved in dendritic protein targeting, we examined whether dynein/dynactin is required for proper localization of other dendritic proteins. Several documented dendritic markers, including homer-GFP, Apc2-GFP, Act5C-GFP, Nod- β -gal and Rdl-HA (Sanchez-Soriano et al., 2005; Rolls et al., 2007), were ectopically expressed in the larval MBs using *GAL4-201Y* as the driver. In this condition, only Nod-β-gal and Rdl-HA showed predominant somatodendritic distribution and were largely excluded from MB axon lobes (Figures 2-4E and C; data not shown).

Nod-β-gal is a fusion protein comprised of the motor domain of Nod and β-galactosidase, and has been shown to be a reliable minus-end reporter for microtubules in *Drosophila*, including MB neurons (Clark et al., 1997; Lee et al., 2000b; Reuter et al., 2003). Microtubules in MB dendrites are bi-directional, but uniformly oriented with plus-end pointing distally in axons. Consistent with previous findings, Nod-β-gal was highly enriched in dendrites, cell bodies and proximal region of peduncles, but largely absent from distal region of peduncles and axonal lobes in wild-type MB neurons (Figure

2-4E). Co-expression with dominant-negative Glued or ectopic induction in dynein/dynactin mutant clones (*Lis1*, *Dmn* and *p24*) did not alter its somatodendritic distribution (Figures 2-4F, 2-5B'-D'). These results indicate that dynein/dynactin dysfunction did not perturb microtubule organization in axons, and that mistargeting of Dscam[TM1]::GFP did not occur as a consequence of abnormal microtubule polarity.

Rdl-HA (*Resistant to Dieldrin*) is a GABA receptor tagged with the HA epitope, and has been shown to be well restricted to dendrites in *Drosophila* embryonic motor neurons (Sanchez-Soriano et al., 2005). In wild-type MB neurons, Rdl-HA was also localized in dendrites, cell bodies and proximal region of peduncles only (Figure 2-4C). Again, perturbation of dynein/dynactin function using dominant-negative Glued or by MARCM with *Lis1*, *Dmn* and *p24* mutations did not alter the somatodendritic distribution of Rdl in the larval MBs (Figures 2-4D, 2-5F'-H'). These results indicate that dynein/dynactin is selectively required for exclusion of dendritic Dscam from axons, implicating utilization of different mechanisms for restricting distinct membrane proteins to the dendrites.

Retrograde transport plays a role in maintaining but not establishing Dscam[TM1] dendritic restriction

We wondered how dynein/dynactin complexes act to ensure restriction of Dscam[TM1] to the dendrites. As a minus-end-directed microtubule motor, dynein/dynactin may actively move Dscam[TM1] from cell bodies to dendrites by selective transport. Alternatively, it may play a scavenging role and constantly remove

mistargeted Dscam[TM1] out of axons via retrograde axonal transport (Burack et al., 2000; Koonce and Samso, 2004; Pilling et al., 2006). To distinguish between these two possibilities, we sought to visualize newly synthesized Dscam[TM1]::GFP and examine how dynein/dynactin dysfunction might affect the initial sorting of Dscam[TM1] and/or the maintenance of its dendritic distribution.

Transient induction of Dscam[TM1]::GFP in the larval MBs was achieved using the TARGET system, in which GAL4-dependent expression of UAS-transgene is acutely controlled by a temperature-sensitive GAL4 repressor, GAL80ts (McGuire et al., 2003). At 18℃, GAL4-OK107 was fully suppressed by GAL80ts (Figure 2-6A and C). Following inactivation of GAL80ts by shifting the organisms to higher temperatures (see Experimental Procedures), we could start to detect mCD8::GFP or Dscam[TM1]::GFP in young MB neurons (whose axons occupy core regions of axonal bundles and are weakly labeled by 1D4 mAb, Mitsuhiko et al., 2002) approximately one hour after induction. Since the enrichment of newly synthesized protein in young MB neurons were seen for both mCD8::GFP and Dscam[TM1]::GFP, this phenomenon could possibly result from the expression profile of GAL4-OK107 at the wandering larval stage or the difference in the intrinsic properties of newly derived MB neurons versus mature ones. Notably, while mCD8::GFP was uniformly distributed (Figure 2-6D), newly synthesized Dscam[TM1]::GFP was consistently located to dendrites (Figure 2-6B). These observations suggest involvement of selective transport in targeting Dscam[TM1] specifically to the dendrites.

We next co-expressed dominant-negative Glued to determine how compromised dynein/dynactin function might affect the sorting of newly synthesized Dscam[TM1]::GFP. Analogous transient co-induction did not alter the dendritic distribution of Dscam[TM1]::GFP (data not shown, similar to Figure 2-6E). However, an acute prolonged induction revealed a requirement for dynein/dynactin in the continuous restriction of Dscam[TM1] to the dendrites (Figures 2-6F-H). Organisms carrying both *UAS-Dscam[TM1]::GFP* and *UAS- Gl*$^{\Delta}$ were reared at 18℃ until the wandering larval stage when they were subjected to a half-hour heat shock at 38℃ followed by continuous incubation at 30℃. Interestingly, starting around six hours after heat shock, Dscam[TM1]::GFP gradually misdistributed into the axons (Figure 2-6M). Dscam[TM1]::GFP was first detected in the proximal region of peduncles (Figure 2-6F), then present in the beginning of axonal lobes (Figure 2-6G), and, by12 hours after heat shock, located throughout the entire axon lobes (Figure 2-6H). By contrast, in the absence of dominant-negative Glued, Dscam[TM1]::GFP remained restricted to the MB calyces even after 28 hours of continuous induction (Figures 2-6I-L). These results indicate that the misdistribution was not due to excessive expression of Dscam[TM1]::GFP, but rather owing to disruption of dynein/dynactin function by dominant-negative Glued.

Two possible scenarios may underlie the time course of mislocalization. First, several hours of continuous induction might be needed to express enough truncated Glued for blocking dynein/dynactin function. Second, dynein/dynactin could be dispensable to the selective transport of Dscam[TM1] from cell bodies to dendrites, and

specifically involved in removing any mistargeted Dscam[TM1] out of the axons. In this case, blocking dynein/dynactin function should not affect the initial dendritic targeting of Dscam[TM1]::GFP, but would compromise the ability of neurons to promptly move Dscam[TM1]::GFP from the axon 'hillock' back to the somatodendritic region.

To determine if such a protracted process of misdistribution occurred as a consequence of slow accumulation of dominant-negative Glued, we further examined how increasing the dosage of dominant-negative Glued affects the misdistribution process. If induction of dominant-negative Glued was the rate-limiting factor, increasing the dosage of truncated Glued should accelerate the onset of mistargeting. As the copy number of *UAS- Gl*$^{\Delta}$ transgene was increased to two and even three, we did not detect any change in the profile of the slow-onset, gradual accumulation of Dscam[TM1]::GFP in the MB axons (Figure 2-6M). These results indicate that the level of dominant-negative Glued was not limiting the misdistribution process. Furthermore, it suggests that blocking dynein/dynactin function did not affect the initial dendritic targeting of Dscam[TM1], but rather disrupted the maintenance of no dendritic Dscam in axons.

DISCUSSION

Multiple lines of evidence indicate that the dynein/dynactin complex has an important function in maintaining proper distribution of dendritic Dscam in MB neurons. First, mutations in three components (*Lis1*, *Dmn* and *p24*) of the dynein/dynactin complex were recovered based on mislocalization of dendritic Dscam through a MARCM-based genetic mosaic screen (Figures 2-2A-C). Second, silencing other

components of the complex with RNAi also resulted in mistargeting of dendritic Dscam to axons (Figures 2-3B-G). Third, disrupting dynein/dynactin function with dominant-negative Glued reproduced the mislocalization phenotype (Figure 2-4B). Further, newly synthesized Dscam[TM1] was preferentially targeted to dendrites (Figure 2-6B). Interestingly, compromising dynein/dynactin function did not affect the targeting from cell bodies to dendrites but disrupted the continuous exclusion of dendritic Dscam from axons (Figures 2-6E-H, and 2-6M). Altogether, our findings show that dynein/dynactin normally acts through retrograde transport to prevent Dscam[TM1] from entering axons.

Acute induction by TARGET revealed two mechanisms underlying the dendritic distribution of Dscam[TM1]. Newly synthesized Dscam[TM1] was largely excluded from axons, suggesting directed dendritic targeting and the involvement of selective transport in the dendritic distribution of Dscam[TM1]. Though dynein/dynactin is essential for restricting Dscam[TM1] to dendrites, knocking down dynein/dynactin function did not disrupt the directed dendritic targeting. This leads us to believe that dynein/dynactin is required for preventing dendritic Dscam from misdistributing into axons. When dynein/dynactin function was compromised, newly synthesized Dscam[TM1] remained consistently targeted to dendrites but later leaked into axons. Dendritic Dscam gradually filled the axons; and it took about six hours for Dscam[TM1] to reach the axon termini. This protracted process of mislocalization suggests that dendritic Dscam passively leaks into the axons, and that dynein/dynactin-mediated retrograde axonal transport normally acts to rapidly move leaked Dscam[TM1]-containing vesicles out of the axons. In summary, these phenomena not only demonstrate

a dynein-dynactin-independent mechanism of selective transport that preferentially targets Dscam[TM1]-containing vesicles to dendrites, but also implicate the involvement of retrograde axonal transport in preventing accumulation of Dscam[TM1] in axons. These two independent mechanisms act together to ensure restriction of dendritic Dscam to the dendrites.

Although the dynein/dynactin complex is essential for maintaining dendritic distribution of Dscam[TM1], our results do not reveal whether mislocalized Dscam[TM1] is on the plasma membrane or in vesicles inside the cytoplasm. It is possible that dendritic Dscam passively leaks into axons either through membrane diffusion or mistargeting of vesicles. Since blocking endocytosis with temperature-sensitive *shibire* mutant showed no obvious effect on Dscam dendritic distribution (data not shown), we favor the model that dynein/dynactin acts to prevent axonal accumulation of Dscam[TM1] by actively moving mistargeted Dscam[TM1]-containing vesicles out of axons by retrograde axonal transport (Figure 2-7).

However, dynein/dynactin is not routinely needed for excluding dendritic proteins from the axons. Since no biological process can be carried out with absolute fidelity, it is conceivable that dendritic molecules of most kinds may accidentally leak into the axons. Some salvage mechanism(s) should exist for actively clearing mislocalized molecules to prevent any significant accumulation in the wrong places. Dynein/dynactin mediates retrograde axonal transport and can serve as a general mechanism for removing dendritic molecules out of axons. Nonetheless, blocking dynein/dynactin function did not affect

the distribution of two other dendritic markers we checked. Nod-β-gal is a reliable minus-end reporter of microtubules, and misdistribution of Nod-β-gal in MB axons has been shown in *short stop* mutant clones, in which microtubule polarity is perturbed (Reuter et al., 2003). Absence of Nod-β-gal from the axons of dynein/dynactin mutant neurons demonstrates that the microtubules in axons remained uniformly polarized with minus ends pointing toward cell bodies, and rules out the possibility that dendritic Dscam became mislocalized due to abnormal microtubule organization. As to Rdl-HA, which, like Dscam[TM1], is a membrane protein, a lack of effect on its somatodendritic distribution indicates that dynein/dynactin is selectively involved in preventing dendritic Dscam from leaking into the axons. Diverse mechanisms may be utilized to efficiently clear different dendritic proteins in axons.

Regarding the mechanism(s) of selective transport, directed dendritic targeting apparently requires motor proteins that selectively move cargos toward the dendrites. Since dendrites, but not axons, carry microtubules with minus ends pointing away from cell bodies, potential candidates that underlie directed dendritic targeting include all minus-end-directed microtubule motors. Notably, dynein/dynactin is dispensable to the initial dendritic targeting of Dscam[TM1] or the continuous dendritic restriction of Rdl, arguing against any critical role for minus-end-directed dynein/dynactin in transporting cargos into the dendrites. Other microtubule motors that might support such directional movement include dendrite-specific plus-end-directed motors (e.g. KIF17 and KIF21B, Marszalek et al., 1999; Setou et al., 2000), though it remains mysterious how a plus-end-directed motor can be well restricted to dendrites. In theory, forward genetic mosaic

screens will ultimately allow us to uncover the diverse mechanisms of dendritic protein targeting. Encouragingly, we have obtained mutants that exhibit different mislocalization phenotypes, further characterization of which should shed additional light on neuron polarity and its underlying cellular/molecular mechanisms. Notably, in DC-B9 mutant clones, mistargeted Dscam[TM1]::GFP existed abundantly in the MB peduncle, preferentially accumulated at the end of the peduncle, but never extended into the axon lobes. This intriguing phenotype suggests the `presence of distribution barriers not only in the beginning of axons but also at the junction between the proximal axon domain (peduncle) and the distal axon segment (lobe), and implies another possible mechanism for restricting Dscam[TM1] to the dendritic membrane.

Furthermore, the functional roles of each subunit of the dynein/dynactin complex have not been fully determined (reviewed in Schroer, 2004). Although several studies of the dynein light chains in mammalian cells indicate that dynein subunits can be functionally specialized (Tai et al., 2001), studies in *Drosophila* show that strong loss-of-function mutations in different dynein/dynactin subunits show extensive overlap in the resulting mutant phenotypes (Reuter et al., 2003; Whited et al., 2004). Our data indicate that *Lis1*, *Dmn*, *Glued*, *p24*, *p25*, *Dhc64C*, *Dhc62B*, and *Dlc90F* all participate in the complete function of dynein/dynactin complex in maintaining dendritic distribution of Dscam. This result supports the idea that all the dynein/dynactin subunits work together to fulfill its diverse functions, and loss of any subunits may result in different degrees of similar dynein/dynactin-dysfunctional phenotypes.

With respect to Dscam targeting motifs, we have reported that the cytoplasmic juxtamembrane domain of Dscam may dictate its TM-dependent subcellular localization (Shi et al., 2007). However, further structure-distribution analysis only allowed us to locate an axonal targeting motif to the cytoplasmic juxtamembrane region of TM2, leaving its dendritic targeting motif(s) still undetermined (unpublished results). In addition, we could not determine using the same system whether any of the mutants recovered here also affects the axonal targeting of Dscam[TM2], since transgenic Dscam[TM2] becomes uniformly distributed upon overexpression following an analogous induction. The involvement of multiple mechanisms in targeting specific Dscams to specific neuronal domains further supports the notion that Dscam isoform compositions in the dendrites versus axons of the same neurons need to be independently regulated, elucidation of the physiological significance of which promises to shed new light on how the brain develops and operates.

In summary, we have uncovered a scavenger mechanism for maintaining dendritic distribution of Dscam[TM1] and provide an in vivo model to study neuron polarity and differential protein targeting. On top of the many known functions of dynein/dynactin (including mitosis, vesicular transport, retrograde signaling, neuronal migration), dynein/dynactin helps restrict certain dendritic proteins to the somatodendritic domain of neurons by preventing them from spreading into the axons. Notably, multiple independent mechanisms act together to locate Dscam[TM1] to dendrites; and diverse mechanisms are utilized to target different dendritic proteins to the dendrites.

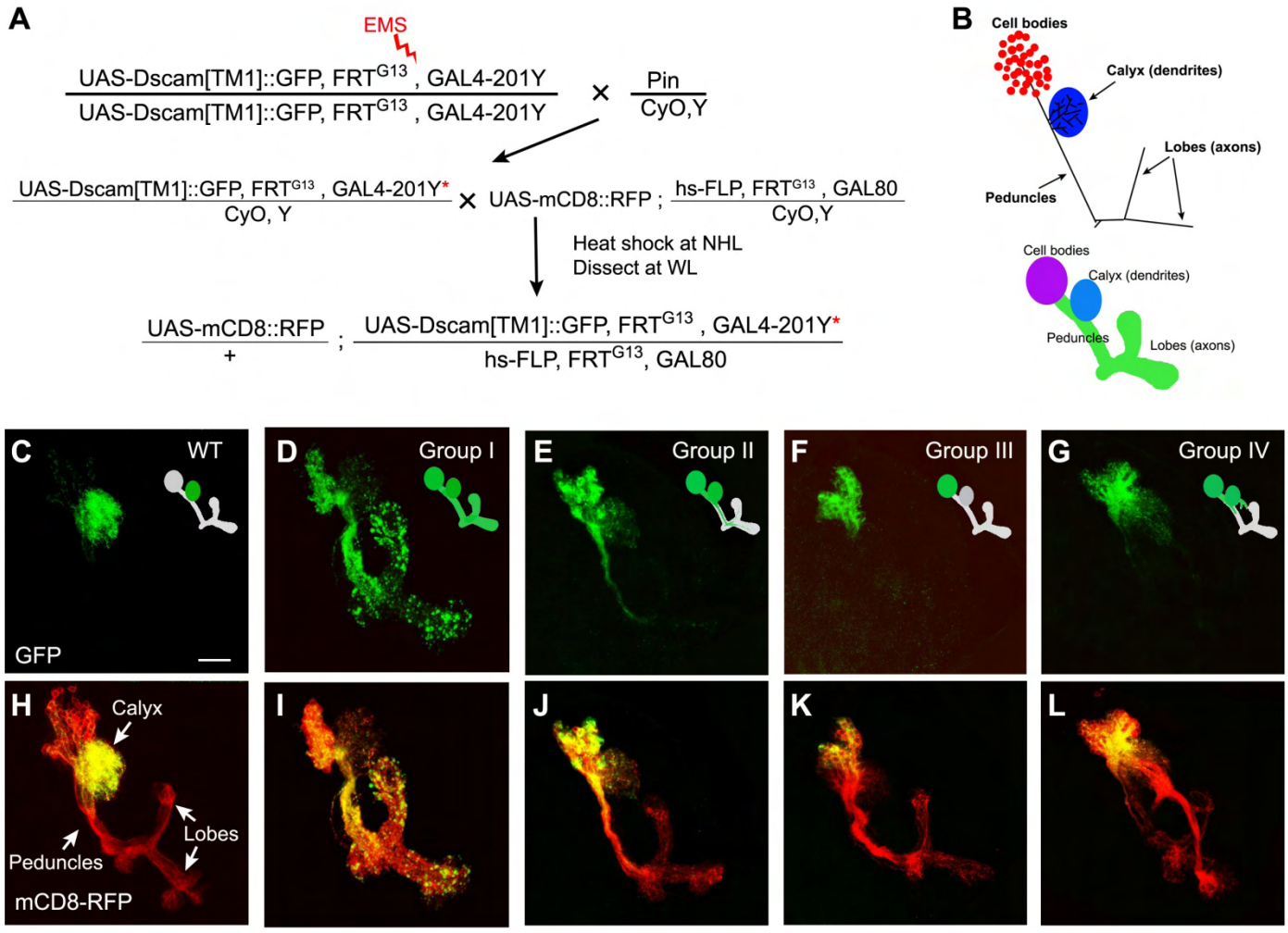

Figure 2-1. Genetic mosaic screen for mutants with abnormal Dscam[TM1] distribution

(A) Schemes of the genetic crosses of the screen. The star represents a mutagenized chromosome. (B) Schematic diagram of MB subcompartments. (C-G') Composite confocal images of MB neuroblast clones co-labeled with mCD8::RFP (red) and Dscam[TM1]::GFP (green). As compared to the wild-type control (C) where transgenic Dscam was absent from axons, various mutant clones (D, E, F, and G) exhibited different Dscam mislocalization phenotypes. Note that mutations of group IV disrupted MB gross morphologies (G and G') and were all mapped to the gene *short-stop*. Scale bar (here and in all figures) represents 20 μm.

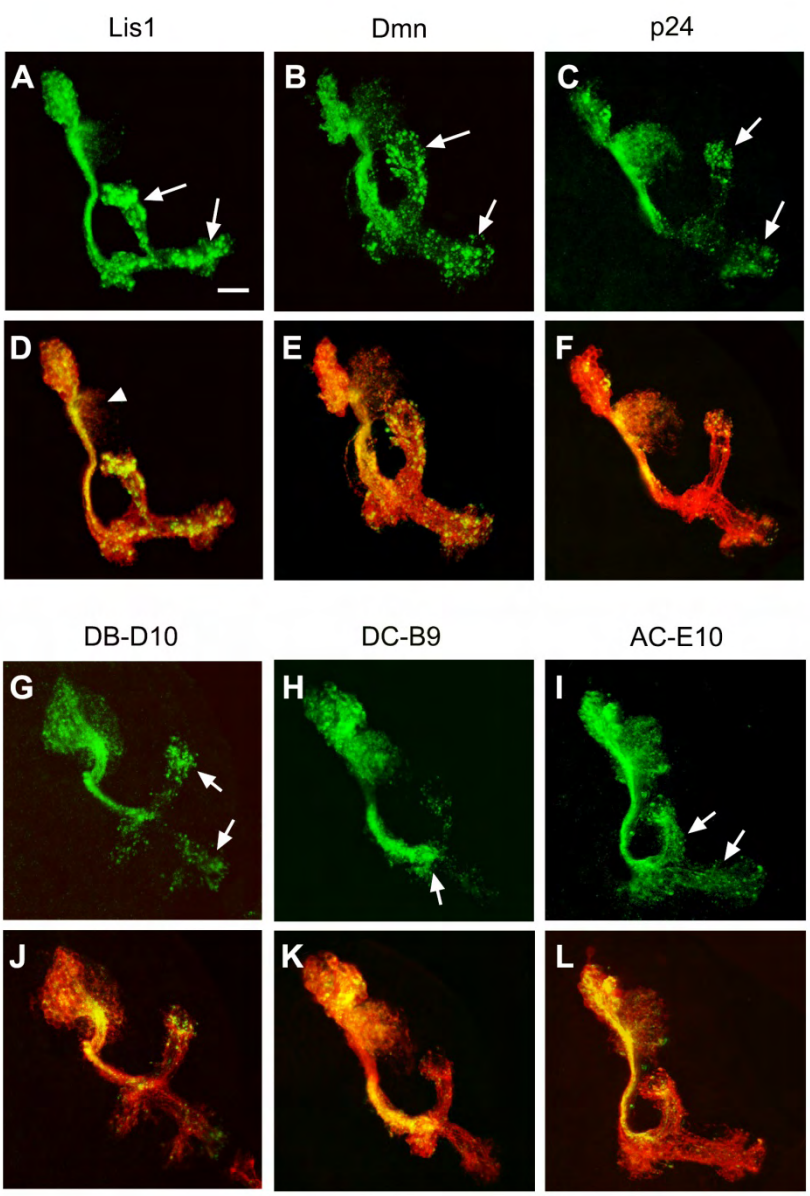

Figure 2-2. Mistargeting of dendritic Dscam in Group I mutant clones
MB clones of different complementation groups of group I. Granular accumulation of Dscam[TM1]::GFP (green) in the MB lobes was observed in four of the six complementation groups, including *Lis1*, *Dmn*, *p24* and DB-D10 (A-D, arrows). In contrast, mistargeted Dscam preferentially accumulated in the peduncles of DC-B9 mutant clones (E, arrow), while Dscam[TM1]::GFP was rather uniformly distributed in AC-E10 clones (F, arrows). MB clones were co-labeled by mCD8::RFP (red). Note the reduced dendritic region in *Lis1* mutant clone (arrowhead).

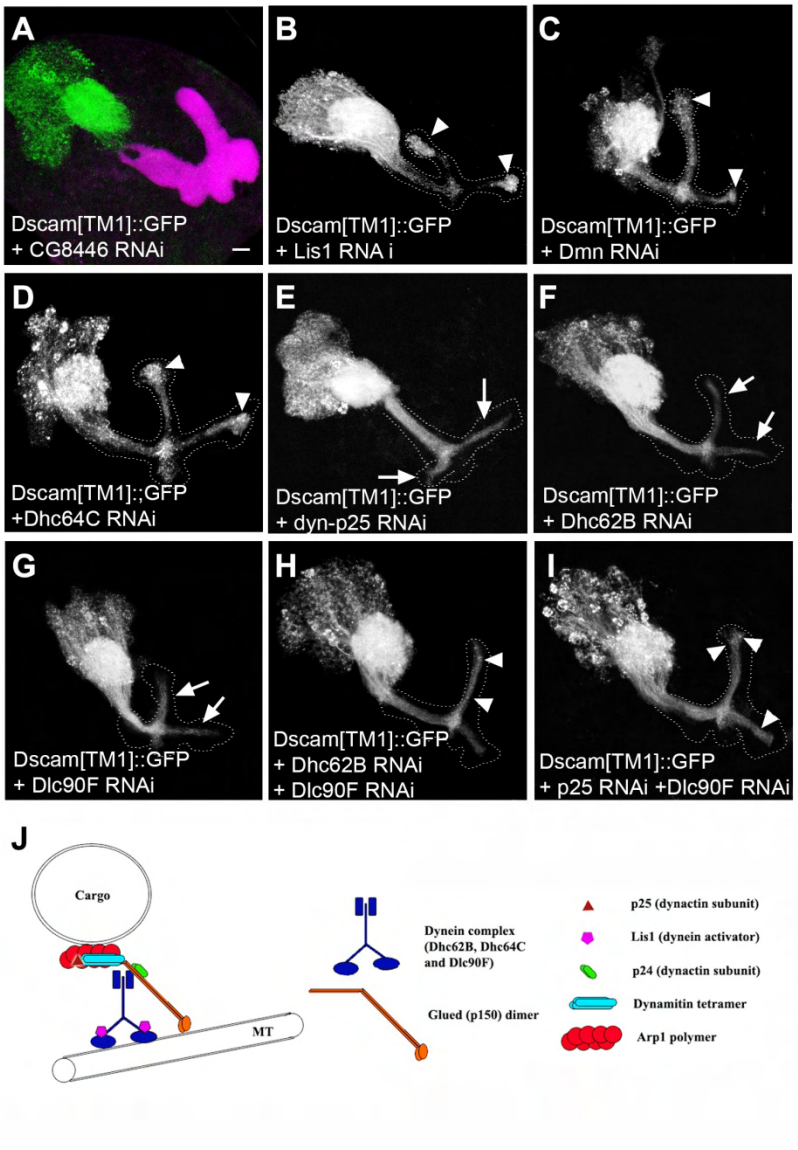

Figure 2-3. Mistargeting of dendritic Dscam following depletion of various components of dynein-dynactin complex

(A-G) Distribution of Dscam[TM1]::GFP in the larval MBs where a dynein/dynactin-unrelated gene *CG8446* (A) or various components of dynein/dynactin complex (B-G) were silenced by induction of *RNAis* with GAL4-OK107. Dscam[TM1]::GFP was no longer restricted to the cell bodies and calyx, when dynein/dynactin components were knocked down (B-G, compared to A). Note granular accumulation at the ends of axon lobes in [B] to [D] (arrowheads) versus uniform distribution in [E] to [G] (arrows). Double knockdown (H and I) showed more granular accumulation at the ends of axons than individual knockdowns (E-G) have. (J) Schematic illustration of dynein/dynactin complex. The entire axonal lobes were outlined by dashed lines according to the 1D4 mAb staining (red in A).

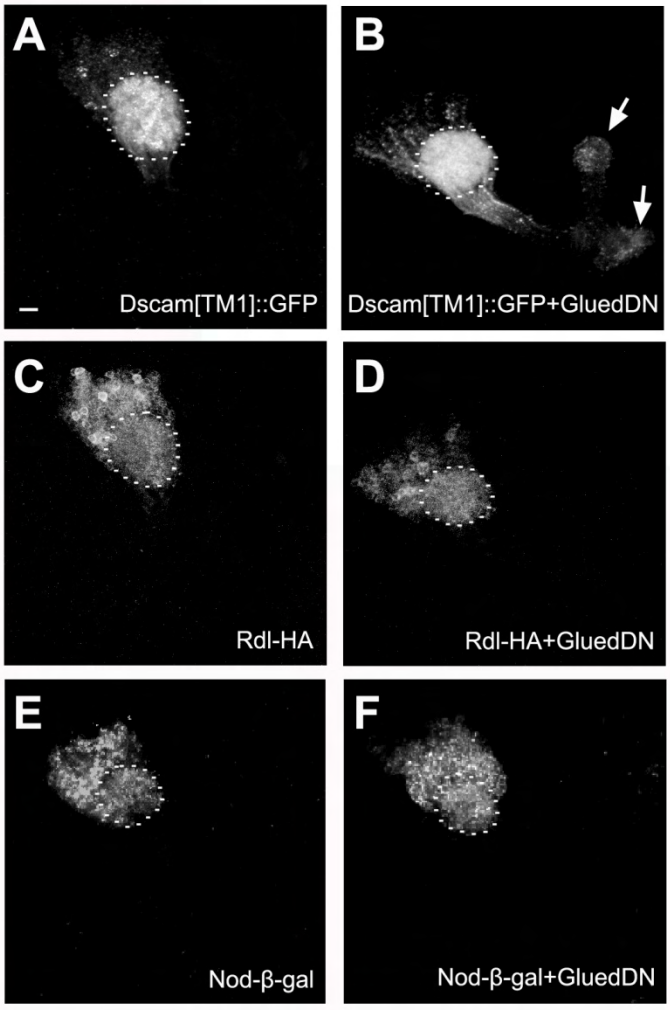

Figure 2-4. Effects of dominant-negative Glued on dendritic protein targeting
Larval MBs expressing various dendritic markers, including Dscam[TM1] (A and B), Rdl-HA (C and D) and Nod-β-gal (E and F), in the absence or presence of dominant-negative Glued. Note that dominant-negative Glued selectively affected the somatodendritic distribution of Dscam[TM1]::GFP (compare B to A), and that mislocalized Dscam[TM1]::GFP preferentially accumulated at the ends of lobes (arrows).

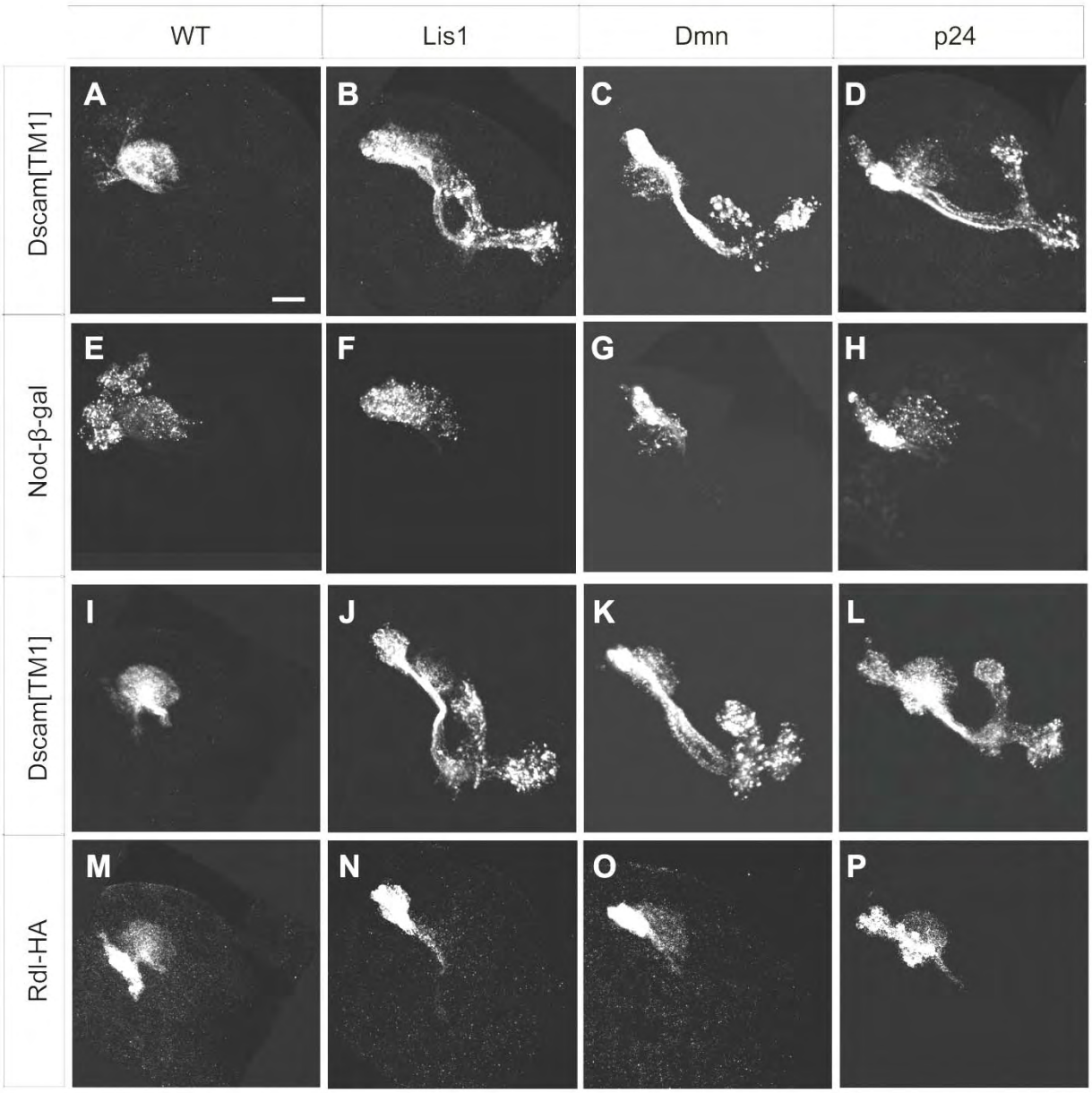

Figure 2-5. Axonal exclusion of Dscam[TM1], but not Nod or Rdl, requires dynein/dynactin

Larval MB clones co-expressing Dscam[TM1]::GFP (A-D and E-H) with Nod-β-gal (A'-D') or Rdl-HA (E'-H'). As compared to wild-type controls, *Lis1*, *Dmn* and *p24* mutant clones had Dscam[TM1]::GFP, but not Nod-β-gal or Rdl-HA, mislocalized to the MB axons.

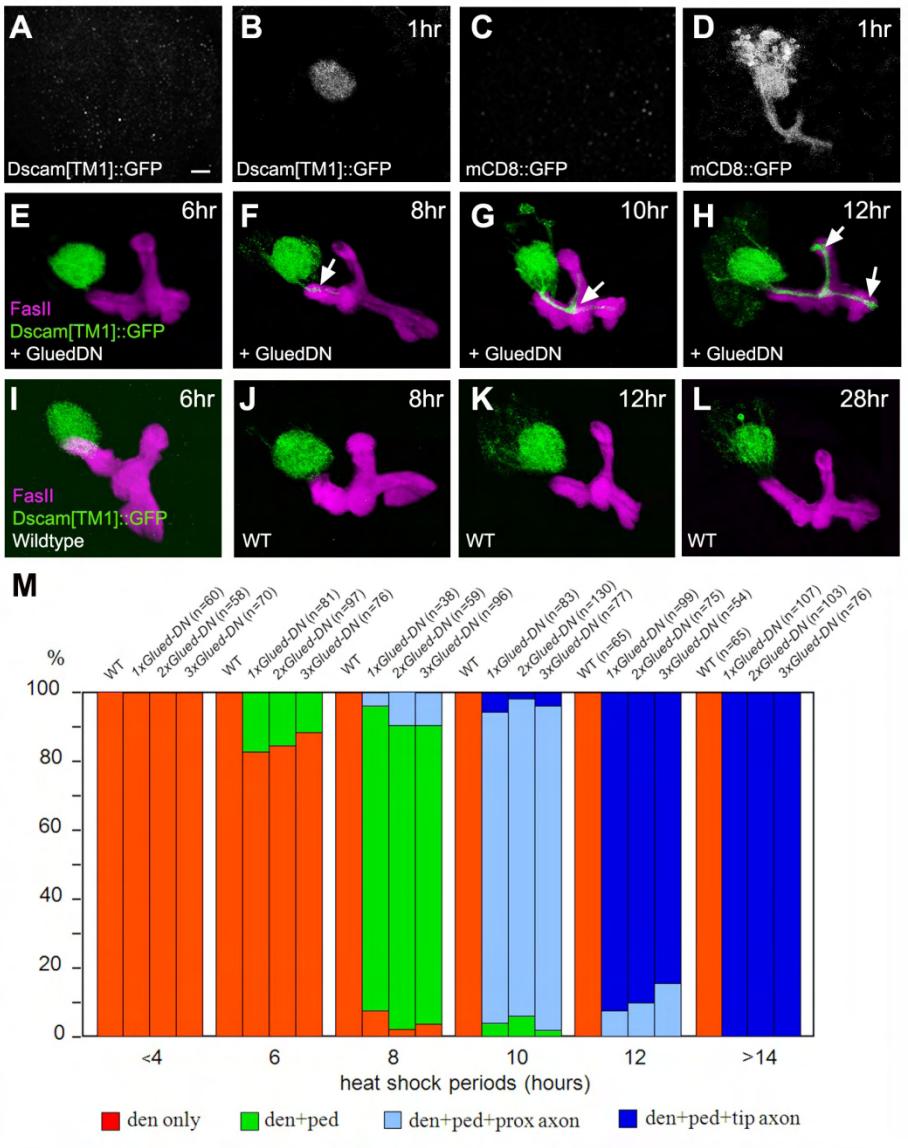

Figure 2-6. Retrograde transport plays a role in restricting Dscam[TM1]::GFP to the somatodendritic domain

(A-D) Transient induction of *UAS-Dscam[TM1]::GFP* or *UAS-mCD8::GFP* by TARGET. Prior to induction, GAL80ts fully suppressed the expression at a permissive temperature (A, C). Notably, one hour after heat-shock inactivation of GAL80ts, Dscam[TM1]::GFP was detected only in MB calyx (B) while mCD8::GFP distributed throughout the entire neurons (D). (E-L) Induction of Dscam[TM1]::GFP with or without GluedDN. Following co-induction with dominant-negative Glued, Dscam[TM1]::GFP gradually spread into MB peduncles and axonal lobes (F-H, arrows). In contrast, Dscam[TM1]::GFP was well restricted to the MB calyx in the absence of dominant-negative Glued (I-L). (M) Effects of GluedDN dosage on the misdistribution of Dscam[TM1]::GFP. Dscam[TM1]::GFP could localize in dendrites only (e.g. [E]), dendrites plus peduncles (e.g. [F]), dendrites, peduncles plus proximal portions of axon lobes (e.g. [G]), or from calyx to the tips of axon lobes (e.g. [H]). Note that increasing GlueDN dosage did not accelerate the mislocalization process.

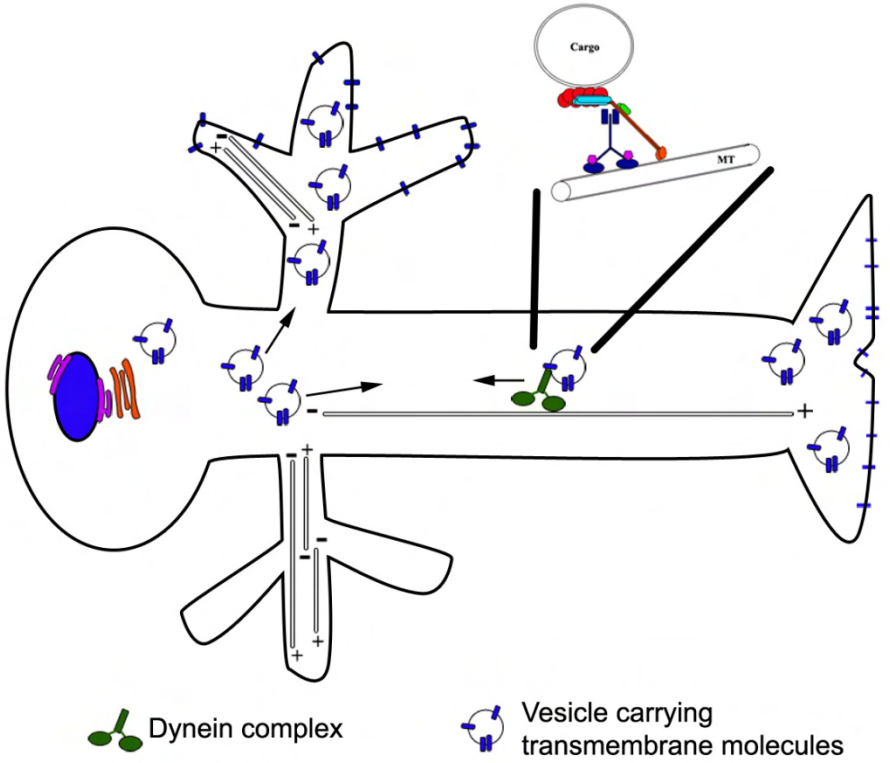

Figure 2-7. Multiple mechanisms govern the dendritic distribution of Dscam[TM1] Dscam[TM1]-containing cargos are primarily targeted to dendrites via a dynein/dynactin-independent process. In addition, they are effectively excluded from the axons by dynein/dynactin-mediated retrograde axonal transport.

Chapter 3

Structural and functional analysis of *Drosophila* Dscam

The following work is the original manuscript in preparation. Author list is:

Jacob Shun-Jen Yang and Tzumin Lee.

ABSTRACT

Dscam, a member of the immunoglobulin superfamily of cell adhesion molecules, is involved in the neuronal morphogenesis in the *Drosophila* brain. *Dscam* generates thousands of isoforms through alternative splicing. The transmembrane (TM) domain of Dscam is encoded by exon 17, for which there are two alternative choices, exon 17.1 (termed TM1) and exon 17.2 (termed TM2). Intriguingly, after pulse induction with the temporal and regional gene expression targeting (TARGET) system, Dscam[TM1] (full length Dscam with TM1 domain) and Dscam[TM2] (full length Dscam with TM2 domain) can be targeted to dendrites and axons, respectively and separately, in *Drosophila* mushroom body (MB) neurons. Here we present structural and functional characterization of Dscam to examine the distribution of various mutant proteins, which allowed us to identify axonal and dendritic targeting motifs of Dscam. An axonal targeting motif has been identified in the cytoplasmic juxtamembrane portion of TM2, and two amino acids (1650Arg and 1654Asp) within this portion are essential for axonal targeting of Dscam. This axonal targeting motif is dominant over the dendritic targeting motif of Dscam, which is present in its ectodomain.

INTRODUCTION

Neurons are highly polarized cells with two types of specialized extensions, dendrites and axons. Dendrites and axons require different sets of cell surface proteins (including receptors, ion channel and cell adhesion molecules) to achieve their distinct physiological functions (Craig et al., 1994). The mechanisms by which these distributions are established, maintained and modified are not well understood.

Dscam is a *Drosophila* homolog of human Down syndrome cell adhesion molecule (DSCAM). Genomic and cDNA analyses demonstrates that *Drosophila Dscam* can generate tens of thousands of isoforms through alternative splicing in its exons 4, 6, 9, 17, 19 and 23 (Schmucker et al., 2000; Wang et al., 2004). All the isoforms share a similar domain structure, with 10 immunoglobulin domains and 6 fibronectin type III repeats in the ectodomain, a single transmembrane (TM) domain and an endodomain. Dscam's transmembrane domain is encoded by exon 17. There are two alternative choices for exon 17, exons 17.1 and 17.2. Previous studies in *Drosophila* mushroom body neurons have shown that ectopically expressed Dscam isoforms with exon 17.1 (termed Dscam[TM1]) were preferentially localized to dendrites and cell body, while Dscam isoforms with exon 17.2 (termed Dscam[TM2]) were distributed throughout the entire neuron including axon, dendrites and cell bodies (Wang et al., 2004). The differential subcellular distribution of Dscam has important implications for the protein's function. Endogenous Dscam[TM1] and Dscam[TM2] primarily regulate dendritic elaboration and axonal arborization, respectively (Shi et al., 2007). Although physiological function of neuronal Dscam is likely to depend critically on the protein's locations in specific regions of neurons, little is known about the mechanisms responsible for this targeting process.

A key step in further defining mechanisms by which the differential distribution of a transmembrane protein is achieved is the identification of targeting motifs within the primary amino acid (aa) sequence of the protein that specify its subcellular localization. Multiple targeting motifs have been identified within several transmembrane molecules in neurons, including voltage-gated potassium channels, sodium channels, and

metabotropic glutamate receptors (West et al., 1997; Francesconi and Duvoisin, 2002; Gu et al., 2003; Garrido et al., 2001; Rivera et al., 2003). However, no targeting motifs of Dscam have been reported to date.

Constitutive overexpression of *Dscam[TM2]* by the traditional *GAL4-UAS* system showed no distribution preference in MB neurons. To better recapitulate the endogenous polarized distribution of Dscam[TM1] and Dscam[TM2], a temperature-sensitive GAL4 repressor, GAL80ts was incorporated to acutely control the expression of UAS transgenes (McGuire et al., 2003). Through this system, we identified an axonal targeting motif in the cytoplasmic juxtamembrane portion of Dscam exon 17.2, which is dominant over a dendritic targeting motif located in the ectodomain of Dscam. Mutation of two amino acids (1650Arg and 1654Asp) in the axonal targeting motif can disrupt the axonal distribution pattern of Dscam[TM2]. The ectodomain of Dscam is sufficient to mediate dendritic targeting of membrane protein mCD8 in neurons. Furthermore, differential distribution of Dscam[TM1] and Dscam[TM2], which are coexpressed in the same MB neurons, suggests the existence of a selective transport mechanism, which can recognize the targeting motifs of Dscam isoforms and transport them to distinct compartments in neurons.

MATERIALS AND METHODS

Fly stocks

For acute induction by the TARGET system, we crossed UAS transgenes to *tubP-GAL80^{ts}; tubP-GAL80^{ts}; GAL4-OK107* (Yang et al., 2008). Other flies stocks used for this study include *UAS-mCD8::RFP* (Yang et al., 2008), *UAS-mCD8::GFP, UAS-*

Dscam[TM1]::GFP, UAS-Dscam[TM2]::GFP (Wang et al., 2004), and *UAS-Dscams* with chimeric TMs (Shi et al., 2007).

Constructs:

Each *Dscam* construct was subcloned into the *pUAST* vector for P element-mediated germline transformation (Brand and Perrimon, 1993; Spradling and Rubin, 1982). For *Dscam[TM1]::RFP,* the monomeric red fluorescence protein (*mRFP*) open reading frame (Campbell et al., 2002) was amplified by PCR and was ligated in frame to the 3' end of the full-length *Dscam[TM1]* cDNA (Wang et al., 2004) via a *BamH*I site. C-terminal truncated mutants of *Dscam* were generated by removing the coding sequence after the *SacI* site in exon 18. Chimeric mCD8-Dscam[TM1] and mCD8-Dscam[TM2] were constructed by replacing the Dscam ectodomain (amino acids 1-4772) with mCD8's ectodomain (amino acids 1-194) through the introduction of a *Hind*III site between the mCD8 ectodomain and Dscam TMs. Chimeric Dscam-mCD8 was constructed by replacing the mCD8 ectodomain with Dscam's ectodomain through the introduction of a *Pst*I site between the Dscam ectodomain and mCD8 TM.

Site-directed mutagenesis

The full-length *Dscam[TM2]* cDNA (4.3-6.36-9.25-17.2+19+23, Wang et al., 2004) was digested with *Hind*III and *Sac*I. The segment (4449 bp-5066 bp) containing exon 17.2 was subcloned into pBluescript via *Hind*III and *Sac*I sites. Mutations were introduced by site-directed mutagenesis following the protocol of the GeneTailer^{TM} Site-Directed Mutagenesis (Invitrogen). Complementary mutagenesis primers were used to amplify the entire plasmid by polymerase chain reaction (PCR). This was followed by the digestion of the parental wild-type template with *Dpn*I and the direct transformation into

Escherichia coli cells. The mutated plasmids were sequenced to ensure presence of the correct mutations, and then subcloned back into the full-length *Dscam[TM2]* cDNA.

Acute Induction of UAS-transgenes by TARGET system

Larvae carrying two copies of *tubP-GAL80^{ts}* (McGuire et al., 2003) were cultured at the permissive temperature of 18°C beginning at embryo state in order to repress GAL4-mediated transcription. Wandering larvae were shifted to 38°C for 30 min, followed by incubation at the non-permissive temperature of 29°C for two hours.

Immunohistochemical staining

The central nervous systems from wandering third instar larvae were dissected out, fixed and immunostained as previously described (Lee and Luo, 1999). Protein expression was detected by the rabbit anti-GFP Ab (1:300, Molecular Probes) and MB lobes were labeled by the 1D4 mAb (1:80). Immunofluorescent signals were collected by confocal microscopy and then processed using Adobe Photoshop to normalize and exclude the background neurons.

RESULTS

Subcellular localization of GFP-tagged Dscam[TM1] versus Dscam[TM2]

Our previous studies suggested that Dscam[TM1] and Dscam[TM2] have separate functions in dendrites versus axons (Shi et al., 2007). According to constitutive overexpression data, Dscam[TM1] is preferentially localized in dendrites and cell bodies in *Drosophila* MB neurons, while Dscam[TM2] is uniformly distributed in axons, dendrites and cell bodies (Figure 3-1A and B). The inconsistency between the uniform distribution and specific function ofDscam[TM2] in axons raised a question whether

Dscam[TM2] may be preferentially expressed in axons in lower expression situations, which better mimic endogenous protein levels. In order to detect distribution of newly synthesized and low level expressed Dscam molecules, we adopted the TARGET system by incorporation of a temperature-sensitive GAL80 (GAL80ts) as a GAL4 repressor. By controlling the culturing temperature, we were able to "turn off and on" the GAL4-UAS transgene expression and to observe Dscam protein distribution through immunofluorescence staining. Previously, we had shown that the TARGET system worked well in Drosophila mushroom body (MB) neurons (McGuire et al., 2004; Yang et al., 2008). Here we applied the TARGET system to Dscam[TM1]::GFP and Dscam[TM2]::GFP. Interestingly, after acute induction for 1.5 hours, Dscam[TM1] can only be detected in dendrites of MB (Figure 3-1C), and Dscam[TM2] is specifically localized to axons (Figure 3-1D). This result indicated that low level expression of Dscam molecules results in specific transportation of Dscam protein to dendrites or axons depending on which exon 17 is expressed. This differential distribution pattern of Dscam[TM1] and Dscam[TM2] is in keeping with the previous findings of their separate functional roles in dendrites versus axons.

Furthermore, because Dscam[TM1] and Dscam[TM2] can be transported to dendrites and axons respectively, we wondered whether the distribution preference of each would be affected if we coexpressed both in the same neurons. We tagged Dscam[TM1] with RFP, and coexpressed Dscam[TM1]-RFP with Dscam[TM2]-GFP in the same neurons with the TARGET system (Figure 3-1E). Interestingly, within the same neurons, Dscam[TM1] is still targeted to dendrites and Dscam[TM2] is transported to axons separately. This result suggested the existence of a sorting mechanism to separate

newly synthesized Dscam[TM1] and Dscam[TM2] into distinct vesicles which, in turn, are selectively transported to different destinations. Next, to confirm the polarized distribution of Dscam does not result from loss of axons or dendrites, we expressed mCD8-RFP to outline the entire neuron (Figure 3-1F). Coexpression of Dscam[TM1]-GFP with mCD8-RFP showed that Dscam[TM1] was restricted to dendrites while mCD8 was evenly distributed in axons, dendrites and cell bodies. This result indicates that dendritic distribution of Dscam[TM1] is mediated by a selective transport mechanism which may not play any role in the distribution of mCD8 protein. Taken together, these observations provide evidence for the involvement of a sorting and selective targeting mechanism in polarized distribution of Dscam in neurons.

Dscam endodomain is not involved in axonal-dendritic distribution of Dscam

To examine whether the endodomain of Dscam plays a role in its differential distribution, we truncated different lengths of the carboxyl terminal domain of Dscam. Two truncations were generated by deleting the 105 and 342 amino acids from the C-terminal end. Despite increased cell body accumulation of these truncated mutant proteins, these mutant proteins showed no effect on their dendritic or axonal distribution, depending on which exon 17 they carried (Figure 3-2A and B). The accumulation of truncated proteins in the cell bodies remains to be further examined, to determine whether these proteins were retained in ER, Golgi or localized in the cytoplasm. These results indicated that although truncation of the C-terminus of Dscam reduced the ability of Dscam proteins to be exported out of the cell body, it did not affect the polarized distribution of Dscam.

Dscam ectodomain contributes to dendritic targeting of Dscam

To examine whether the ectodomain of Dscam plays a role in its polarized distribution, we swapped the ectodomain of Dscam with the ectodomain of mCD8, which is used as a membrane marker without a distribution preference in *Drosophila* neurons (Lee et al., 1999; Yang et al., 2008). We generated two chimeric constructs, *mCD8[TM1]::GFP* (Figure 3-2C) and *mCD8[TM2]::GFP* (Figure 3-2D). Both chimeric proteins exhibited more cell body accumulation than Dscam[TM1]::GFP and Dscam[TM2]::GFP. However, outside the cell body regions, mCD8[TM1]::GFP was distributed evenly throughout the entire MB neuron including axons and dendrites; while mCD8[TM2]::GFP was still preferentially targeted to axons. Comparing the distribution patterns of mCD8[TM1]:: GFP and Dscam[TM1]-GFP raised the possibility that the Dscam ectodomain may carry a dendritic targeting motif. On the other hand, the axonal distribution pattern of mCD8[TM2]::GFP indicated that the Dscam ectodomain may not be involved in the axonal targeting of Dscam.

To confirm that the ectodomain of Dscam encodes a dendritic targeting motif, we replaced the ectodomain of mCD8 with the ectodomain of Dscam and generated a chimeric construct, *Dscam-mCD8::GFP* (Figure 3-2E). Intriguingly, Dscam-mCD8::GFP was preferentially transported to dendrites. This result suggested that the ectodomain of Dscam carries a dendritic targeting motif, which is sufficient to direct membrane proteins to neuronal dendrites.

Mapping the targeting motifs in exon17.1 and exon17.2 of Dscam

Because the difference in amino acid sequences between Dscam[TM1] and Dscam[TM2] is the alternative exon 17, we postulated the existence of targeting motifs in exon 17.1 or exon 17.2. Exon 17.1 and 17.2 encode single transmembrane domains and two juxtamembrane segments in extracellular and cytoplasmic regions (Figure 3-3A). The protein sequences of exon 17.1 and exon 17.2 share 80% similarity in their transmembrane domains, 33% similarity in the extracellular juxtamembrane segments and 35% similarity in the cytoplasmic juxtamembrane segments. To identify the targeting motifs in exons 17, we swapped the counterparts of juxtamembrane portions between exon 17.1 and exon 17.2 and expressed in MB neurons (Figure 3-3A). Intriguingly, the chimeric proteins Dscam[17.1/17.2] (Figure 3-3B) and Dscam[17.2/17.1] (Figure 3-3C) exchanged their distribution preferences. The chimeric protein with the cytoplasmic juxtamembrane segment from exon 17.2 and the remaining parts from exon 17.1 was transported to axons, while the chimeric protein carrying the cytoplasmic juxtamembrane segment from exon 17.1 and the remaining parts from exon 17.2 was targeted to dendrites. These results indicated that the cytoplasmic juxtamembrane portions of exons 17 are important in the polarized distribution of Dscam[TM1] and Dscam[TM2].

In comparison between the juxtamembrane domains of 17.1 and 17.2 (Figure 3-3A), we found that there was an additional RRRADDMR segment in 17.2, which is absent from 17.1. To determine which amino acids in this region are involved in axonal targeting of Dscam[TM2], we conducted site-directed(scanning) alanine mutagenesis. Several mutants were generated and their protein distribution was examined with transient induction, including 17.2[AAAADDMR] (3-3D), 17.2[RRAAAAA] (3-3E), 17.2[RARADDMR] (3-3F), 17.2[RRAADDMR] (3-3G), 17.2[RRRAAAMR] (3-3H),

17.2[AAAAADMR] (3-3I). Taken together, we found that the second Arginine (1650aa) and the second Aspartate (1654aa) are essential for axonal targeting of Dscam[TM2]. Mutations of either one to alanine caused partial mislocalization of Dscam[TM2] to dendrites.

DISCUSSION

Neurons are one of the most highly polarized cell types. Polarized distribution of distinct cell surface molecules in different compartments underlies most aspects of their physiological functions. The molecular bases for differential sorting and trafficking of these membrane proteins are still being uncovered. Most of our current understanding about sorting and trafficking mechanisms comes from studying Madin-Darby Canine Kidney (MDCK) epithelial cells. It is evident that some of the signals and the machinery involved in polarized distribution are conserved between epithelial cells and neurons (Dotti and Simons, 1990), but cell-type specific mechanisms have also been described (Silverman et al., 2005). Similarities between dendritic targeting in neurons and basolateral targeting in epithelial cells have been suggested by experiments (Matter et al., 1994; Odorizzi and Trobridge, 1997; West et al, 1997). However, sorting to the apical and axonal compartments is less well understood.

Recent studies confirmed that peptide motifs mediate polarized targeting of membrane proteins in neurons (reviewed by Arnold, 2007). Several dendritic and axonal targeting motifs have been identified. For instance, a dileucine-containing motif in potassium channel Kv4.2 and tyrosine-based motifs found in neuroligin-1, transferrin receptor and nicotinic acetylcholine receptors have been shown to mediate dendritic

targeting (Rivera et al., 2003; West et al., 1997; Silverman et al., 2005; Xu et al., 2006). In addition, a dileucine-containing motif of $Na_v1.2$, a leucine-cotaining motif in nicotinic acetylcholine receptors, a tripeptide RRK in mGluR1b, and a T1 tetramerization domain in Kv1 have been determined to act as axonal targeting signals (Garrido et al., 2001; Gu et al., 2003; Rivera et al., 2005; Xu et al., 2006). It is well documented that both dendritic and axonal proteins rely on short amino acid sequences within their cytoplasmic tails for polarized sorting. In our results, the dendritic targeting motif of Dscam is located in the ectodomain. How could a motif in an ectodomain be recognized by the sorting machinery while it is embedded inside a vesicle? One possibility is that Dscam interacts with another protein through its ectodomain to achieve its dendritic sorting. A similar phenomenon can be observed for axonal targeting of Kv1, which depends on another protein, Kvβ, that interacts with Kv1 through its T1 domain. In addition, the axonal targeting motif of Dscam located in the cytoplasmic juxtamembrane domain of TM2 bears no similarity to other identified axonal targeting motifs. This suggests that the axonal targeting of Dscam[TM2] could be mediated by novel targeting mechanisms. To define the targeting mechanisms of Dscam, the identification of proteins that bind to targeting motifs will make it possible to determine whether other polarized proteins share a common targeting mechanism.

Polarized distribution of exogenous proteins has been shown in *Drosophila* neurons (Rolls et al., 2007). However, one difficulty in analyzing the distribution of tagged exogenous proteins in *Drosophila* neurons is the loss of localization when the expression level is much higher than the endogenous level. To reduce the expression level of exogenous proteins, Rolls *et al.*, used different approaches including raising

larvae at 18℃, reducing the number of UAS sequences from five to two, and using certain lowly expressed GAL4 lines. In our study, we incorporated the TARGET system to detect the polarized distribution of newly synthesized proteins at very low expression levels. In the constitutively overexpressed situation, Dscam[TM1]::GFP was localized to dendrites and cell bodies of MB neurons while Dscam[TM2]::GFP was distributed throughout the entire neurons. In the acute induction with the TARGET system, newly synthesized Dscam[TM1] was only detected in dendrites, and Dscam[TM2] was localized to axons. This result demonstrated that TARGET will be a powerful system to study the polarized distribution of exogenous proteins *in vivo*.

Through TARGET, we identified an axonal targeting motif of Dscam and showed that two residues (1650Arg and 1654Asp) are involved in axonal targeting. Furthermore, we suggest a polarized sorting and targeting mechanism exists in MB neurons because Dscam[TM1] and Dscam[TM2] were targeted to dendrites and axons separately when coexpressed in the same neurons simultaneously. It would be interesting to conduct a genetic screen in MB neurons to identify mutants which disrupt the polarized distribution of Dscam. Through this, we can further elucidate how neurons create and maintain the complex expression patterns of polarized proteins.

Taken together, this study provides four important new findings: (1) dendritic targeting of Dscam relies on its ectodomain; (2) an axonal targeting motif of Dscam is located in the cytoplasmic juxtamembrane region of TM2, which is dominant over the dendritic targeting motif; (3) a polarized sorting mechanism exists in Drosophila MB neurons; and (4) TARGET is a good system to study polarized targeting mechanisms of proteins *in vivo*.

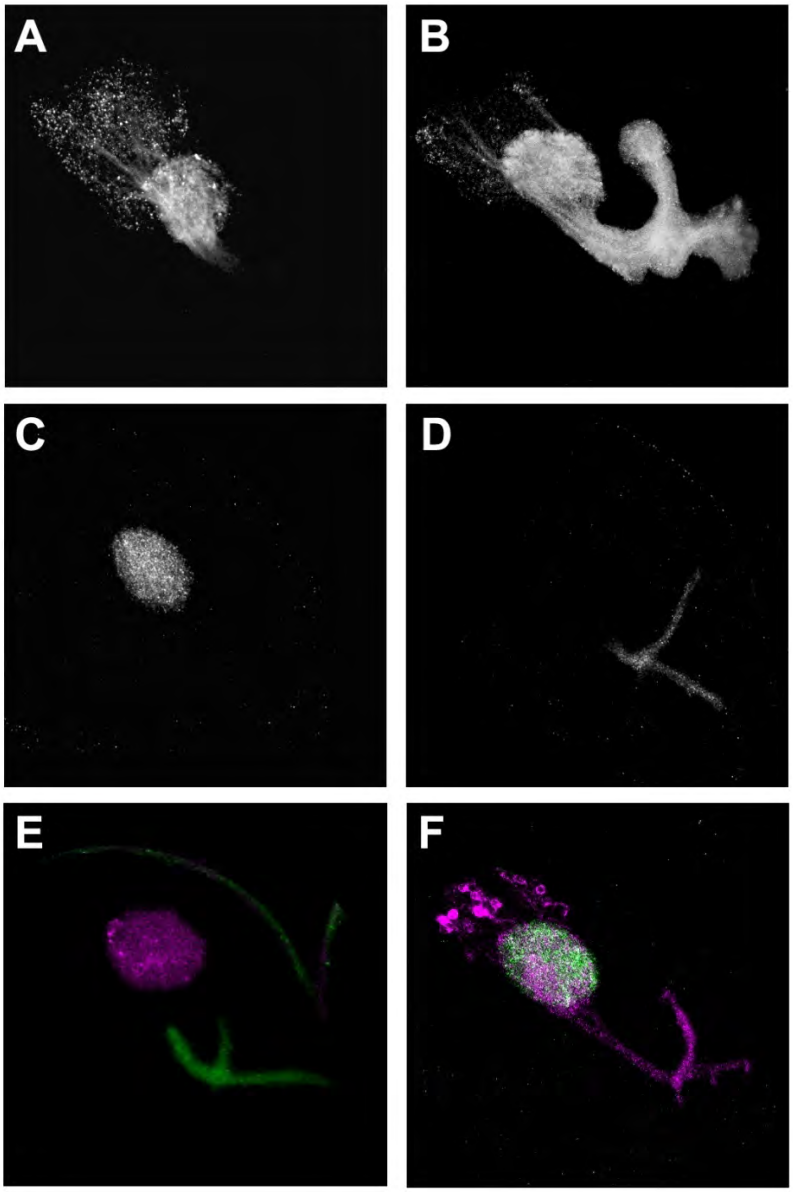

Figure 3-1. Polarized distribution of Dscam[TM1] and Dscam[TM2] in *Drosophila* MB neurons.
(A-B) Constitutive overexpression of Dscam[TM1]::GFP (A) and Dscam[TM2]::GFP (B) with GAL4-OK107.
(C-D) Transient induction of Dscam[TM1]::GFP (C) and Dscam[TM2]::GFP (D) with GaL4-OK107 using the TARGET system. In contrast to constitutive overexpression results, Dscam[TM1] was specifically targeted to dendrites and Dscam[TM2] was only detected in axons.
(E) Transient induction of both Dscam[TM1]::RFP and Dscam[TM1]::GFP in the same MB neurons. Coexpression of Dscam[TM1] and Dscam[TM2] did not interfere with their individual polarized targeting.
(F) Transient induction of both Dscam[TM1]::GFP and mCD8::RFP in the same MB neurons. mCD8 showed no distribution preference.

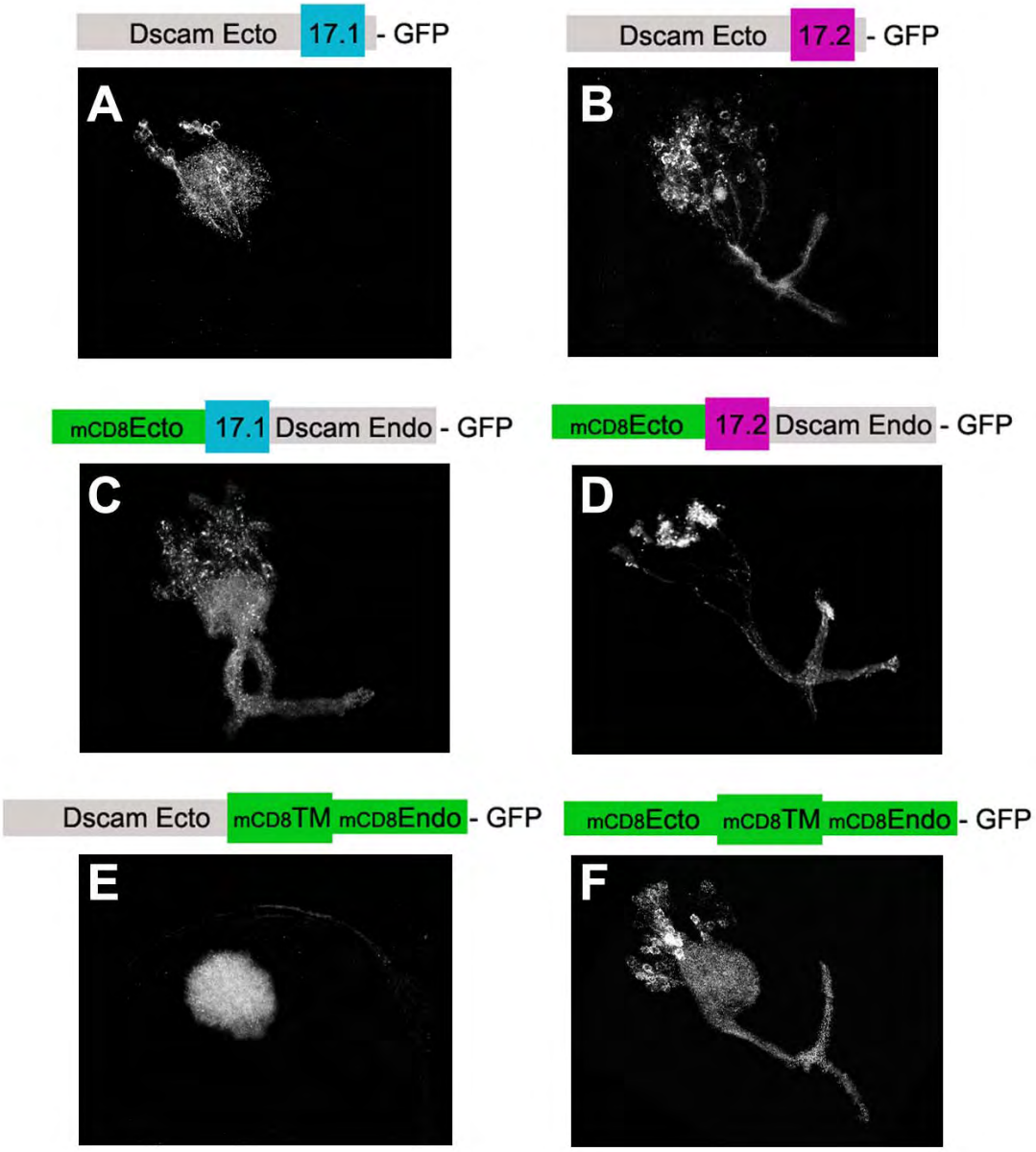

Figure 3-2. Dscam ectodomain carries a dendritic targeting signal.
(A-B) Transient induction of cytoplasmic truncation mutants of *Dscam[TM1]Δ::GFP* (A) and *Dscam[TM2]Δ::GFP* (B). Deletion of Dscam endodomain did not affect the polarized distribution patterns between dendrites and axons. Instead, truncation resulted in more accumulation in cell bodies.
(C-D) Transient induction of chimeric transgenes *mCD8[TM1]::GFP* (C) and *mCD8[TM2]::GFP* (D). mCD8[TM1] was distributed uniformly in MB neurons. mCD8[TM2] was localized in axons and cell bodies, but less in dendrities.
(E) Transient induction of chimeric transgene *Dscam-mCD8::GFP*. Dscam ectodomain carries a dendritic targeting signal which is sufficient to localize the chimeric protein to dendrites only.
(F) Transient induction of *mCD8::GFP*.

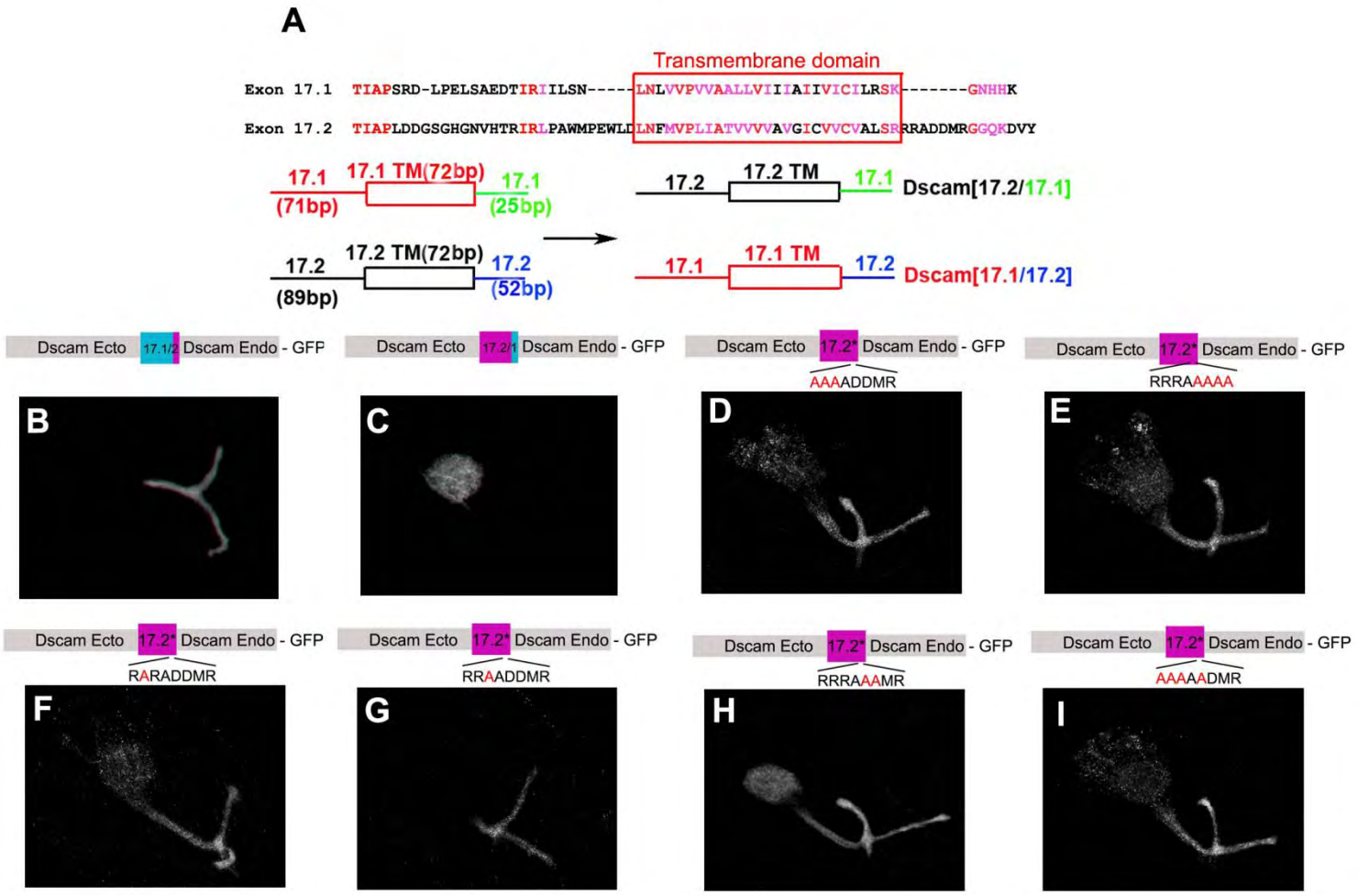

Figure 3-3. An axonal targeting motif of Dscam is located in the cytoplasmic juxtamembrane portion of TM2

(A) A diagram shows the amino acid sequences of TM1 and TM2. Swapping the cytoplasmic juxtamembrane portions between TM1 and TM2 generates two chimeric TM constructs: *Dscam[17.2/17.1]::GFP* and *Dscam[17.1/17.2]:GFP*.

(B-C) Transient induction of *Dscam[17.1/17.2]::GFP* (B) and *Dscam[17.2/17.1]::GFP* (C). After swapping the cytoplasmic juxtamembrane portions, the polarized distribution patterns were exchanged.

(D-I) Site-directed mutagenesis was used to mutate different amino acids in the axonal targeting motif to alanines. Transient induction of these mutant Dscam[TM2]::GFP constructs: 17.2[AAAADDMR] (D), 17.2[RRRAAAAA] (E), 17.2[RARADDMR] (F), 17.2[RRAADDMR] (G), 17.2[RRRAAAMR] (H) and 17.2[AAAAADMR] (I). Mutated amino acids are colored in red in the diagram and underlined in the legend.

Chapter 4

Specific *Drosophila* Dscam juxtamembrane variants control dendritic elaboration and axonal arborization

The following work is reprinted from the Journal of Neuroscience article of the same name published as:

Lei Shi*, Hung-Hsiang Yu*, Jacob Shun-Jen Yang* and Tzumin Lee. J. Neurosci, 20 June 2007: Vol. 27. No.25, pp. 6723-6728.

*These authors contributed equally to this study

ABSTRACT

Drosophila Dscam isoforms are derived from two alternative transmembrane/juxtamembrane domains (TMs) in addition to thousands of ectodomain variants. Using a microRNA-based RNA interference technology, we selectively knocked down different subsets of Dscams containing either the exon 17.1- or exon 17.2-encoding TM. Eliminating Dscam[TM1] reduced Dscam expression but minimally affected postembryonic axonal morphogenesis. In contrast, depleting Dscam[TM2] blocked axon arborization. Further removal of Dscam[TM1] enhanced the loss-of-Dscam[TM2] axonal phenotypes. However, Dscam[TM1] primarily regulates dendritic development, as evidenced by the observations that removing Dscam[TM1] alone impeded elaboration of dendrites and that transgenic Dscam[TM1], but not Dscam[TM2], effectively rescued *Dscam* mutant dendritic phenotypes in mosaic organisms. These distinct Dscam functions can be attributed to the juxtamembrane regions of TMs that govern dendritic versus axonal targeting of Dscam as well. Together, we suggest that specific *Drosophila* Dscam juxtamembrane variants control dendritic elaboration and axonal arborization.

INTRODUCTION

The insect *Dscam* gene encodes thousands of distinct immunoglobulin/fibronectin-type cell adhesion molecules that mainly differ in their extracellular domain and can carry one of the two well-conserved transmembrane/juxtamembrane segments (TMs) (Schmucker et al., 2000). The variations in the ectodomain have drastic impacts on the inter-Dscam binding *in vitro* (Wojtowicz et al., 2004), whereas distinct TMs may target Dscam to different subcellular compartments (Wang et al., 2004; Zhan et al., 2004).

Such a huge repertoire of diverse homophilic cell adhesion molecules may help govern how a complex nervous system is specifically wired.

In *Drosophila*, Dscam is widely required for proper neuronal morphogenesis, especially the bifurcation/arborization of neurites. Interestingly, loss of Dscam function affects neurite trajectories selectively at the loci where bifurcation normally occurs (Wang et al., 2002; Chen et al., 2006). Some *Dscam* mutant neurites stall with clumps of possibly numerous short branches at the ends, resulting in truncation of axonal trees at their first points of bifurcation. These characteristic phenotypes are probably derived from excessive repetitive bifurcations of mutant growth cones, because others that have fully extended frequently exhibit evidence for additional bifurcations at the normal branching points. In addition, proper guidance of individual growth cones at the points of ramification, especially with respect to their sister growth cones, requires Dscam. It appears that Dscam controls neurite arborization by preventing comigration of sister growth cones, thus preventing the number of sister growth cones from exceeding the number of available fascicles. Dynamic stochastic expression of distinct Dscam ectodomains (Neves et al., 2004) would permit self recognition in such "like-kill-like" morphogenetic processes. Consistent with this model, most Dscam ectodomain exon alternatives are not conserved through evolution, arguing that the overall diversity is more critical than the identities of individual variants (Graveley et al., 2004).

In contrast, the two exon alternatives that encode the TM of Dscam are well conserved (Graveley et al., 2004). Interestingly, ectopic Dscam can be preferentially localized to dendrites by selective utilization of exon 17.1 (encoding TM1) or localized to axons by using exon 17.2 (encoding TM2) (Wang et al., 2004). To determine the roles of

Dscam[TM1] versus Dscam[TM2], we previously created *Dscam*s lacking either exon 17.1 or exon 17.2. Deletion of either exon 17 led to skipping of the other exon 17 in many *Dscam* transcripts (our unpublished results). Manipulating genomic *Dscam* can be problematic for other reasons (see Discussion). We, thus, resorted to a microRNA(miRNA)-based RNA interference (RNAi) technology (Chen et al., 2007) for specifically silencing exon 17.1- or exon 17.2-containing *Dscam* transcripts. We found that endogenous Dscam[TM1] and Dscam[TM2] primarily act to mediate dendritic elaboration and axonal arborization, respectively. Consistent results were obtained with transgenic Dscam alleviating dendrite versus axon phenotypes in *Dscam* mutant clones depending on the nature of its TM. In addition, the cytoplasmic juxtamembrane regions of the TMs are sufficient to control Dscam localization as well as its differential roles in dendrites versus axons. Together, we suggest that Dscams with distinct TMs control dendritic elaboration versus axonal arborization.

MATERAILS AN METHODS

Transgenes

Standard molecular biological techniques were used to generate *UAS-17.1 miRNA*, *UAS-17.2 miRNA*, and *UAS-18 miRNA*, which encode microRNAs carrying unique *Dscam* sequences derived from exon 17.1, exon 17.2, and exon 18, respectively. The complete nucleotide sequences of the microRNA constructs are in the appendix. In addition, the two *UAS-Dscams* with chimeric TMs were constructed by swapping the cytoplasmic juxtamembrane segment of TM1 (amino acid 1631-1648) with the cytoplasmic

juxtamembrane segment of TM2 (amino acid 1645-1661) through the introduction of an *Acc*I site between the transmembrane and cytoplasmic juxtamembrane regions.

Flies

Transgenic flies carrying various *UAS-miRNA* and *UAS-Dscam* with chimeric TM were obtained by P element-mediated germ line transformation with technical support from Genetic Services.

Tissue-specific induction of RNAi and phenotypic analysis by immunohistochemistry

Targeted induction of *UAS-miRNA* involved use of various tissue-specific galactosidase-4 (GAL4) drivers, and their phenotypic analysis mainly involved coexpression of various upstream activation sequence (UAS)-reporter genes. Both flip-out-marked clones of ellipsoid body (EB) neurons and MARCM (mosaic analysis with a repressible cell marker)-labeled clones of projection neurons (PNs) were induced in newly hatched larvae by heat shock for 40 min at 37°C. Whole fly brains were prepared for immunostaining as described previously (Lee et al., 1999). Detection of endogenous Dscam proteins involved a mouse monoclonal antibody (mAb) that was raised against the peptide ATLDKRRPDLRDELG. The anti-Dscam mAb, 1D4 mAb, and anti-mCD8 mAb were used at 1:20, 1:50, and 1:100, respectively. Fluorescence signals were captured with confocal microscopy and processed using Adobe Photoshop (Adobe Systems, San Jose, CA).

RESULTS

microRNA-based RNA interference permits selective depletion of Dscam[TM1] versus Dscam[TM2]

Transgenic *Drosophila* Dscams with distinct TMs are enriched in dendrites or axons (Wang et al., 2004) and, consistent with such differential protein targeting phenomena, potently affect different aspects of neuronal morphogenesis (Wang et al., 2004; Zhan et al., 2004). To determine whether endogenous Dscam with TM1 versus TM2 indeed helps govern different neuronal morphogenetic processes, we examined whether and how targeted depletion of Dscam[TM1] or Dscam[TM2] perturbs distinct aspects of neuronal morphogenesis in intact *Drosophila* brains. We first explored whether one can effectively knock down Dscam[TM1] versus Dscam[TM2] by specifically silencing the *Dscam* transcripts that carry exon 17.1 or exon 17.2 using a miRNA-based RNAi technology (Chen et al., 2007). We engineered three *UAS-miRNA* constructs, *UAS-17.1 miRNA*, *UAS-17.2 miRNA*, and *UAS-18 miRNA*, to specifically target the *Dscam* exon 17.1, exon 17.2, and exon 18 (a common *Dscam* exon), respectively. For each *UAS-miRNA* transgene, we identified the most potent transgenic line from multiple independent transformants by individually assaying its ability to antagonize GAL4-induced coexpression of *UAS-Dscam::GFP* (green fluorescent protein). We resorted to transgenic Dscam::GFP, because direct visualization of Dscam[TM1] versus Dscam[TM2] was not possible without antibodies against different TMs. Pairing transgenic miRNA with Dscam::GFP that carries the miRNA target sequences consistently led to a drastic reduction in the level of Dscam-GFP expression (Figure 4-S1C and F). In contrast, even with the most potent transgenic line, UAS-17.1 miRNA and

UAS-17.2 miRNA exerted no detectable effect on the alternative isoform (Figure 4-S1D and E). It assures no cross-reactivity, also eliminating the trivial explanation that suppression of *Dscam* transgenes might result from the presence of multiple UAS transgenes. These observations provide us with the opportunity to use transgenic miRNA to knock down specific subsets of Dscam isoforms in intact fly brains.

We then examined how a broad induction of various Dscam-targeted miRNAs affects the endogenous Dscam expression in the developing *Drosophila* CNS. We could normally detect abundant Dscam proteins in the larval neuropils by immunostaining with a peptide antibody against some Dscam common motif(s) (Wang et al., 2004) (Figure 4-1A). Interestingly, such Dscam immunoreactivity was differentially abolished after pan-neuronal induction of various miRNA transgenes. First, we were encouraged by the lack of detectable residual Dscam after induction of UAS-18 miRNA (Fig. 4-1B) or coinduction of UAS-17.1 miRNA and UAS-17.2 miRNA (Figure 4-1C), which are both expected to silence all Dscam splice variants. Second, induction of UAS-17.1 miRNA or UAS-17.2 miRNA alone, even in multiple copies, left its overall pattern of expression essentially unchanged (Figure 4-1D and E). Depleting Dscam[TM1] versus Dscam[TM2] should provide insight into the spatial/temporal patterns of TM1 versus TM2 expression. Interestingly, close inspection revealed that Dscam[TM1] apparently exists more abundantly than Dscam[TM2] in the larval CNS, especially within the abdominal ganglion (Figure 4-1, compare D with *E*). Together, these observations demonstrate the general feasibility of knocking down Dscam[TM1] versus Dscam[TM2] using *UAS-17.1 miRNA* or *UAS-17.2 miRNA*. Additionally, both *UAS-18 miRNA* alone and *UAS-17.1*

miRNA plus *UAS-17.2 miRNA* should allow us to determine the *Dscam* "null" phenotypes one can obtain with various GAL4 drivers.

Dscam[TM2], but not Dscam[TM1], plays an essential role in governing axon arborization, probably because of differential protein targeting

To determine the roles of Dscam[TM1] versus Dscam[TM2] in Dscam-dependent axonal morphogenesis, we first examined how expression of specific *Dscam*-targeted miRNAs affects the morphogenesis of mushroom body (MB) axons. Transgenic miRNA was induced through MB development using *GAL4-OK107*. We selectively focused on its effects on the orthogonal and ß lobes, because they are normally derived via Dscam-governed axon bifurcation, and one can readily identify the MB /ß axons based on their strong immunoreactivity with the 1D4 monoclonal antibody (Wang et al., 2002). Interestingly, induction of *UAS-18 miRNA* or *UAS-17.2 miRNA* alone, but not *UAS-17.1 miRNA*, drastically disrupted the formation of /ß lobes (Figure 4-2). Abnormal /ß lobes were often misshapen and variably truncated (Figure 4-2B–E), reminiscent of the deformed MBs in *Dscam* mutant organisms (Wang et al., 2004). This suggests involvement of Dscam[TM2], but not Dscam[TM1], in MB axonal morphogenesis. We further classified the anomalies based on the presence or absence of any /ß lobe residue and its degree of extension (severe, no /ß neurite extended beyond the peduncle terminus; strong, no neurite reached the tips of /ß lobes; medium, small subsets of /ß neurites were fully extended; weak, grossly intact lobes failed to segregate). Quantitative analysis of the above phenotypes ($n > 100$, each) revealed that *UAS-17.2 miRNA* alone did not cause as much of a defect as *UAS-18 miRNA* (Figure 4-2I) (5.0 ± 2.0 vs $52.7 \pm 4.5\%$ for the severe

phenotype). This is apparently a result of the possibility that endogenous Dscam[TM1] could partially compensate for the loss of Dscam[TM2] in the Dscam-governed bifurcation of MB axons, because doubling the dosage of *UAS-17.2 miRNA* did not enhance the phenotypes (8.7 ± 2.5%), but coinduction of *UAS-17.1 miRNA* and *UAS-17.2 miRNA* fully recapitulated the 18 miRNA-derived null phenotypes (59.0 ± 6.0%) (Figure 4-2I). Together, these results provide direct evidence for differential involvement of Dscam[TM1] and Dscam[TM2] in supporting neuronal morphogenesis.

Preferential usage of exon 17.2 over exon 17.1 might explain why Dscam[TM2] plays a dominant role in this particular developmental event. To rule out this possibility, we attempted to rescue the 18 miRNA-derived null phenotypes by supplementing transgenic Dscam[TM1] or Dscam[TM2]. We reasoned that both *Dscam* transgenes carry wild-type exon 18 and should be suppressed by 18 miRNA to an analogous degree, if they were comparably induced. Additionally, their ability to antagonize silencing of endogenous *Dscam* by 18 miRNA should be identical. Thus, any difference in their rescue of 18 miRNA-derived loss-of-Dscam phenotypes can be ascribed to the presence of TM1 or TM2 in the comparably residual transgenic Dscam. We previously identified UAS-Dscam::GFPs that exhibit similar levels of induction (Wang et al., 2004). Using these lines, we obtained substantially better rescue after coinduction of UAS-18 miRNA with UAS-Dscam[exon 17.2]::GFP than with UAS-Dscam[exon 17.1]::GFP (Figure 4-2I) (38.0 ± 1.8 vs 6.9 ± 0.4% for the weak plus normal phenotypes). This supports the notion that Dscam[TM2] and Dscam[TM1], which differ only in the TMs, are functionally distinct. To locate the structural basis for such a functional distinction between

Dscam[TM1] and Dscam[TM2], we conducted structural-functional analysis and generated two chimeric TMs by swapping the cytoplasmic juxtamembrane portions between TM1 and TM2 (Figure 4-2F). Interestingly, this exchange reversed the functional distinction (Figure 4-2I) (rescued to 69.0 ± 3.0% with 17.1/17.2 vs 7.3 ± 2.4% with 17.2/17.1) as well as their differential protein targeting between Dscam[TM1] and Dscam[TM2] (Figure 4-2G and H). These results suggest that the cytoplasmic juxtamembrane domains of Dscam govern its TM-dependent differential subcellular localization and further imply that, probably because of differential targeting, TM2-containing Dscam isoforms function primarily in axons, whereas TM1-containing Dscams possibly act in dendrites within neurons.

To examine whether Dscam[TM2], but not Dscam[TM1], is broadly used to mediate diverse axonal morphogenesis, we further investigated whether and how knocking down Dscam[TM1] or Dscam[TM2] levels affects the morphogenesis of EB neurons. We reported previously that Dscam-dependent proper arborization of axons is also required for full elaboration of EB neurites in the centrally placed EB neuropil (Wang et al., 2002). Interestingly, after separate induction of *UAS-17.1 miRNA* and *UAS-17.2 miRNA* using *asense-GAL4* (Zhu et al., 2006b) plus *GAL4-EB1* (Wang et al., 2002), only *UAS-17.2 miRNA* could phenocopy the morphogenetic defects characteristic of Dscam mutant EB neurons (Figure 4-S2A–D) (100%; $n = 10$, each). This observation again supports the notion that Dscam[TM2], but not Dscam[TM1], plays an essential role in governing diverse axonal morphogenetic processes, and, as addressed above, this difference in function is probably derived from differential protein targeting.

Dscam[TM1] is involved primarily in dendritic elaboration

Transgenic Dscam[TM1]::GFP is selectively enriched in dendrites in diverse model neurons, including the antennal lobe (AL) PNs (Wang et al., 2004). To determine whether Dscam[TM1] is preferentially involved in dendritic morphogenesis, we resorted to PNs for additional analysis of the TM-dependent distinct Dscam morphogenetic functions. In contrast with MB and EB neurons where Dscam appears dispensable for dendritic morphogenesis (Wang et al., 2002), the PNs, especially the ventral lineage-derived multiglomeruli-targeting PNs (in the vPN clones), require Dscam for full elaboration of their dendrites in the ALs in addition to proper arborization of their axons in the lateral horns (LHs) (Zhu et al., 2006a).

We first demonstrated that *GAL4-GH146*-dependent induction of *UAS-18 miRNA* in the otherwise wild-type vPN neuroblast (Nb) clones potently suppressed the elaboration of MARCM-labeled dendrites in the ALs and disrupted their axonal arborization in the LHs (Figure 4-3D, H and L) (100%; n = 10). The dendrites of multiglomeruli-targeting PNs became aberrantly restricted to the AL medial upper portion where the axon passage resides (Figure 4-3H, arrow). In the LHs, their axonal branches failed to extend away from one another and often stalled with abnormal aggregates (Figure 4-3L, arrow). In addition, the projection out of the LH (Figure 4-3I and J, arrowheads) is essentially missing. These morphogenetic defects are analogous to the previously documented Dscam loss-of-function PN phenotypes (Zhu et al., 2006a). We then wondered whether depleting Dscam[TM1] versus Dscam[TM2] in the same neurons might differentially affect the morphogenesis of their dendrites versus axons. UAS-17.1 miRNA and UAS-17.2 miRNA were separately induced by GAL4-GH146 in

the vPN Nb clones. Remarkably, the loss-of-Dscam dendritic and axonal phenotypes were uncoupled and well correlated with the protein targeting phenomena. Induction of UAS-17.1 miRNA alone effectively suppressed PN dendritic elaboration but minimally affected their axonal arborization (Figure 4-3B, F and J) (100%; n = 9). In contrast, induction of UAS-17.2 miRNA alone selectively disrupted the arborization of PN axons in the LHs (Figure 4-3C, G and K) (100%; n = 15). We further quantified dendrite phenotypes by counting the glomeruli that became not innervated by GAL4-*GH146*-positive PNs in the above vPN Nb clones. Given the presence of several *GAL4-GH146*-positive pan-glomerular PNs in the vPN lineage, there is normally no glomerulus where we could not detect any vPN-lineage-derived *GAL4-GH146*-labeled neurites. Such vPN dendrites were also fully elaborated after depletion of endogenous Dscam[TM2], as revealed by no *GAL4-GH146*-unlabeled glomerulus despite induction of 17.2 miRNA. In contrast, depleting endogenous Dscam[TM1] with 17.1 miRNA made a significant and comparable number of AL glomeruli devoid of MARCM-labeled vPN dendrites as knocking down all Dscam isoforms by 18 miRNA (17.1, 10.86 ± 0.69 vs 18, 11.00 ± 0.82). These results collectively suggest that differential protein targeting of Dscam[TM1] and Dscam[TM2], respectively, controls dendritic elaboration and axonal arborization.

Consistent with this notion, single-ectodomain transgenic Dscam significantly rescued certain *Dscam* mutant phenotypes in dendrites versus axons, depending on the presence of TM1 or TM2. Briefly, using two distinct *Dscam* transgenes that differ only in their exon 17, we had shown previously that transgenic Dscam[TM2], but not

Dscam[TM1], could effectively rescue various axonal morphogenetic defects in single-cell clones of *Dscam* mutant MB neurons (Wang et al., 2004). Interestingly, when the same pair of *Dscam* transgenes were respectively examined for its effects on *Dscam* mutant DL-1 PNs, we found that PN dendrite defects were rescued only by transgenic Dscam[TM1], whereas only transgenic Dscam[TM2] partially rescued PN bouton formation in the MB calyces (Figure 4-4). This provides RNAi-independent evidence for involvement of Dscam[TM1] and Dscam[TM2] in the morphogenesis of dendrites and axons, respectively.

DISCUSSION

Our use of an miRNA-based RNAi technology permits depletion of distinct subsets of Dscam isoforms based on their exon compositions. Reducing TM1-containing (encoded by exon 17.1) versus TM2-containing (encoded by exon 17.2) Dscams during morphogenesis of various model neurons allowed us to demonstrate that Dscam[TM1] and Dscam[TM2] are preferentially involved in dendritic elaboration and axonal arborization, respectively. This differential involvement of distinct Dscams is likely a result of differential protein targeting, because they are specified by similar cytoplasmic juxtamembrane portions of the *Dscam* exon 17-encoding TMs. However, after strong binary induction, transgenic Dscam[TM2] can exist abundantly in both dendrites and axons, whereas Dscam[TM1] remains primarily restricted to dendrites, although Dscam[TM1] exhibits more broad function than Dscam[TM2]. Knocking down both further impeded MB axons (Figure 4-2I), whereas eliminating exon 17.1-containing Dscam was equally potent as silencing all *Dscam* transcripts in the inhibition of PN

dendrites (Figure 4-3). These discrepancies suggest targeting-independent functional distinction between Dscam[TM1] and Dscam[TM2].

Despite some recently raised concerns on the specificity of RNAi-mediated gene silencing (Ma et al., 2006), we are confident in this study for several reasons. First, it should be more straightforward to obviate potential off-target effects with the microRNA-based RNAi constructs, because each of them only yields two 22-nucleotide-long double-stranded RNAs. Second, we generated an independent miRNA-based RNAi construct against a common *Dscam* exon in addition to the ones targeting exon 17.1 versus exon 17.2 and have obtained the expected results after analogous induction of RNAi against these discrete *Dscam* sequences. Third, the specificity and effectiveness of our RNAi was also confirmed by direct visualization of specific Dscam proteins *in vivo*. Fourth, all of our RNAi-induced phenotypes were comparable both qualitatively and quantitatively to previously known *Dscam* loss-of-function phenotypes. Fifth, we could also rescue the RNAi-mediated silencing of *Dscam* using appropriate *Dscam* transgenes. In addition, our demonstration that endogenous Dscam mediates dendritic versus axonal morphogenesis depending on the presence of TM1 or TM2 has been implicated by multiple independent lines of research. In particular, whereas transgenic Dscam with TM2 consistently rescues of *Dscam* mutant axons, Dscam[TM1] is much more potent than Dscam[TM2] in the rescue of *Dscam* mutant dendrite elaboration.

Alternative methods for knocking out subsets of isoforms mainly involve deletion of specific exon alternatives at the genomic level. In theory, by gene targeting (Gong and Golic, 2003), one can modify a genomic *Dscam* to carry only exon 17.1 or exon 17.2 in *Drosophila*. But such genomic manipulation is potentially problematic. Assuming simple

gene targeting does not alter the levels of Dscam expression, elimination of subsets of isoforms could inevitably lead to expression of other isoforms in much broader patterns and/or at higher levels than the normal unperturbed conditions. This may attenuate the defects resulting from the loss of specific isoforms and/or elicit additional phenotypes because of ectopic expression of the residual isoforms, further complicating interpretation. In contrast, knocking down various subsets of Dscam isoforms at the level of translation (e.g., by microRNA) should deplete the isoforms of interest without affecting the expression of others. This way, one can potentially map the endogenous patterns of expression for various specific subsets of Dscam isoforms and, more importantly, unequivocally determine the contributions made by given subsets of Dscam isoforms to various neural developments. In the case of Dscam[TM1] versus Dscam[TM2], we found that, although the relative abundance might differ at various developmental stages, they are apparently coexpressed in most cells. The coexpression with differential requirements implies that they are functionally distinct. Dscam[TM1] selectively concentrates in dendritic growth cones, whereas Dscam[TM2] is preferentially located to axonal growth cones. Nevertheless, we could not observe their differential targeting after depletion of one versus the other, because most neuropils are made up of both dendrites and axons. We also recently learned that retrograde transport plays an essential role in the dendritic enrichment of Dscam[TM1] (our unpublished results), potentially explaining why both Dscam[TM1] and Dscam[TM2] could be detected in the cores of larval MB peduncles where newly derived MB axons are selectively fasciculated (our unpublished observation). Finally, compared with the constitutive changes associated with gene targeting, GAL4/UAS-mediated targeted induction of RNAi permits more

varied control over when and/or where to knock down the isoforms of interest and should better illustrate the stage- as well as tissue-specific isoform-characteristic functions.

Together, our results indicate Dscams with distinct TMs are differentially involved in morphogenesis of dendrites versus axons, most likely because of differential protein targeting. What might be the advantages for having two exon alternatives to specify where a Dscam protein should be located? One possible advantage is the ability to independently control the Dscam repertoire at dendrite and axon within a single neuron. For instance, coupling different ectodomains with TM1 would permit selective enrichment of Dscams with distinct homophilic binding specificities in the dendrites but not axons. Additionally, for a given ectodomain, varying the ratio of TM1/TM2 could simultaneously alter the amounts of dendritic and axonal Dscams. Given that dendrites and axons of the same neurons often acquire different morphological characteristic features, it would be interesting to determine whether the TM1/TM2-governed differential distribution of Dscam directly underlies some aspects of the differential morphogenesis of dendrites versus axons.

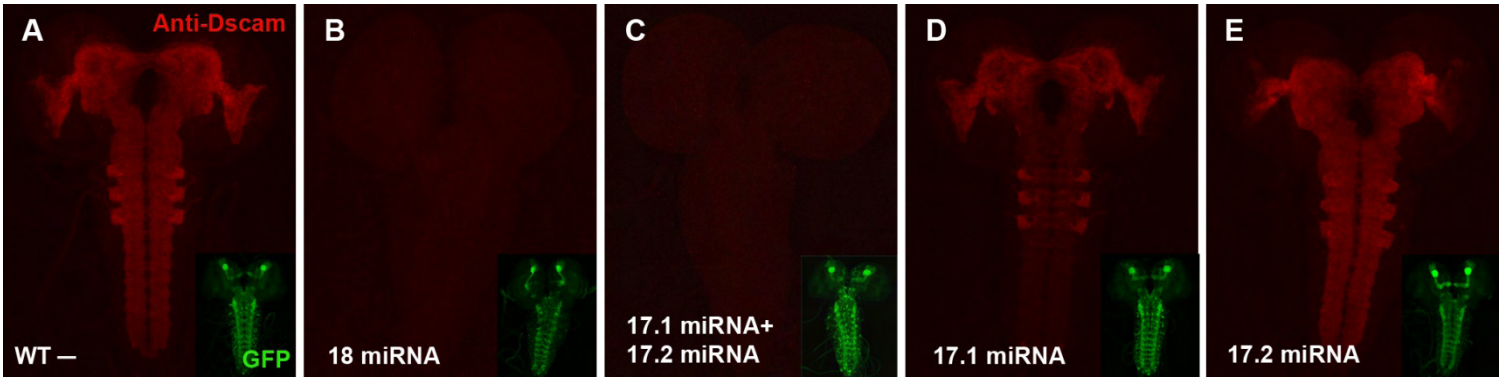

Figure 4-1. Silencing of endogenous Dscam expression by various transgenic miRNAs.

Composite confocal images of wandering larvae CNS showing endogenous Dscam expression (magenta; as revealed by immunostaining with an anti-Dscam exon 18 peptide mAb), in wild-type (WT) and after asense-GAL4/GAL4-C155-dependent induction of various anti-Dscam miRNAs (B–E). (A) Wild-type control. Note that UAS-18 miRNA alone (B) or only UAS-17.1 miRNA plus UAS-17.2 miRNA (C) could effectively eliminate the entire Dscam expression. In addition, regardless of the levels of Dscam, major neural structures, as revealed by coinduction of UAS-mCD8::GFP (green), remained comparable (insets). Scale bar: (here and in all figures) 20 μm.

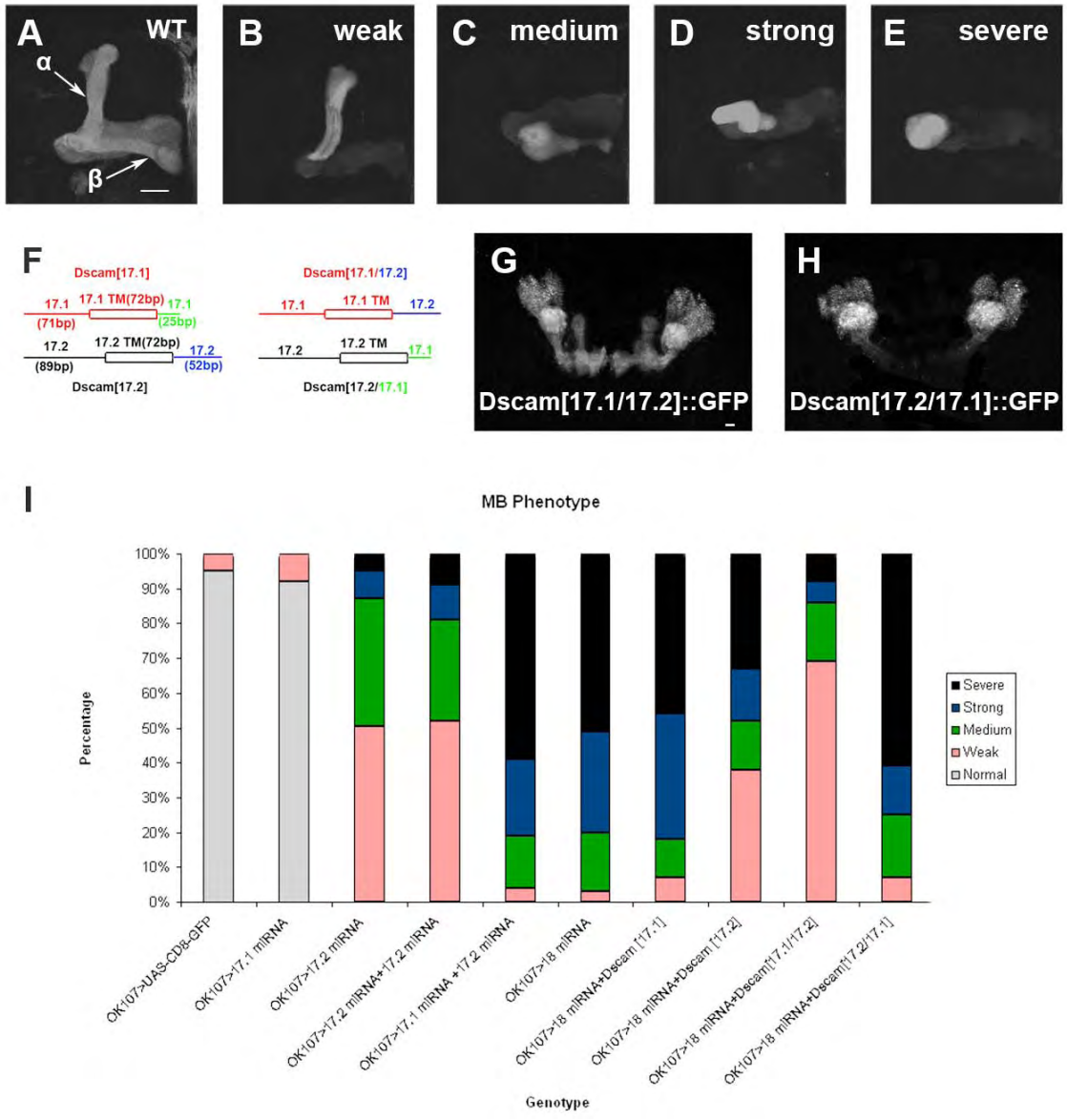

Figure 4-2. Dscam[TM2], but not Dscam[TM1], plays an essential role in MB axonal morphogenesis

(A-E) Adult MB lobes visualized by 1D4 mAb. Compared with the wild type (A), induction of certain anti-Dscam miRNAs (see I) disrupted the formation of MB lobes to various extents (B-E). (F-H) Derivation of two chimeric Dscam TMs (F) and their effects on Dscam::GFP (green) protein targeting. After binary induction with *GAL4-201Y*, Dscam[17.1/17.2]::GFP, like Dscam[TM2]::GFP, is uniformly distributed in the larval MBs (G). In contrast, Dscam[17.2/17.1]::GFP, like Dscam[TM1]::GFP, is enriched in dendrites (H). Additionally, both Dscam[17.1/17.2]::GFP and Dscam[TM2]::GFP are preferentially targeted to axons after suppression of the induction by RNAi (data not shown) (similar to Figure 4-S1F and H).
(I) Quantitative analysis of MB lobe phenotypes, based on the above classification (A-E), after *GAL4-OK107*-dependent induction of various anti-Dscam miRNAs and in the absence or presence of distinct transgenic Dscam::GFP.

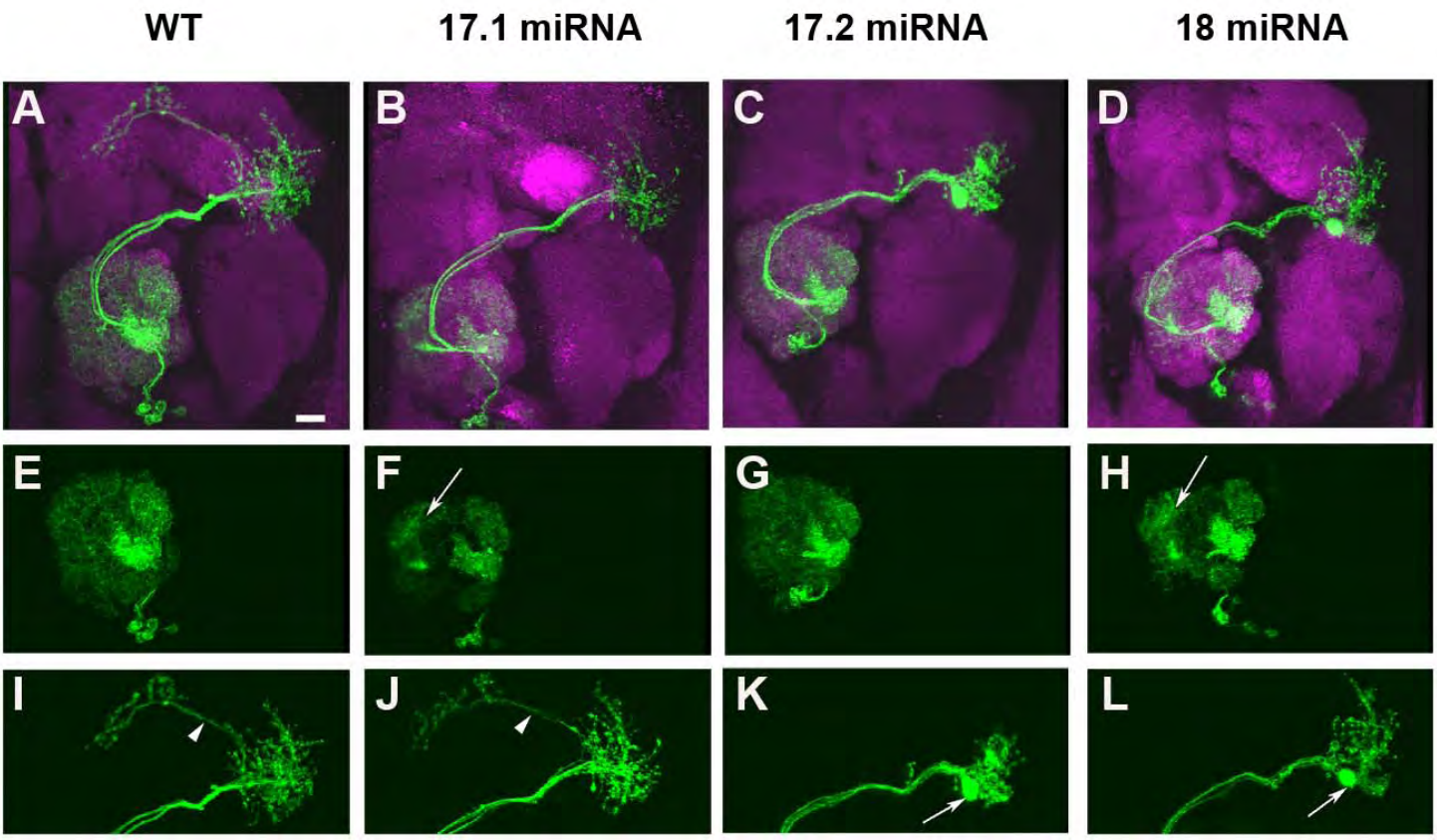

Figure 4-3. Dscam[TM1] and Dscam[TM2] primarily govern dendritic and axonal morphogenesis, respectively

MARCM-labeled adult vPN Nb clones. Compared with the wild-type clone (A, green), induction of 17.1 miRNA, 17.2 miRNA, and 18 miRNA in vPN Nb clones (B–D, green) specifically disrupted dendritic elaboration (F, arrow), axonal arborization (K, arrow), and both (H, L; arrows), respectively. Adult fly brains were counterstained with nc82 mAb (magenta). The cropped images selectively show dendritic elaboration (E–H) or axonal arborization (I–L) of the clones.

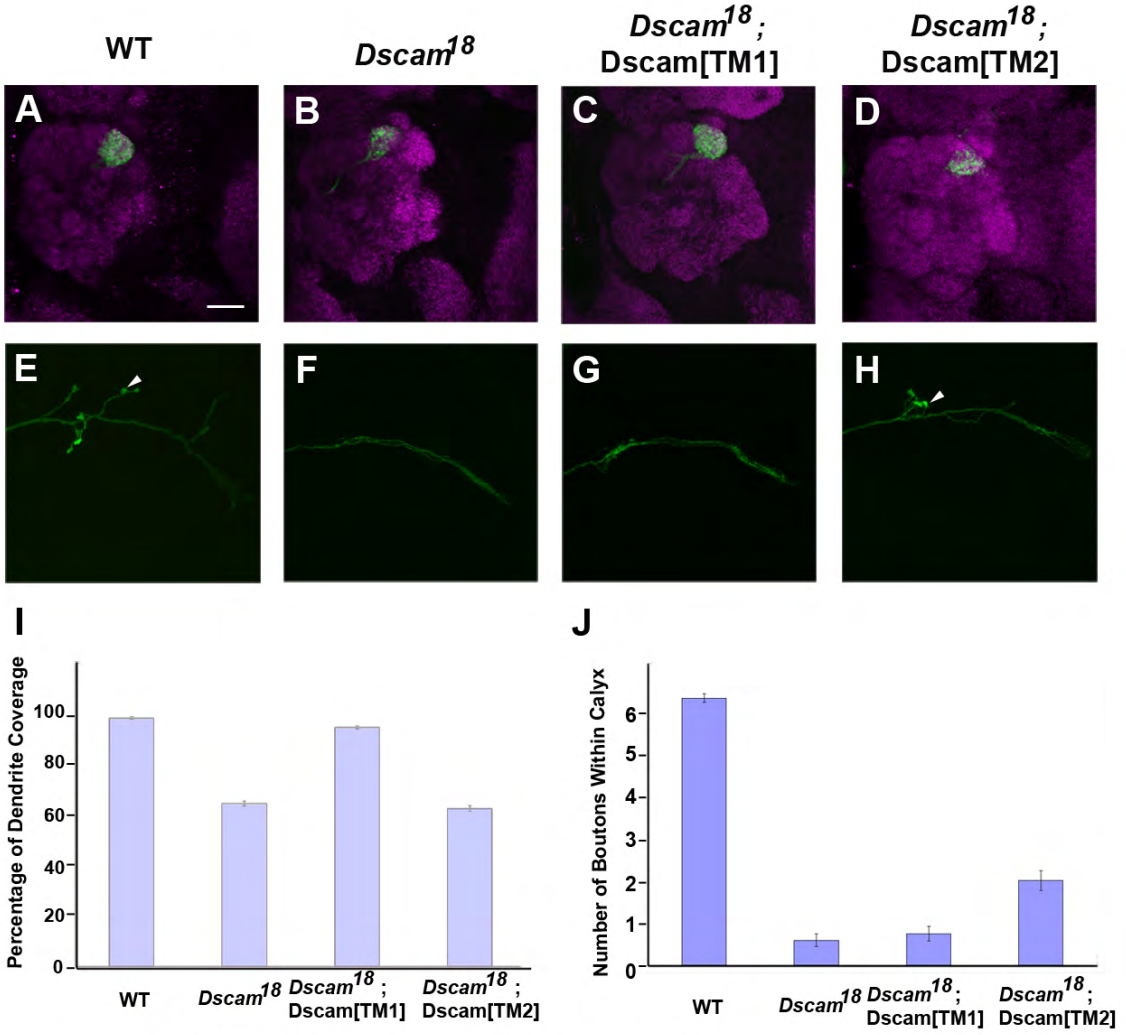

Figure 4-4. Rescue of *Dscam* mutant PN morphogenesis by transgenic Dscam with TM1 versus TM2.

(A-H) Adult single-cell clones of DL-1 PNs (green) of which the dendrite elaboration in the DL-1 glomeruli (as revealed by nc82 immunostaining; magenta) and axon arborization in the MB calyces and the LHs are, respectively, shown in (A-D) and (E-H). (A) and (E), Wild-type clones. (B) and (F), *Dscam* mutant clones. (C) and (G), Rescueof mutant clones with *pDscam-Dscam[3.36.25.1-genomic 18-24]*. (D) and (H), Rescue with *pDscam-Dscam[3.36.25.2-genomic 18-24]*. Note partial coverage of DL-1 glomeruli by the green PN dendrites in (B) and (D) and the absence of bouton-like structures (arrowheads) in (F) and (G).

(I-J) Quantitative analysis of the coverage of DL-1 glomeruli by single-cell PN clones (I) and the numbers of PN-derived bouton-like structures in the MB calyces (J). n=25 in every condition.

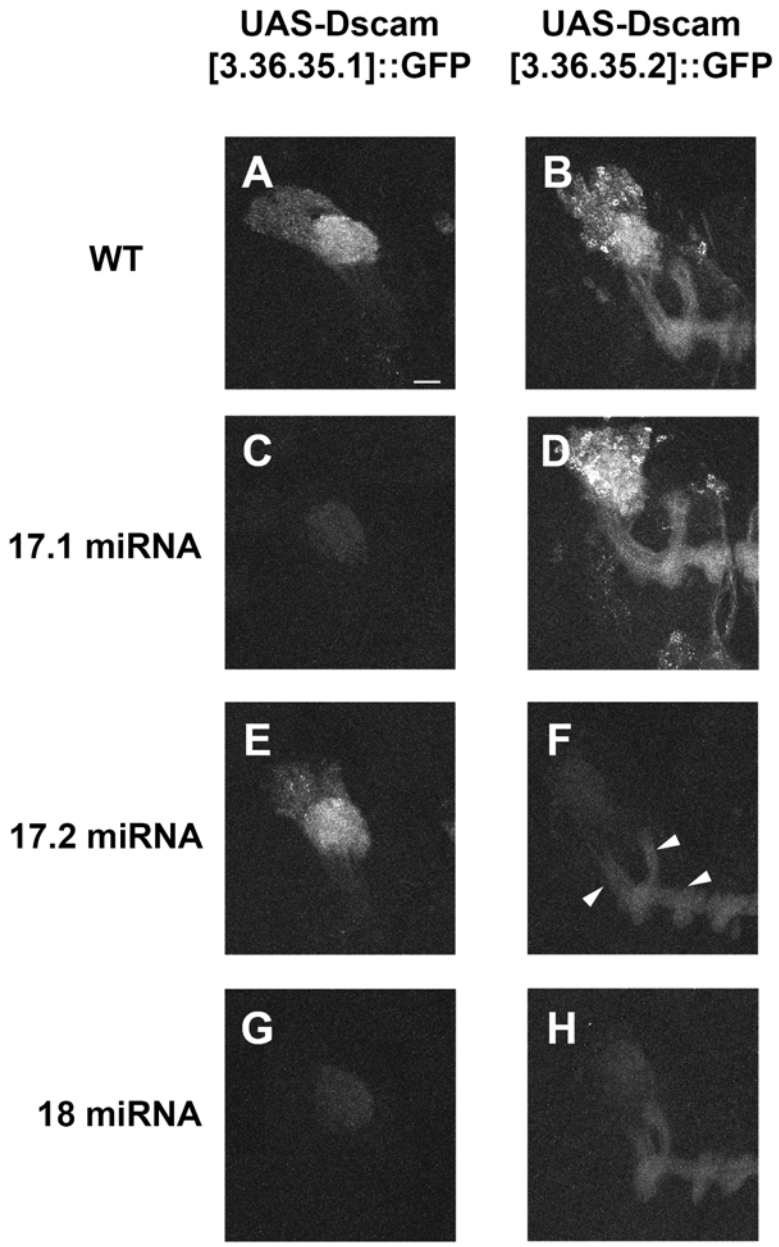

Figure 4-S1. Silencing of various UAS-transgenes by specific UAS-miRNAs
Composite confocal images of wandering larval (WL) MBs showing suppression of the GAL4-201Y-dependent induction of UAS-Dscam3.36.25.1::GFP and UAS-Dscam3.36.25.2::GFP by UAS-17.1 miRNA (C) and UAS-17.2 miRNA (F), respectively. In addition, UAS-18 miRNA antagonized the induction of both UAS-Dscam3.36.25.1::GFP (G) and UAS-Dscam3.36.25.2::GFP (H), but not UAS-mCD8::GFP (data not shown). Note that weak induction is necessary for demonstrating the preferential axon targeting of DscamTM2. For instance, the MB axon peduncle and lobes (e.g. arrowheads in F) are better labeled than the calyx when Dscam3.36.25.2::GFP was weakly expressed (F, H).

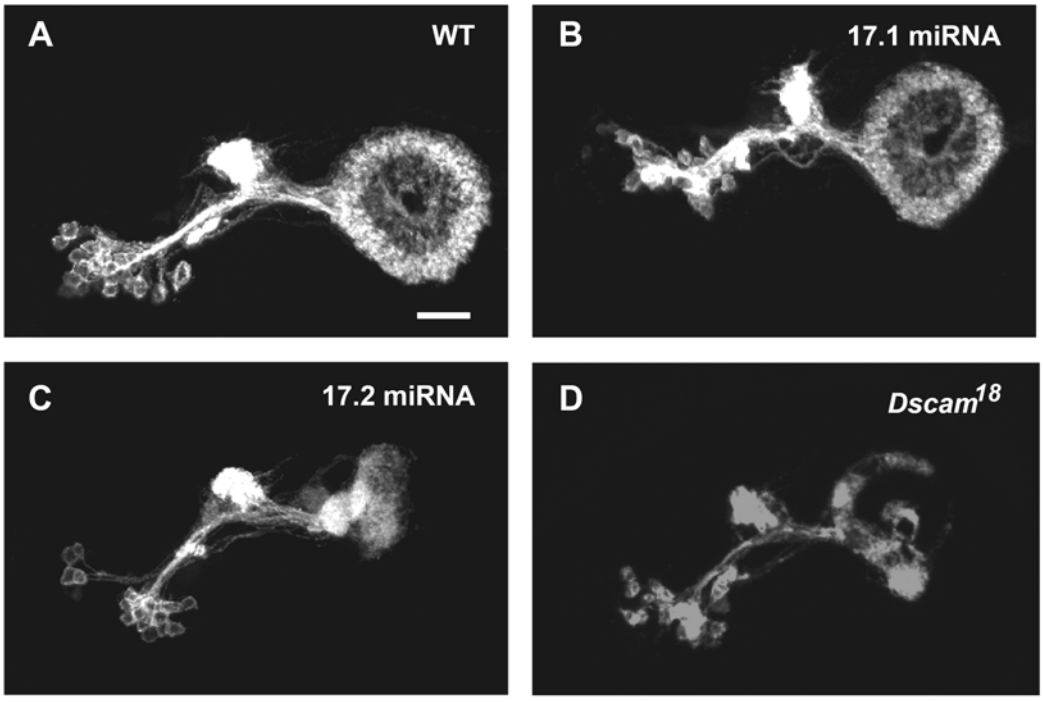

Figure 4-S2. Requirement of DscamTM2 for EB axonal morphogenesis

Nb clones of adult EB neurons labeled with a flip-out reporter gene (A-C) or MARCM (D). Clones were generated in the absence of transgenic miRNA (A) or in the presence of UAS-17.1 miRNA (B) or UAS-17.2 miRNA (C). Note malformation of the EB ring following induction of UAS-17.2 miRNA (C). Similar phenotypes are observed in Dscam mutant clones (D).

Chapter 5

Endodomain diversity in the *Drosophila* Dscam and its roles in neuronal morphogenesis

The following work is the original manuscript submitted to Journal of Neuroscience in Sep 2008 and is currently under review. Author list is:

Hung-Hsiang Yu*, Jacob S. Yang*, Jian Wang, Lei Shi, Yaling Huang and Tzumin Lee.

*These authors contributed equally to this study

ABSTRACT

Drosophila Dscam can be variably spliced to encode 152,064 different single-pass transmembrane proteins. This involves derivation of 19,008 distinct ectodomains, two alternative transmembrane segments, and four endodomain variants. Intriguingly, the wiring of adult fly neural circuitry primarily involves Dscam isoforms that lack both exon 19 and exon 23 in their coding of the endodomain. Use of exon 19 is largely restricted to embryogenesis, and exon 23 is seldom included through development. Consistent with these patterns of exon usage, silencing of transcripts lacking exon 19 or 23 effectively elicits loss-of-*Dscam* phenotypes in post-embryonic neuronal morphogenesis, while repressing exon 19-containing *Dscam* transcripts affects embryonic neuronal wiring. Further, as compared to exon 19-containing Dscam, transgenic Dscam without exon 19 is more efficiently targeted to neurites and more potently suppresses axon bifurcation in *Dscam* mutant neurons. In sum, Dscam with or without exon 19 in its endodomain potentially governs differential stage-specific neuronal morphogenesis.

INTRODUCTION

The assembly of functional neural circuits from numerous neurons requires a series of cellular recognition events to specify correct axonal and dendritic patterns throughout development. Neurite projection following the birth of neurons brings axons and dendrites into proximity where they often branch to make synaptic contacts with multiple targets. One major challenge in this process is to distinguish self-branches from those of their neighboring neurons to prevent redundant connections. In *Drosophila*,

Dscam (Down syndrome cell adhesion molecule) is primarily involved in the above process during neuronal morphogenesis including axonal guidance, axonal targeting and proper arborization of axons and dendrites (Chen et al., 2006; Wang et al., 2002; Zhu et al., 2006).

Drosophila Dscam can encode 152,064 distinct immunoglobulin/fibronectin-type-III cell adhesion molecules (Schmucker et al., 2000; Wang et al., 2004). This derives from the presence of 19,008 variations, two alternatives, and four possibilities in its extracellular, transmembrane, and cytoplasmic domains, respectively. The huge diversity in the ectodomain, known to bind with high affinity only to the ectodomain of the same kind, potentially underlies self-recognition for individual neurons (Wojtowicz et al., 2004; Wojtowicz et al., 2007). Repulsion as a consequence of the homophilic Dscam-Dscam interactions may mediate self-avoidance among the neurites derived from the same cell while permitting fasciculation of neurites of different origins, to ensure proper patterning of multiple growth cones migrating simultaneously (Hughes et al., 2007; Matthews et al., 2007; Soba et al., 2007; Wojtowicz et al., 2004). Further, elaboration of dendrites versus axons in the same neuron may involve different subsets of Dscam ectodomains, since a Dscam ectodomain can be selectively targeted to dendrites or axons depending on the nature of its transmembrane/juxtamembrane domain (Shi et al., 2007).

Compared to well studied Dscam variants in the ectodomain and transmembrane/ juxtamembrane domain, little is known about the role of Dscam endodomain variants in neuronal morphogenesis. A previous report has suggested that four possible Dscam

endodomains, ranging from exon 18 continuously extending to exon 24 or skipping exon 19 and/or exon 23, are generated from independent alternative splicing of exon 19 and exon 23 (Wang et al., 2004). The full-length Dscam endodomain, located on the carboxyl side of the exon 17-encoded transmembrane/juxtamembrane segment, consists of 367 amino acids. It carries several putative SH3 binding sites, two 33 amino acid repeats that contain two consensus SH2 binding motifs, a proline-rich motif, an immunoreceptor tyrosine-based activation like motif (ITAM-like) , an immunoreceptor tyrosine-based inhibition motif (ITIM), and a putative postsynaptic density, disc large and ZO-I protein (PDZ)-binding motif (Schmucker et al., 2000). However, skipping exon 19 produces a Dscam protein without a proline-rich motif (PPVP) and an ITAM-like ($YxxLx_{(12)}YxxA$) sequence (Figure 5-1A). By contrast, the exon 23 encodes 22 and one third amino acids, so skipping exon 23 makes a reading frame shift in the last exon 24 that results in the loss of the ITIM (TAYDTM) and an PDZ-binding motif (TMAV) (Figure 1A). Due to use of a different splicing donor site, four additional amino acids (TVIS) are added at the junction where exon 18 connects with exon 20 (Figure 5-1A). These differences in the primary sequence may confer different signaling and/or protein targeting properties on the Dscam endodomain variants, but their function in neural development still remains to be investigated.

Here, we knocked down Dscam isoforms with specific endodomains to determine whether distinct Dscam endodomains are utilized to govern different Dscam-dependent neuronal morphogenetic processes. A microRNA (miRNA)-based inducible RNA interference (RNAi) approach silences specific transcripts based on discrete 22-

nucleotide sequences (Chen et al., 2007; Shi et al., 2007). The miRNA-based silencing approach knocks down isoform expression after splicing, rather than in the transcriptional level through genomic manipulation. Thus, this technique should minimally affect the normal usage of isoforms that permits determination of isoform expression patterns and a direct demonstration of the involvement of distinct Dscam isoforms in different places and at different times. Using this miRNA-based silencing technique, we were able to specifically silence *Dscam* transcripts carrying exon 19 or exon 23 via targeting the exon 19- or exon 23-characteristic sequences, and to selectively deplete *Dscam* transcripts lacking exon 19 or exon 23 through RNAi against the unique sequences around the junction between exon 18 and exon 20 or between exon 22 and exon 24. Selective elimination of *Dscam* isoforms either containing or lacking exons 19 and 23 followed by analysis of residual Dscam, as well as characterization of neuronal morphogenesis, revealed differential involvement of distinct Dscam endodomains in specific neuronal morphogenetic processes. Notably, the wiring of adult fly neural circuitry primarily involves Dscam isoforms lacking both exon 19 and exon 23. However, Dscam with exon 19 plays a more dominant role than Dscam without exon 19 in supporting wiring of embryonic neural circuitry. In addition, Dscam with exon 23 and Dscam without exon 23 are expressed in different compartments of the developing nervous system. Through characterization of transgenic Dscams with different endodomains, we further found that transgenic Dscam without exon 19 is more efficiently targeted to neurites and more potently suppresses axon bifurcation in *Dscam* mutant neurons than does exon 19-containing Dscam. Taken together, the huge repertoire of *Drosophila* Dscam ectodomains can govern diverse neural developmental processes not only through

alternative exon 17s to be targeted to dendrites versus axons, but also potentially via the use of four different endodomains to support distinct stage-specific or context-dependent neural development.

MATERIALS AND METHODS

Transgenic Constructs

Standard molecular biological techniques were used to generate *UAS-19 miRNA*, *UAS-23 miRNA*, *UAS-18/20 miRNA* and *UAS-22/24 miRNA*, which encode microRNAs carrying unique *Dscam* sequences derived from exon 19, exon 23, the junction between exon 18 and exon20, and the junction between exon 22 and exon 24, respectively. The complete nucleotide sequences of the microRNA constructs are indicated in Figure 1A and listed in the appendix. *UAS-18miRNA* and four *UAS-Dscam endodomain variants* with the same ectodomain composition (*UAS-Dscam[3.36.25.2]::GFPs*) were described previously (Shi et al., 2007; Wang et al., 2004).

Flies

Transgenic flies carrying various *UAS-miRNAs* were obtained by P element-mediated germ line transformation with technical support from Genetic Services.

Acute Induction of UAS-transgenes by TARGET system

Larvae carrying two copies of *tubulin promoter* (*tubP*)-*GAL80*^{ts} (McGuire et al., 2003) were cultured at the permissive temperature of 18°C throughout embryogenesis in order

to repress GAL4-mediated transcription. Wandering larvae were shifted to 38°C for 30 min, followed by incubation at the non-permissive temperature of 29°C for various periods.

Isolation and analysis of Dscam exon 15-24 cDNAs

Dscam exon 15-24 cDNAs were amplified by RT-PCR with the primers CAGGTCTATGCCACAGGATTCA and GACTCTAGATTACACTGCCATAGTATCG and subcloned into pBluescript with *Hind*III and *Xba*I as the cloning sites. Multiple independent subclones were then individually analyzed for presence or absence of exon 19 and/or exon 23 in their inserts. Analysis was largely based on presence or absence of various exon-specific restriction enzyme sites and isoform-characteristic lengths of specific PCR products.

RNAi induction and phenotypic analysis

Targeted induction of *UAS-miRNA* involved use of various tissue-specific GAL4 drivers; and their phenotypic analysis mainly involved co-expression of various UAS-reporter genes. The complete nucleotide sequences of the microRNA constructs are in the appendix. Rescue experiments by four different *UAS-Dscam endodomain variants* were analyzed in MARCM-labeled clones of α/β mushroom body neurons (MBs), which were induced one day before eclosion by heat shock for 30 min at 37ºC. Whole fly brains were prepared for immunostaining as described previously (Lee et al., 1999). Dscam 18 monoclonal antibody (mAb) (Shi et al., 2007) and Dscam 19 rabbit polyclonal antibody (pAb), used to detect all versus exon 19-containing endogenous Dscam proteins, were a

mouse monoclonal antibody and a rabbit polyclonal antibody raised against epitopes in Dscam exon 18 (ATLDKRRPDLRDELG) and exon 19 (HSTWDPRRNPNLY), respectively. The anti-Dscam 18 mAb, anti-Dscam 19 pAb1D4 mAb, anti-GFP and anti-mCD8 mAb were used at 1:20, 1:1000, 1:500, and 1:100, respectively. Fluorescence signals were captured with Zeiss confocal microscopy and processed using Adobe Photoshop to subtract background or adjust the signals by altering the linearity of the signals.

RESULTS

microRNA-based RNA interference permits differential silencing of *Dscam* transcripts encoding distinct endodomains

Based on analysis of RT-PCR products, there are four possible Dscam endodomain variants spanning the *Dscam* exon-16-to-polyA segment (Wang et al., 2004). The variations in the Dscam endodomain derive from presence or absence of exon 19 or exon 23 (Figure 5-1A). To determine if Dscam uses different endodomains in support of different neural developmental processes, we selectively knocked down *Dscam* transcripts containing or lacking exons 19 and/or exon 23 using a miRNA-based RNAi technology that permits silencing of specific transcripts based on the presence of unique sequences that are only 22 nucleotide-long (Chen et al., 2007; Shi et al., 2007).

By targeting exon 19- or exon 23-characteristic sequences or the unique sequences at the exon-exon junctions derived from skipping of exon 19 or exon 23 (Figure 5-1A), we successfully silenced the expression of specific Dscam transgenes

based on presence or absence of exon 19 or exon 23. Multiple independent transformants carrying *UAS-19RNAi*, *UAS-18/20RNAi*, *UAS-23RNAi*, or *UAS-22/24RNAi* were obtained and individually examined to identify the most effective RNAi transgenes for silencing their target-sequence-containing Dscam::GFPs in mature larval mushroom body (MB) neurons (Figure 5-1 and data not shown). *GAL4-201Y*-dependent co-induction of distinct *UAS-RNAis* with a full-length Dscam (Dscam+19+23)::GFP or its derivative that skips both exon 19 and exon 23 (Dscam-19-23::GFP) further revealed that *UAS-19RNAi* (Figure 1C) and *UAS-23RNAi* (Figure 5-1E) effectively antagonized the expression of Dscam+19+23::GFP while minimally affecting the induction of Dscam-19-23::GFP which lacks the target sequences for these transgenic miRNAs (Figure 5-1G and I). Opposite results were obtained following co-induction of the Dscam::GFPs with *UAS-18/20RNAi* or *UAS-22/24RNAi* (Figure 5-1B, D, F and H). These observations justified the use of *UAS-19RNAi*, *UAS-18/20RNAi*, *UAS-23RNAi*, and *UAS-22/24RNAi* for selectively silencing exon 19-containing (*Dscam+19*), exon 19-lacking (Dscam-19), exon 23-containing (Dscam+23) and exon 23-lacking (Dscam-23) *Dscam* transcripts, respectively.

Differential expression of Dscams with different endodomains

We have made a *UAS-18RNAi* transgene targeting the exon 18 shared by all *Dscam* transcripts, and previously demonstrated that ubiquitous induction of *UAS-18RNAi* abolished endogenous Dscam expression in the developing nervous system (Shi et al., 2007). To determine the effectiveness of the above miRNA transgenes in silencing the endogenous expression of Dscam, we examined how induction of individual or

multiple *Dscam* miRNAs affected the endogenous patterns of Dscam expression at different developmental stages.

In control embryos, immunostaining with an anti-Dscam exon 18 monoclonal antibody (Ab18) revealed concentration of endogenous Dscam on the ladder-like axonal tracks of the ventral ganglion (Figure 5-2A). Such a stereotyped pattern of Dscam distribution was completely eliminated by *tubulin promoter* (*tubP*)-*GAL4*-dependent ubiquitous induction of *UAS-18RNAi*, *UAS-19RNAi* plus *UAS-18/20RNAi* or *UAS-23RNAi* plus *UAS-22/24RNAi* (Figure 5-2D, E and H). It was noted that pan-neuronal induction of *UAS-18RNAi* by *GAL4-C155* plus *Asense-GAL4* could not deplete the ladder-like axonal expression of endogenous Dscam, possibly due to late or insufficient induction of RNAi (data not shown). In contrast, residual Dscam persisted following *tubP-GAL4*-dependent induction of only one of the paired *UAS-RNAis*, even with multiple copies (data not shown). Comparing the induction of *UAS-19RNAi* versus *UAS-18/20RNAi*, the ladder-like patterns of immunostaining, though weakened, looked morphologically indistinguishable from those seen in control embryos (Figure 5-2B and C). Intriguingly, when endogenous Dscam was silenced by *UAS-23RNAi* or *UAS-22/24RNAi*, we found that the whole Dscam distribution can be subdivided into two non-overlapping compartments that exclusively contain Dscam+23 and Dscam-23, respectively (Figure 5-2F-G). Residual Dscam was completely restricted to the midline of the ventral ganglion, following induction of *UAS-22/24RNAi* (Figure 5-2F). Closer inspection revealed the midline localization of Dscam in control embryos as well (Figure 5-2A, 5-3A and D); and the midline expression of Dscam was only abolished by

induction of *UAS-23RNAi* that otherwise did not affect the pattern or intensity of the endogenous Dscam expression (Figure 5-2F versus Figure 5-2B, C and G). These phenomena indicate that, in embryos, Dscam+19 or Dscam-19 is coexpressed in the same neurons while Dscam+23 or Dscam-23 is differentially expressed.

Similar analysis of Dscam expression in the late larval central nervous system (CNS) revealed that the endogenous Dscam mostly lacks exon 19 and exon 23. Pan-neuronal induction of either *UAS-19RNAi* or *UAS-23RNAi* to deplete Dscam+19 or Dscam+23 minimally affected the expression pattern or level of endogenous Dscam (Figure 5-2K and O). Consistent with these observations, depleting the Dscams-19 or Dscam-23 drastically reduced the Dscam expression in the late larval CNS (Figure 5-2J and N). Intriguingly, distinct patterns of residual Dscam were detected. Upon induction of *UAS-18/20RNAi* to eliminate Dscam-19, the residual Dscam, though barely detectable, existed in a similar pattern to that of control animals (Figure 5-2I and J). In contrast, induction of *UAS-22/24RNAi* to silence *Dscam*-23 transcripts selectively depleted endogenous Dscam from those neuropil structures where Dscam is normally enriched (Figure 5-2N). These results suggest that larval development of the *Drosophila* CNS is mainly supported by Dscam-19-23 isoforms. In addition, Dscam+23 or Dscam-23 exists in distinct patterns, though not as exclusive as in embryos, and potentially governs different morphogenetic processes through development of the *Drosophila* CNS.

To validate some of the above conclusions, we sought to locate Dscam+19 directly by immunostaining with exon 19-targeted antibody (Ab19), a polyclonal

antibody raised against a peptide sequence characteristic of Dscam exon 19. The Ab19 selectively bound to ectopic Dscam+19::GFP (data not shown). Further, a similar ladder-like pattern of immunocytochemical signals, which was eliminated in *Dscam-null* embryos, was detected following immuonstaining of wild-type embryos with the Ab18 or Ab19 (Figure 5-3A-B and 5-3D-E). These results demonstrate that the Ab19 specifically binds with Dscam+19. When the Ab18 and the Ab19 were used to label all the Dscam isoforms or Dscam+19 isoforms in the late larval CNS, we detected abundant Dscam expression only with the Ab18 (Figure 5-3C and F). This substantiates the notion that Dscam+19 is largely absent during post-embryonic development of the fly CNS. These results are also consistent with the use of transgenic miRNAs to silence alternative transcripts in identifying the expression patterns of distinct isoforms *in vivo*.

Analysis of *Dscam* transcripts by RT-PCR revealed that the dynamic usage of exon 19 and exon 23 is evident even at the mRNA level. The relative abundance of *Dscam* transcripts encoding distinct endodomains varied at different developmental stages. The expression of *Dscam+19* transcripts in the CNS drastically decreased from embryos (65.8%) to larvae (15.8%), became negligible by puparium formation (0%), and returned after eclosion (31.6%). In contrast, *Dscam+23* transcripts rarely existed in embryos (2.6%), significantly increased in larvae (7.9%) and pupae (10.4%), and further doubled in the relative abundance in adult brains (21.1%). The differential expression of *Dscam* mRNA splicing variants at different developmental stages can account for the differences we detected in the abundance of distinct endodomains at the protein level.

These results suggest that the dynamic expression of distinct Dscam endodomains is likely controlled through regulation of alternative splicing.

Taken together, these observations not only indicate that distinct Dscam endodomain isoforms do exist in vivo, but also demonstrate that the miRNA-based RNAi reagents work effectively to antagonize expression of each isoform while minimally affecting the alternative splice form. Differential induction of these isoforms should allow us to determine where Dscams with specific endodomains are distributed *in vivo*. Notably, examining the expression of Dscam+23 uncovers two distinct populations of Dscam-positive structures that may potentially utilize different Dscam endodomains for supporting different morphogenetic processes.

Wiring of the adult fly neural circuitry primarily involves *Dscam-19-23* transcripts

Based on the above analysis on endogenous expression patterns of Dscam endodomain variants, Dscam-19-23 may support diverse neuronal morphogenesis during larval and pupal stages. This raises the possibility that wiring of the fly neural circuitry primarily involves Dscam-19-23. To test this hypothesis, we examined how silencing of *Dscam* transcripts encoding specific endodomains by targeted RNAi affects morphogenesis of two distinct types of larval-born neurons where *Dscam* loss-of-function phenotypes are known. We found in both MB neurons and the ellipsoid body (EB) neurons, that induction of *UAS-18/20RNAi* or *UAS-22/24RNAi*, but not *UAS-19RNAi* or *UAS-23RNAi*, effectively elicited the phenotypes characteristic of loss of *Dscam* function (Figure 5-4A-C and data not shown).

For example, Dscam governs axon bifurcation by preventing sister growth cones from migrating along the same path in the MB neurons (Wang et al., 2002). It ensures formation of paired MB lobes that normally lie perpendicular to each other and are comparable in bundle thickness. By contrast, when Dscam is absent, MB axons undergo excessive bifurcation, and their sister branches are no longer consistently segregated. These abnormalities underlie overgrowth of one MB lobe at the expense of its paired one. To determine the roles of Dscam+19, Dscam-19, Dscam+23 or Dscam-23 in MB morphogenesis, we examined which of the above anti-*Dscam* miRNA transgenes could be induced to elicit these loss-of-*Dscam* MB phenotypes. We first demonstrated that *GAL4-OK107*-driven induction of *UAS-18RNAi* caused defects in MB lobe morphology (Figure 5-4A and B). Instead of having two comparable axon lobes, 88% of the MBs acquired one huge and one skinny lobe (Figure 5-4C). This anomaly replicated *Dscam* mutant MB phenotypes (Wang et al., 2002). Since silencing Dscam with *UAS-18RNAi* eliminates all Dscam isoforms, this result has not only confirmed the efficiency of knocking down endogenous Dscam by transgenic miRNA, but also given us an opportunity for learning what *Dscam* "null" phenotypes to expect in the MBs following the suppression of specific Dscam endodomain isoforms. Notably, induction of *UAS-19RNAi* and *UAS-18/20RNAi* or with *UAS-23RNAi* versus *UAS-22/24RNAi* yielded different effects (Figure 5-4C). While induction of *UAS-19RNAi* or *UAS-23RNAi* to deplete Dscam+19 or Dscam+23 failed to affect MB morphogenesis, 68% and 77% of the MBs acquired asymmetric axon lobes following silencing of Dscam-19 or Dscam-23 using *UAS-18/20RNAi* or *UAS-22/24RNAi* (Figure 5-4C). This suggests that Dscam-19

and Dscam-23 are indispensable for gross morphogenesis of the MBs. However, the penetrance of *UAS-18/20RNAi*-induced MB phenotypes increased from 68% to 89% following co-induction with *UAS-19RNAi*, supporting a lesser role for Dscam+19 in mediating the neuronal morphogenetic processes mainly governed by Dscam-19-23. By contrast, co-induction of *UAS-22/24RNAi* and *UAS-23RNAi* minimally enhanced the MB phenotype, suggesting again that Dscam-23 is dispensable in the neuronal morphogenesis. Taken together, these results indicate that the Dscam-dependent MB lobe formation primarily involves Dscams-19-23, which is consistent with Dscam-19-23 being predominantly expressed through post-embryonic CNS development.

Dscam-19 is selectively involved in embryonic neuronal morphogenesis

In contrast with Dscam-23 whose usage remains low through different developmental stages, both Dscam+19 and Dscam-19 are abundantly expressed in embryonic CNSs. To reveal the role of Dscam exon 19 variants in neural development, we examined if eliminating Dscam+19 or Dscam-19 affects embryonic neuronal morphogenesis. We characterized neurite tracks in the embryonic ventral ganglion that typically consists of bilaterally symmetric longitudinal fascicles connected across the midline via repeated pairs of commissure bundles. Although aberrant neurite tracks in *Dscam* mutant embryos have been reported (Schmucker et al., 2000), ubiquitous induction of *UAS-18RNAi* failed to disrupt the ladder-like neuronal tracks in otherwise wild-type embryos (Figure 5-4F). Recent studies showed that *Dscam* loss-of-function phenotypes in embryos can be significantly enhanced in tyrosine kinase *abelson* (*abl)* mutant backgrounds (Andrews et al., 2008). Prompted by this unpublished observation,

we examined how silencing *Dscam* by *RNAi* might affect neural track development in *abl* mutant embryos (Figure 5-4D and E). Similar to the *Dscam*-depleted embryos caused by *tubP-GAL4*-dependent induction of *UAS-18RNAi*, the ladder-like neurite tracks were grossly normal in abl^{2}/abl^{4} mutant embryos (Figure 5-4F). In contrast, the ubiquitous induction of *UAS-18RNAi* in abl^{2}/abl^{4} mutant embryos effectively blocked midline crossing of neurites and caused commissureless phenotypes in 19% of the ventral ganglion segments (Figure 5-4E and F). This sets a stage for determining the roles of various Dscams in embryonic neuronal morphogenesis by *RNAi* using distinct *Dscam*-targeted *miRNAs*.

To tell the respective contributions made by Dscam+19 and Dscam-19, we silenced *Dscam* transcripts containing or lacking exon 19 in the abl^{2}/abl^{4} mutant background. Following analogous induction with *tubP-GAL4*, *UAS-19RNAi* and *UAS-18/20RNAi* elicited commissureless phenotypes in 9% and 1% of the ventral ganglion segments, respectively (Figure 5-4F). This demonstrates that Dscam+19 plays an essential and more dominant role than Dscam-19 in the development of the *Drosophila* embryonic CNS. Again consistent with the differential usage of exon 19 during versus after embryogenesis, endogenous Dscam+19 is preferred in supporting embryonic neuronal morphogenesis while governing post-embryonic neuronal development utilizing the Dscam-19.

Differential rescue of axon branching phenotypes by transgenic Dscam +19 or Dscam-19

To start understanding why Dscam with specific endodomains is utilized in specific contexts, we examined whether ectopic expression of Dscams with different endodomains may act differentially *in vivo*. Although MB morphogenesis primarily involves Dscam-19-23, past studies have shown that the *Dscam+19+23* transgene, no matter which ectodomain it carries and whether it is fused with GFP at the carboxyl terminus or not, can effectively prevent sister branches from extending into the same axon bundle in single-cell clones of *Dscam* mutant neurons (Wang et al., 2004; Zhan et al., 2004; Soba et al., 2007). We wondered if *Dscam* transgenes that encode Dscams with distinct endodomains may vary in their ability to restore the normal pattern of axon bifurcation and segregation in *Dscam* mutant MB neurons.

*UAS-Dscam::GFP*s that encode the same ectodomain connected to one of the four possible endodomains through the exon 17.2-defined transmembrane domain were identified by their comparable induction expression level with the same *GAL4* driver (Figure 5-5A). We examined how expression of each of the representative *Dscam* transgenes exclusively in *Dscam* mutant single-cell MARCM clones affects their axon bifurcation and segregation at the MB peduncle terminus. We focused on the analysis of MB α/β neurons, whose axons extend through the peduncle, undergo bifurcation at the peduncle end, and then innervate the MB α and β lobes with only one primary branch from each neuron (Figure 5-5C). Single-cell MARCM clones of MB α/β neurons were derived following mitotic recombination induced during mid-pupal development. Loss of the GAL4 repressor, GAL80, in the clones led to derepression of *GAL4-OK107*, which in turn drove expression of *UAS-mCD8::GFP* for marking the clones uniquely. In the

rescue experiments, the derepressed *GAL4-OK107* also activated one of the *UAS-Dscam::GFPs* specifically in the clones. Given that these *Dscam* transgenes vary only in the presence or absence of exon 19 or 23, any differences in the phenotypes of *Dscam* mutant α/β neurons that have expressed different *UAS-Dscam::GFPs* can be fully ascribed to the differences in Dscam protein distribution and/or function due to the involvement of different endodomains.

As reported previously, single-cell MARCM clones of *Dscam* mutant MB α/β neurons could not effectively segregate their sister branches to prevent multiple neurites of the same cellular origin from extending into the same MB lobe (Wang et al., 2002). Although *Dscam* mutant neurons might acquire supernumerary branches, this segregation problem was evident even in the mutant axons that only bifurcated once at the peduncle end. Failure in the divergent segregation of sister branches appears to be the primary defect (Figure 5-5D-F). 97% of *Dscam* mutant single-cell MARCM clones of MB α/β neurons sent two or more neurites into one MB axon, exhibiting the multi-branches/lobe phenotype (Figure 5-5B-F). By this measure, single-isoform *Dscam-19* transgenes were similar to single-isoform *Dscam+19* transgenes in restoring the *Dscam* mutant multi-branches/lobe phenotype to the wild-type phenotype (Figure 5-5B). Failure in divergent segregation (multi-branches/lobe) was observed in 22%, 16%, 25%, and 22% of *Dscam* mutant MB α/β neurons (as opposed to 97% in the absence of any rescuing construct) that were rescued by the transgenes of *Dscam+19+23*, *Dscam-19+23*, *Dscam+19-23* and *Dscam-19-23*, respectively (Figure 5-5B). In addition, among the rescued single-cell MARCM clones (without the multi-branches/lobe phenotype), we detected a single-

branch/neuron phenotype in which the axon did not bifurcate at the peduncle end and stochastically projected into the α or β lobe. Intriguingly, many more rescued single-cell MARCM clones exhibited the single-branch/neuron phenotype (no bifurcation despite presence of both α and β lobes), when the mutant clones were supplemented with *Dscam-19* transgenes (Figure 5-5G). For the *Dscam-19+23* and *Dscam-19-23* transgenes, 11% and 13% of *Dscam* mutant single-cell clones extended their single axonal processes into the α and β lobes without branching at the normal bifurcation point around the peduncle terminus (Figure 5-5B). In contrast, only 5% and 5% were obtained with the *Dscam+19+23* and *Dscam+19-23* transgenes, respectively, (Figure 5-5B). In addition, overexpressing the *Dscam-19+23* transgene in wild-type single-cell MARCM clones only resulted in 3% single-branch phenotype (Figure 5-5B). Taken together, no matter whether exon 23 is present or not, *Dscam-19* transgenes more potently modulate the axon bifurcation and segregation patterns than *Dscam+19* transgenes. These observations suggest some exon 19-dependent modification of protein distribution or function that is relevant to where or how Dscam may signal to govern MB axonal morphogenesis.

Transgenic Dscam-19 is preferentially targeted to neurites while Dscam+19 can be significantly sequestered in neuronal cell bodies

To understand the logic behind the exon 19-dependent functional differences, we visualized the protein distribution of *Dscam+19::GFP* and *Dscam-19::GFP* transgenes *in vivo*. Previously, we have reported the differential protein distribution in the larval MBs when *UAS- Dscam+19::GFP* and *UAS-Dscam-19::GFP* transgenes were ectopically expressed in mature larval MB neurons using *GAL4-201Y* (Wang et al.,

2004). Notably, the Dscam+19::GFP and Dscam-19::GFP were found to be enriched in cell bodies and neurites of the larval MBs, respectively. This raises the possibility that Dscam protein distribution may vary depending on the presence or absence of exon 19.

However, *GAL4-201Y* drove expression of Dscam::GFPs in excessive amounts and in mature MB neurons, which is in great contrast with the endogenous Dscam being expressed at a much lower level and typically in newly derived post-mitotic neurons. To ascertain the role of exon 19 in Dscam protein distribution, we examined whether Dscam+19::GFP and Dscam-19::GFP remain differentially localized upon weak induction in young MB neurons. Transient binary induction of *UAS-transgene* is possible with the TARGET system, in which GAL4 activity is suppressed until inactivation of temperature-sensitive GAL80 at a restrictive temperature (McGuire et al., 2003). Derepression of *GAL4-OK107* following a heat shock to inactivate $GAL80^{ts}$ allowed one to weakly express *UAS-transgene* in young MB neurons as judged by the central localization of neurites in the age-dependent concentrically organized axon bundles. Similar transient induction of *UAS-Dscam::GFPs* again revealed that Dscam-19::GFP, but not Dscam+19::GFP, was selectively enriched in the neurites (Figure 5-6A-D). While Dscam-19::GFP primarily labels the MB axon bundles (Figure 5-6B and 5-6D), Dscam+19::GFP significantly accumulates in cell bodies despite a low-level induction in the MB neurons where endogenous Dscam is expressed (Figure 5-6A and C). This result indicates that Dscam-19 is better targeted to the extending neurites, potentially explaining why transgenic Dscam-19 is more potent than the Dscam+19 in modulating post-embryonic neuronal morphogenesis.

DISCUSSION

Besides the huge diversity in the ectodomain and two choices in the transmembrane domain, endogenous Dscam can carry four distinct endodomains resulting from the alternative splicing of exon 19 and exon 23. Dscams with different endodomains are differentially expressed through development of the *Drosophila* CNS. These conclusions are supported by multiple observations, including (1) the analysis of *Dscam* transcript compositions by RT-PCR, (2) the localization of specific Dscam endodomains by depleting the alternatives via miRNAs against exon 19, exon 23, or the unique exon-exon junctions derived from skipping of exon 19 or exon 23 (Figure 5-2), and (3) the direct visualization of Dscam+19 using Ab19 as opposed to labeling all the Dscam isoforms with Ab18 (Figure 5-3). The differential expression of distinct Dscam endodomain variants suggests diverse Dscam function and implicates possible involvement of Dscams with different endodomains in governing differential neuronal development or function. Interestingly, post-embryonic neuronal morphogenesis primarily utilizes Dscam-19-23 (Figure 5-4C). In contrast, Dscam+19 plays a more dominant role in the wiring of embryonic neural tracks (Figure 5-4F). Skipping exon 19 promotes targeting of Dscams to the neurites in post-embryonic neurons, suggesting a mechanism for regulating Dscam protein targeting by the alternative splicing of exon 19 (Figure 5-6). In addition, exon 23 is dispensable to most Dscam-dependent neuronal morphogenetic processes but present in probably all the Dscam molecules in certain neural structures, suggesting an unidentified Dscam function in the developing *Drosophila* CNS (Figure 5-3C and F).

Four different Dscam endodomain variants exist from independent alternative splicing by skipping exon 19 or exon 23. Possible approaches to study the role of these Dscam endodomain variants in neuronal morphogenesis include: (1) manipulating *Dscam* at the genomic level by gene-targeting (Gong and Golic, 2003), or (2) silencing different *Dscam* endodomain transcripts by RNAi (Chen et al., 2007; Shi et al., 2007). Deleting genomic sequence to manipulate alternative exon choice might be problematic, since elimination of specific *Dscam* endodomain variants inevitably leads to expression of other isoforms in much broader patterns and/or at higher levels than the normal unperturbed conditions. In contrast, knock-down of Dscam endodomain variants at the translational level by RNAi should deplete the isoforms of interest without affecting the expression of others. Further, by targeting the junction spanning different exons (Figure 1), the miRNA-based silencing approach allowed us to selectively deplete isoforms that lack any unique exon shared by the isoform subset. It is also noted that this miRNA-based knock-down could eliminate endogenous Dscam expression at the embryonic stage, while double-stranded RNA-based knock-down generally did not work at this stage (Figure 2E; Yu et al., unpublished observation).

Using miRNA-based knock-down and immonostaining of isoform-specific antibodies, we found that Dscam+19 or Dscam-19 may redundantly govern neuronal morphogenesis but is preferentially utilized at different developmental stages (Figure 5-2 and 5-3). In contrast, most neuronal morphogenetic processes might exclusively use Dscam-23 (Figure 5-3C); and Dscam+23, though weakly expressed in the developing CNS, potentially supports some unknown Dscam function (Figure 5-2F and N). With

respect to the alternative splicing of exon 19, Dscam+19 is primarily used during embryogenesis, but becomes rarely expressed in the post-embryonic nervous system (Figure 5-3D and F). However, Dscam+19 and Dscam-19 exhibit similar spatial expression patterns despite the dynamic changes in the relative abundance (Figure 5-2B-C and 5-2J-K). Consistent with these expression profiles, endogenous Dscam-19 plays an essential role in post-embryonic neuronal morphogenesis, while Dscam+19 plays a supportive role in the same morphogenetic processes (Figure 5-3C). The opposite situation applies in the embryonic ventral ganglion (Figure 5-3F). In contrast, Dscam+23 and Dscam-23 are enriched in different neural structures at the same developmental stages (Figure 5-2F-G and 5-2N-O). It appears that the dominant Dscam expression domains exclusively consist of Dscam-23. And, locating Dscam+23 has revealed previously uncharacterized Dscam expression regions (Figure 5-2F). Consistent with this, depleting *Dscam-23* transcripts only was sufficient to recapitulate the loss-of-*Dscam* phenotype (Figure 5-3C). Elucidation of the function of Dscam+23 may depend on the identification and better characterization of the neural structures whose Dscams invariantly contain exon 23.

Analysis of the differences in the primary sequences of distinct endodomains may confer insights about different signaling and/or protein-targeting properties of the Dscam endodomain variants. For example, skipping exon 19 produces the Dscam without a proline-rich motif and an ITAM-like (Figure 5-1A). An ITAM is defined by a motif containing two tyrosine residues within the consensus sequence of $YxxI/Lx_{(6\text{-}12)}YxxI/L$ (Fodor et al., 2006). Instead of the conserved Ile/Leu adjacent to the second tyrosine

residue in most of ITAM containing proteins, Ala is used in that position in Dscam (Figure 5-1A). Although rare, it is not unprecedented since a similar variation has been found in RhoH, a hematopoietic-specific GTPase-deficient member of Rho GTPase family (Gu et al., 2006). Whether the ITAM-like domain in Dscam can mediate the canonical ITAM-involved signal transduction pathway to control cellular responses awaits investigation. Nonetheless, transgenic Dscams are enriched in different subcellular compartments depending on the presence or absence of exon 19 (Figure 5-6). In the MBs, transgenic Dscam-19 is preferentially targeted to neurites while transgenic Dscam+19 can be significantly sequestered in neuronal cell bodies. Similar patterns of differential protein distribution were detected in the projection neurons (PNs) following targeted induction of transgenic *Dscams* with different endodomains (Yu et al., unpublished observation). This nicely correlates with the phenomena that transgenic Dscam-19 acted more potently than Dscam+19 in altering neurite projection patterns in both MB neurons and PNs (Yu et al., unpublished observation). Whether the proline-rich motif and/or the ITAM-like sequence within the exon 19 make Dscam-19 variants easier to target to neurite projections also awaits further investigation. But this primary sequence analysis sometimes is unable to provide insight into why Dscams with specific endodomains are utilized in specific contexts. The difference between Dscam+23 and Dcam-23 is that the latter variant lacks exon 23, which results in the loss of the ITIM and PDZ-binding motif (Figure 5-1A). However, transgenic Dscams behaved indiscriminately in the presence or absence of exon 23, yielding no insight into why Dscam-23 is pre-selected in most, if not all, known Dscam-dependent neuronal morphogenetic processes (Figure 5-5B). In addition, it is paradoxical for Dscam+19,

which may not be as efficiently targeted to the extending neurites as is Dscam-19, to be predominantly used in supporting embryonic neuronal morphogenesis (Figure 3F). Nevertheless, the spatial distribution of endogenous Dscam in the embryonic ventral ganglion did not change following depletion of Dscam+19 or Dscam-19, suggesting that exon 19 may regulate Dscam protein targeting differentially in a stage-specific manner (Figure 5-2B-C and 5-2J-K).

Transgenic Dscam-19 not only effectively prevents multiple self-branches from extending into the same MB lobe in *Dscam* mutant single-cell MARCM clones, but also blockes axon bifurcation, which results in a single-branch/neuron phenotype in a significant number of the rescued single-cell MARCM clones (Figure 5-5). The single-branch/neuron phenotype is apparently elicited by a cell-autonomous mechanism, and cannot be readily explained based on our current model about the roles of Dscam in controlling axon arborization (Figure 5-5B and 5-5G). Two known mechanisms may suppress MB bifurcation at the peduncle end. First, the competition among self-branches for the available separate fascicles probably underlies the phenomenon that neurons can reliably make the correct numbers of branches based on the numbers of fascicles that project off the branch point. This may explain why MB α/β axons do not bifurcate when the α or β lobe is missing (Wang et al., 2002). Second, promiscuous competition from non-self-branches is thought to occur and, as a consequence, stops most axons from extending beyond the bifurcation point when the endogenous *Dscam* gene loses its ectodomain diversity or a single-isoform *Dscam* transgene is ubiquitously expressed (Wang et al., 2004; Hattori et al., 2007). Both pathological conditions are caused by

environmental factors through non-autonomous mechanisms. By contrast, in the clone-specific rescue experiments, the α and β lobes were both normal, and the Dscam transgene was only expressed in the neuron that exhibited the single-branch/neuron phenotype (Figure 5-5G). These results clearly suggest a novel cell-autonomous mechanism for Dscam in governing neurite arborization. Further, it is unlikely to be due to excessive Dscam expression, since the UAS transgenes can only be barely expressed in the newly-derived single-cell MARCM clones owing to the perdurance of GAL80 inherited from the heterozygous ganglion mother cells. In addition, overexpressing an *UAS-Dscam-19+23 transgene* in the wild-type MB α/β MARCM clones which should increase the overall Dscam amount did not result in obvious single-branch/neuron phenotype (Figure 5-5B). Therefore, the suppression of axon bifurcation is likely to result from loss of Dscam ectodomain diversity in a single neuron, suggesting that the huge molecular diversity in the Dscam ectodomain is not only essential for self-recognition among numerous migrating growth cones but also critical to the behavior of an isolated growth cone. It is possible that the complexity of the expressed Dscam ectodomains in a given neuron at a given time may determine the strength of Dscam-Dscam homophilic signaling between the nascent split growth cones and, thus, help govern how divergently the sister growth cones should migrate away without compromising each other.

Taken together, we substantiate the presence of four possible Dscam endodomains and demonstrate that Dscams with specific endodomains are involved in supporting specific neural developmental processes. The identification and

characterization of the diversity and function in the Dscam endodomain has laid a solid ground for further elucidating the roles of Dscam, a huge repertoire of cell adhesion molecules, in neural development as well as the innate immunity of insects (Watson et al., 2005). It also provides new insights into how the diversity in the Dscam ectodomain may cell-autonomously govern neurite arborization, and suggests an exon 23-dependent unidentified Dscam function for supporting the development of *Drosophila* CNS.

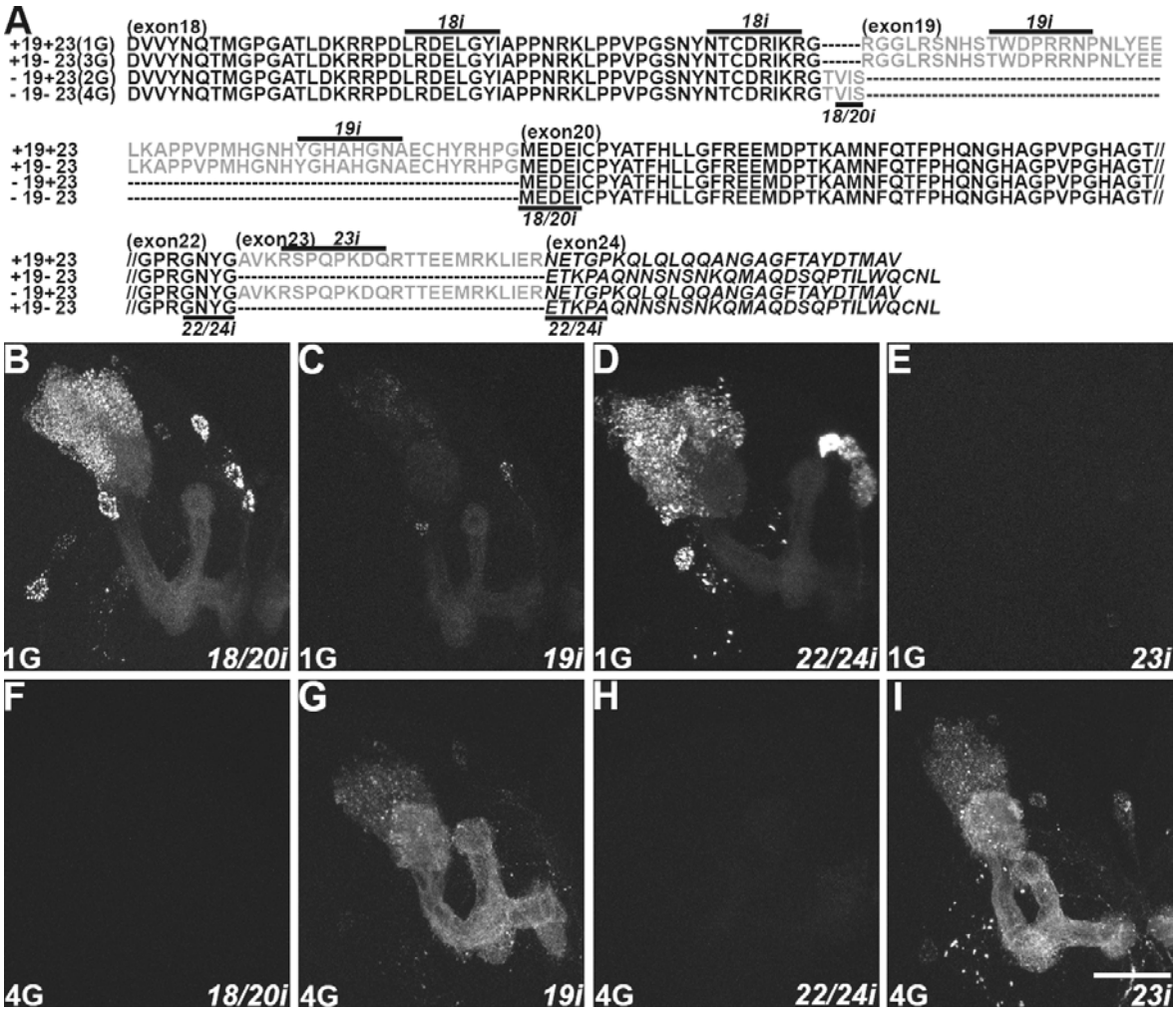

Figure 5-1. Amino acid sequences of four different Dscam endodomain variants and silencing of various *UAS-transgene*s by specific *UAS-miRNA*s

(A) Amino acid sequences of four Dscam endodomain variants, full length (+19+23), missing exon 19 only (-19+23), lacking exon 23 only (+19-23), and omitting both exon 19 and exon 23 (-19-23), are aligned within the cytoplasmic domain from exon 18 to exon 24. Common sequence between exon20 and exon22 is not shown. Four extra amino acids (TVIS) are in the Dscam variants which skip exon 19. Amino acids shown in italicized resulting from a reading frame shift on exon 24 is observed when the Dscam variants skip exon 23. Target sequences for different *UAS- miRNAs* (*18i*, *18*/*20i*, *19i*, *22*/*24i* and *23i*) to eliminate different Dscam variants are indicated. (B-I) Composite confocal images of wandering larval MBs showed suppression of the *GAL4-201Y*-dependent induction of *UAS-Dscam+19+23::GFP* (B-E) and *UAS-Dscam-19-23::GFP* (F-I) by *UAS-18/20 miRNA* (B, F), *UAS-19 miRNA* (C, G), *UAS-22/24 miRNA* (D, H) and *UAS-23 miRNA* (E, I), respectively. The scale bar in this and all other figures equals 50 μm.

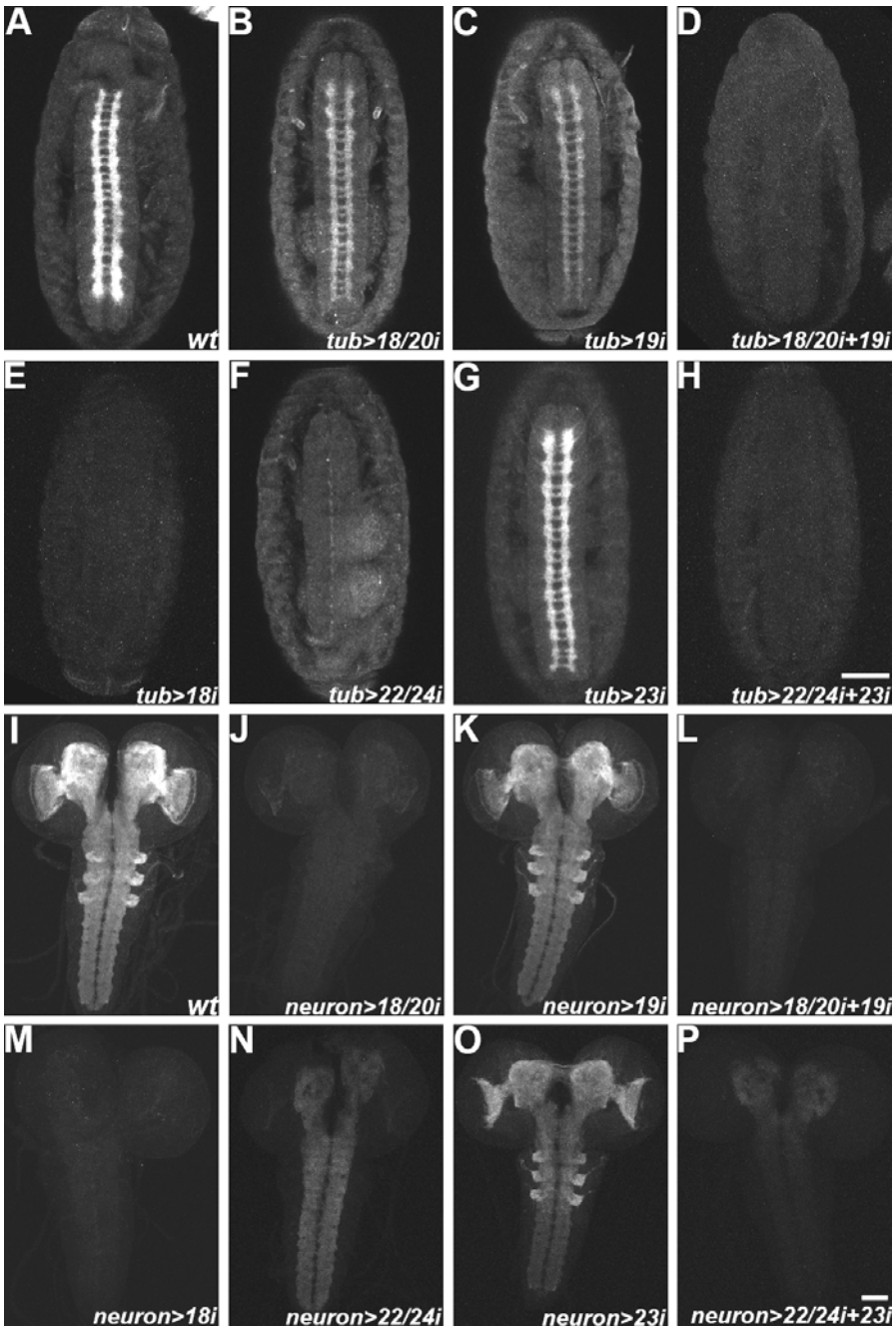

Figure 5-2. Differential and dynamic endogenous expression of Dscam endodoamin variants revealed by transgenic miRNAs knock-down

Composite confocal images of embryonic and wandering larval CNS showing endogenous Dscam expression (revealed by immunostaining with an anti-Dscam exon 18 monoclonal Ab), following *tubP-GAL4*-dependent (A-H) or *GAL4-OK107*-dependent (I-P) induction of various anti-Dscam miRNAs, including *UAS-18 miRNA* (E, M), *UAS-18/20 miRNA* (B, J), *UAS-19 miRNA* (C, K), *UAS-18/20 miRNA* plus *UAS-19 miRNA* (D, L), *UAS-22/24 miRNA* (F, N), *UAS-23 miRNA* (G, O) or *UAS-22/24 miRNA* plus *UAS-23 miRNA* (H, P). Arrows point at the midline in F.

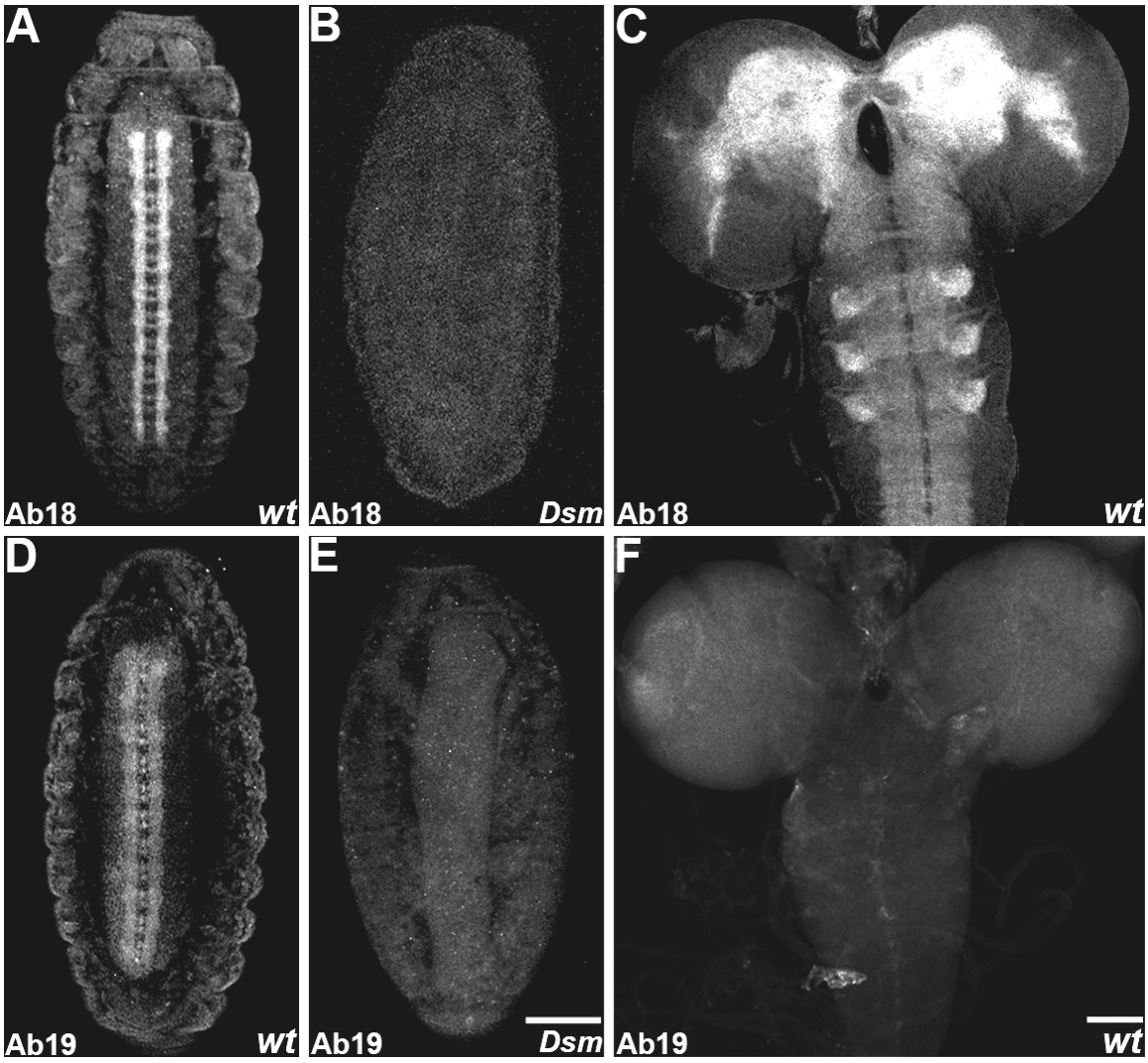

Figure 5-3. Endogenous expression of Dscam exon 19 variants revealed by Dscam antibodies

An anti-Dscam exon 18 monoclonal antibody (Ab18) recognizing all Dscam proteins (A-C) and an anti-Dscam exon 19 polyclonal antibody (Ab19) recognizing Dscam+19 proteins (D-F) were used to reveal the endogenous expression pattern of Dscam+19 during development. Both Ab18 and Ab19 are specific for detecting Dscam endogenous proteins as evidently by lack of immunostaining in *Dscam* null mutant embryos (B, E). Arrows point at the midline in A and D.

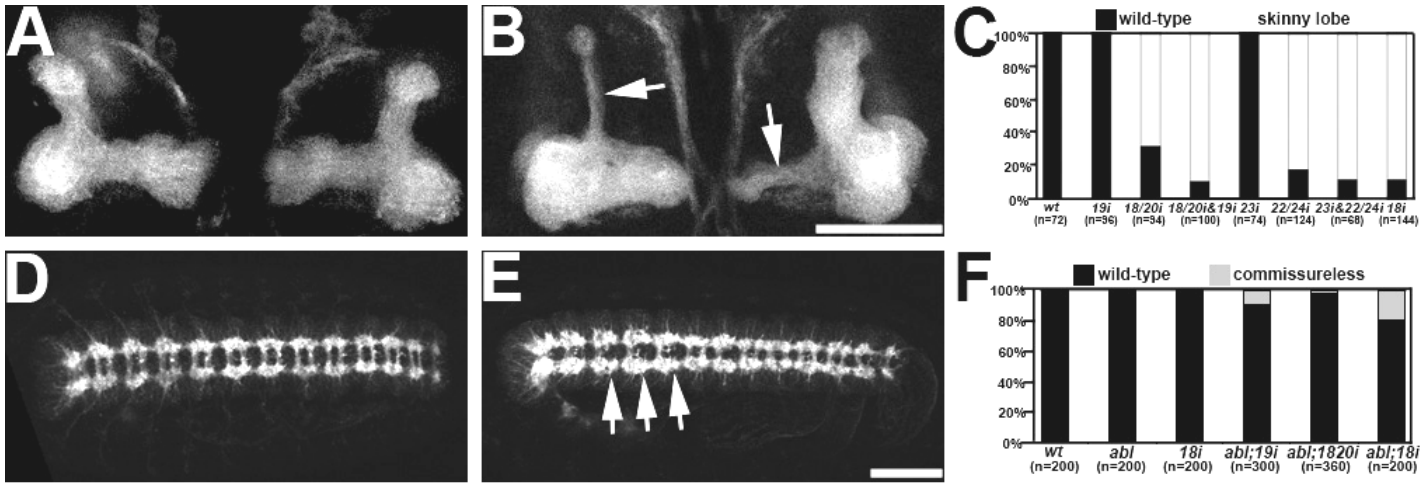

Figure 5-4. The role of Dscam endodomain variants in embryonic CNS and larval MB axonal morphogenesis

(A-C) Quantitative analysis of wandering larval MB lobe phenotype followed *GAL4-OK107*-dependent induction of various *UAS-Dscam miRNAs*. Skinny lobe phenotype (arrows) was observed when Dscam-19 and/or Dscam-23 were eliminated. (D-F) Quantitative analysis of embryonic CNS commissureless phenotype (arrows) followed *tubP-GAL4*-dependent induction of various *UAS-Dscam miRNAs*. No phenotype was observed when all Dscam proteins were knocked down alone or in *abelson (abl)* mutant embryos. However, the commissureless phenotype was observed when all Dscam or Dscam+19 proteins were eliminated in the *abl* mutant embryos.

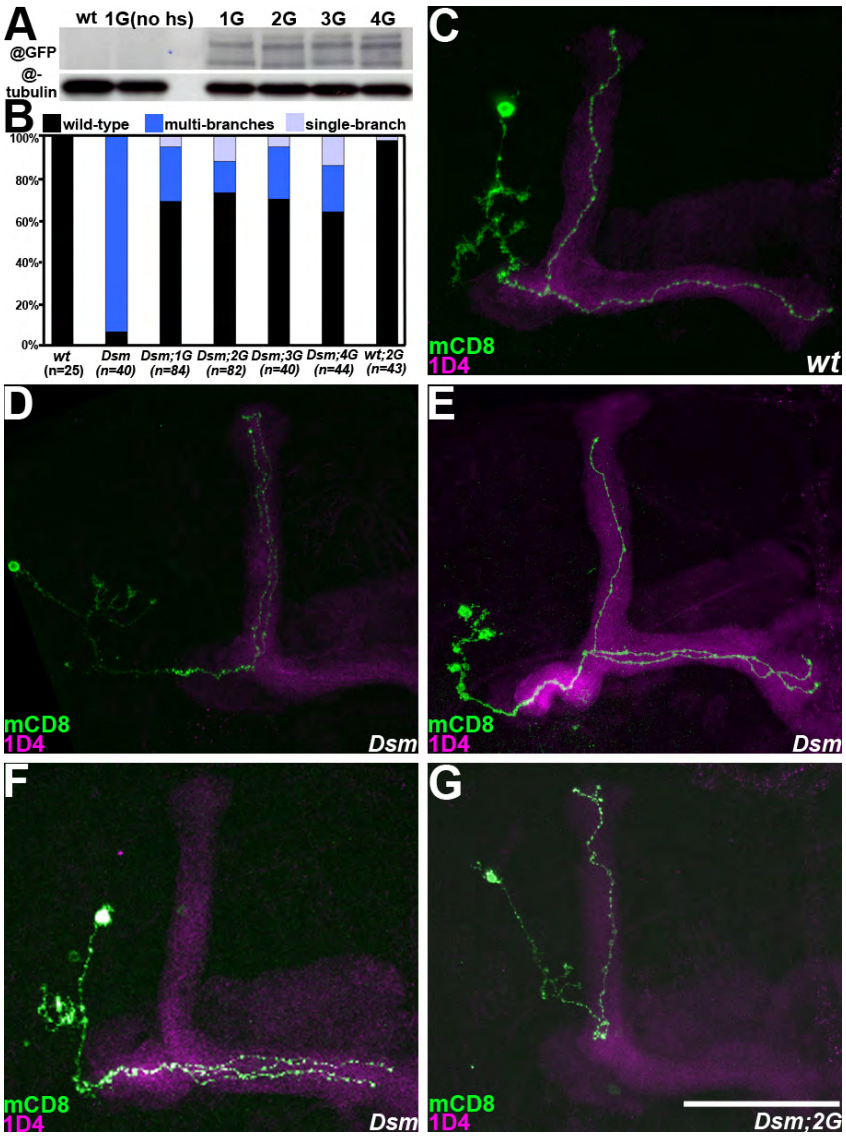

Figure 5-5. Rescue of multi-branch *Dscam* mutant MB α/β phenotype by transgenic Dscam with four different Dscam endodomain variants

(A) Dscam endodomain variants with a similar expression level were chosen to rescue the multi-branch *Dscam* mutant MB α/β phenotype. *Heat shock-GAL4* was used to drive the expression of different Dscam endodomain variants by brief heat shock at 37ºC. The expression level of heat shock animals were analyzed by the Western blot. (B-G) Quantitative analysis of different MB α/β neuronal phenotypes was shown when different Dscam endodomain variants were introduced in *Dscam* mutant MARCM clones (B). Normally, only one primary branch from each neuron was observed in each adult MB α and β lobes (C). However, multi-branch phenotype with two or three branches on one MB lobe was observed in *Dscam* mutant MARCM clones (D-F). In addition, an unusual single-branch phenotype was also observed when Dscam endodomain variants were overexpressed in *Dscam* mutant MARCM clones (G). Antibody 1D4 (magenta) was used to reveal adult MB α/β lobes. Anti-mCD8 antibody (green) was used to reveal mCD8::GFP in MARCM single-cell clones.

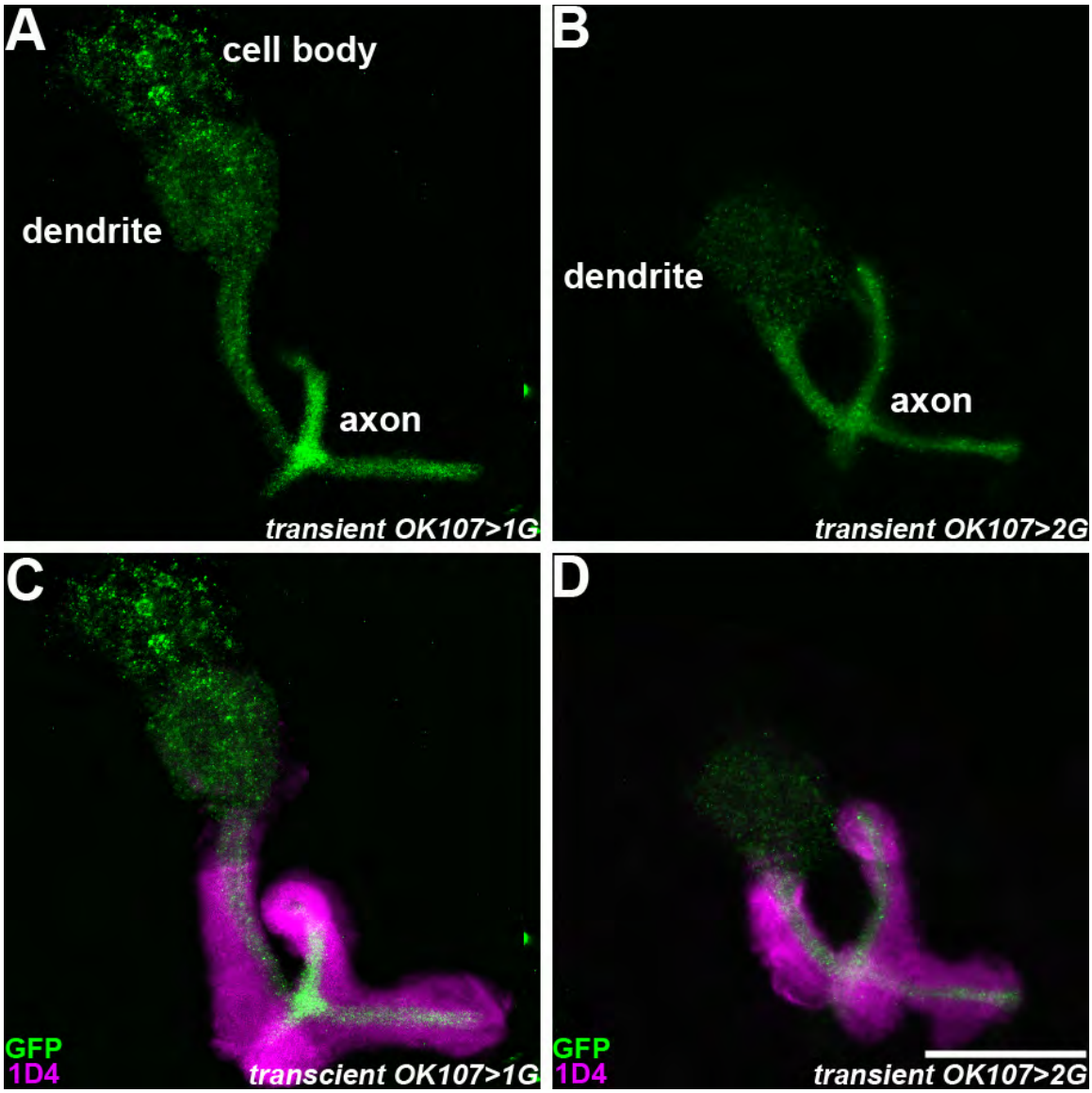

Figure 5-6. Preferential cell body and neurite localization of Dscam exon 19 variants

(A-D) The TARGET system was used to transiently expressed Dscam exon 19 variants, Dscam+19 and Dscam-19, respectively. Transgenic Dscam-19::GFP was primarily targeted to the larval MB axon bundles and weakly to the dendritic calyx (B, D). Besides significantly accumulated in MB axon bundles and the dendritic calyx, transgenic Dscam+19::GFP was also abundantly present in cell bodies (A, C). Antibody 1D4 (magenta) was used to reveal larval MB lobes. Anti-GFP antibody (green) was used to reveal transiently expressing transgenic Dscam::GFP.

Chapter 5

Final Conclusions and General Discussion

The work presented in this dissertation is focused on the molecular mechanisms that govern the polarized distribution of distinct Dscam isoforms and the elucidation of the role of distinct Dscam isoforms in neuronal morphogenesis. These studies indicated that distinct Dscam isoforms execute their functions in different neuronal subcellular compartments, most likely due to their differential protein distribution. Dscam[TM1], which is preferentially targeted to dendrites, mediates dendritic elaboration, while Dscam[TM2], which is specifically localized to axons, regulates axonal arborization. In addition, Dscam-19 (Dscam lacking exon 19) was more efficiently targeted to neurites and acted more potently in altering neurite projection patterns than Dscam+19 (Dscam with exon 19). Through the structural functional analysis, dendritic and axonal targeting motifs of Dscam were identified in the ectodomain and cytoplasmic juxtamembrane segment of TM2, respectively. The dynein/dynactin complex, identified from a MARCM-based genetic screen, was shown to be involved in the dendritic restriction of Dscam[TM1] through retrograde transport. A dynein/dynactin-independent selective transport mechanism and a dynein/dynactin-dependent salvage mechanism were demonstrated to work together to ensure the proper localization of Dscam[TM1] to dendrites. A sorting mechanism for Dscam[TM1] and Dscam[TM2] into distinct vesicles was also suggested.

New insights into the mechanisms underlying the polarized distribution of membrane proteins in neurons

Compelling evidence has been provided that, as a major minus-end-directed motor, the dynein/dynactin complex may not play any role in the initial dendritic

targeting of membrane proteins Dscam and Rdl in *Drosophila* MB neurons. These observations raised the possibility that other dendrite-specific plus-end-directed motors may be responsible for the selective transport of membrane proteins to dendrites (Marszalek et al., 1999; Setou et al., 2000). It is also possible that cargos, not motors, determine the destinations of proteins during selective transport (Satpute-Krishnan et al., 2006). In both situations, identification of the associated motors that specifically recognize Dscam[TM1] versus Dscam[TM2] vesicles would help to further dissect out the possible roles for these motors in the selective transport mechanism.

Axonal retrograde transport, which is mediated by dynein/dynactin, sends chemical messages and endocytosis products from the axon terminals to cell bodies. For example, earlier studies show that distal uptake and retrograde transport of nerve growth factor (NGF) is necessary for survival responses and other trophic effects (Ibáñez, 2007). However, it is not clear if retrograde transport is also involved in the polarized distribution of membrane proteins. In our study, we uncovered a new function of retrograde transport, a salvage mechanism that actively removes mislocalized dendritic Dscam from axons. Although this salvage mechanism may not be required for all dendritic membrane proteins, such as Rdl, it suggests that a secondary system for proper sorting and targeting of membrane proteins may exist in polarized neurons.

It would be worth examining whether dynein/dynactin is involved in the polarized distribution of other membrane proteins in other model neurons. Recently, a study in *Drosophila* dendritic arborization (da) neurons showed that dynein is required for dendritic localization of Golgi outposts and the ion channel Pickpocket. They also suggested that dynein function is required for uniform microtubule orientation in axons

(Zheng et al., 2008). These findings are different from what we observe in the *Drosophila* MB neurons. Dynein/dynactin dysfunction does not affect the dendritic distribution of Rdl and also does not perturb the microtubule orientation in axons. There are some intrinsic differences between da neurons and MB neurons. For example, da neurons are multipolar while MB neurons are unipolar (Sanchez-Soriano et al., 2005). Taken together, these data indicate that dynein/dynactin function could differ among model neurons.

The vesicular transport of Dscam[TM1] and Dscam[TM2] was observed in *Drosophila* embryonic cultured neurons (data not shown). The speed of vesicle movement was about 1.2 μm/s, which falls into the category of microtubule-based fast transport conducted by motors (0.5-2.0 μm/s, Burack et al., 2000). Compared to the slow mislocalization process (0.006 μm/s) of Dscam[TM1] caused by dynein/dynactin dysfunction, we believe that the mislocalization process is not mediated by motor transport. Instead, it could occur through accidental leakage of vesicles into axons which cannot be brought back to cell bodies by dynein/dynactin. It could also occur through lateral diffusion which cannot be removed from the axonal membrane through the endocytotic pathway, although it remains unclear how dynein/dynactin dysfunction would affect endocytosis. Further examination of whether mislocalized Dscam[TM1] localizes to the plasma membrane or in the cytoplasm would help to clarify the mechanisms involved.

Multiple mechanisms are involved in the polarized distribution of membrane proteins

Our data support the idea that multiple mechanisms act together to achieve the polarized distribution of membrane proteins in neurons. First, from our screen mutants, we found that some mutations (group 3) result in cell body retention of Dscam[TM1], while another mutation (DC-B9) causes aberrant accumulation of Dscam[TM1] in the peduncles of MB neurons, and the other mutation (AC-E10) results in Dscam[TM1] evenly distributed throughout the axons without granular accumulation. These intriguing phenotypes, which are different from those of dynein/dynactin mutants, suggest presence of localization mechanisms other than those involving dynein/dynactin. In addition, a mutation in the ion transport peptide (ITP) also leads to the mislocalization of Dscam[TM1] in axons. Although there are no reported data on the molecular function of *Drosophila* ITP, the ITP in locusts, which displays sequence similarity to *Drosophila* ITP, is a neuropeptide which has been shown to stimulate the transport of ions across the ileal epithelium (Vanden Broeck, 2001). It would be interesting to examine how neuropeptide signaling pathways are involved in the polarized distribution of Dscam[TM1].

Second, more recent work has found that peptide motifs can target membrane proteins to specific subcellular compartments in neurons (Arnold, 2007). However, peptide motifs are not conserved across different membrane proteins. In Dscam, we found that an axonal targeting motif that consists of both basic (Arg) and acidic (Asp) residues. This type of bipartite motif has not been reported before. Interestingly, most peptide motifs are located in the endodomains of membrane proteins. However, the dendritic targeting motif of Dscam is localized in the ectodomain and is not directly recognized by motor proteins, because it is embedded inside the cargo vesicle during

transport. These novel findings indicate that the Dscam may utilize different polarized targeting mechanisms from the other membrane proteins.

Third, it has been shown that the axonal distribution of vesicle-associated membrane protein (VAMP)-2 is achieved by uniform delivery to the surface of both axons and dendrites and preferential endocytosis from the dendritic membrane. In contrast, the targeting of neuron-glia cell adhesion molecule (NgCAM) depends on selective transport of cargo proteins to the axonal membrane (Sampo et al., 2003). In the case of Dscam, blocking endocytosis with a temperature-sensitive *shibire* mutant showed no obvious effect on its dendritic distribution. However, it remains to be examined whether axonal targeting of Dscam depends on the endocytic pathway. Finally, we found that the salvage pathway mediated by the dynein/dynactin complex is essential for dendritic restriction of Dscam[TM1] but is dispensable for dendritic distribution of Rdl. In summary, we believe that different membrane proteins are distributed in a polarized fashion in neurons by different combinations of known and unknown mechanisms.

Future studies on the polarized distribution and molecular functions of Dscam

Our findings demonstrate that Dscam[TM1] primarily mediates dendritic elaboration, and Dscam[TM2] mainly regulates axonal arborization. These distinct functional roles in dendrites and axons correlate to the polarized distribution patterns of Dscam[TM1] and Dscam[TM2]. The next question to ask is why neurons need some Dscam molecules localized to dendrites while others are distributed to axons. Previous studies show that Dscam undergoes isoform-specific homophilic binding through its ectodomain, and this interaction cell-autonomously leads to the formation of complex

morphology of dendrites and axons (Soba et al., 2007; Wang et al., 2002; Wojtowicz et al., 2004). Single-cell RT-PCR documented that an individual neuron expresses 14-50 distinct *Dscam* mRNAs from the spectrum of thousands of splice variants, and Dscam alternative splicing is differentially regulated in different cells (Neves et al., 2004). It would be interesting to examine whether, within a single neuron, dendritic Dscam[TM1] always couples with certain kinds of ectodomain variants and axonal Dscam[TM2] binds to other types of ectodomains. It is possible that the morphological difference between dendrites and axons is related to the usages of different *Dscam* ectodomain repertoires. To verify this hypothesis, genetic manipulation of genomic exon 17.1 and exon 17.2 with gene targeting could possibly reverse the choices of ectodomain variants. Reversal of the choices of ectodomains between Dscam[TM1] and Dscam[TM2] may result in the functional and morphological changes between dendrites and axons.

Identification of Dscam[TM1]-specific and Dscam[TM2]-specific associated proteins would definitely help to elucidate the polarized distribution mechanisms and differential functions of Dscam[TM1] and Dscam[TM2]. To achieve this goal, several approaches can be conducted. First, co-immunoprecipitation of GFP-tagged Dscam[TM1] and Dscam[TM2] with anti-GFP or anti-Dscam antibodies can enrich neuronal lysates for specific associated proteins. The isolated proteins can be distinguished from each other and compared using SDS-PAGE. Second, the yeast two-hybrid system can be employed by using Dscam axonal and dendritic targeting motifs as bait to identify associated molecules. Third, genetic screens could also identify additional molecules involved in the polarized distribution of Dscam. Further characterization of mutants from these screens could reveal potential Dscam-interacting proteins.

In summary, the studies detailed in this dissertation have addressed fundamental questions regarding the polarized distribution mechanisms of membrane proteins in neurons. The polarized distribution of Dscam[TM1] and Dscam[TM2] serves as a good model system to dissect out how neurons properly sort and target different membrane proteins to distinct subcellular compartments. The identification of a novel salvage mechanism mediated by dynein/dynactin, several prominent mutants involved in polarized distribution mechanisms, axonal and dendritic targeting motifs by which Dscam is differentially targeted, and potential functions of Dscam associated with its polarized distribution have significantly advanced our mechanistic understanding of how various Dscam isoforms are differentially expressed and distributed in neurons to regulate neuronal morphogenesis. Further elucidation of these basic mechanisms may lay the groundwork for future characterization of membrane protein trafficking in polarized neurons and help us to understand complex processes that occur in the brain during development and daily activities.

Appendices

microRNAs was designed according to the paper Chen et al., 2007. Target recognition sequences are underlined.

Exon 17.1 Target 1:

(1) D-M7d887-1:

GGCAGCTTACTTAAACTTAATCACAGCCTTTAATGTCGAGGACACGATCCGCATTATCTAAGTTAATATACCATATC

(2) D-Myd887-2:

AATAATGATGTTAGGCACTTTAGGTACCGAGGACACGATCCGCATTATCTAGATATGGTATATTAACTTAGATA

Exon 17.1 Target 2:

(1) D-M7d888-1:

GGCAGCTTACTTAAACTTAATCACAGCCTTTAATGTCGATAATTGTTATTTGTATACTTAAGTTAATATACCATATC

(2) D-Myd888-2:

AATAATGATGTTAGGCACTTTAGGTACCGATAATTGTTATTTGTATACTTAGATATGGTATATTAACTTAAGTA

Exon 17.2 Target 1:

(3) D-M7d889-1:

GGCAGCTTACTTAAACTTAATCACAGCCTTTAATGTCAACTTCATGGTGCCCCTAATTTAAGTTAATATACCATATC

(4) D-Myd889-2:

AATAATGATGTTAGGCACTTTAGGTACCAACTTCATGGTGCCCCTAATTTAGATATGGTATATTAACTTAAATT

Exon 17.2 Target 2:

(3) D-M7d888-1:

GGCAGCTTACTTAAACTTAATCACAGCCTTTAATGTGACATGCGCGGCGGCCAAAAGGTAAGTTAATATACCATATC

(4) D-Myd888-2:

AATAATGATGTTAGGCACTTTAGGTACGACATGCGCGGCGGCCAAAA
GGTAGATATGGTATATTAACTTACCTT

Exon 18 Target 1:

(1) D-18 1-1:

GGCAGCTTACTTAAACTTAATCACAGCCTTTAATGTGCGGGATGAGCT
CGGATACATCTAAGTTAATATACCATATC

(2) D-18 1-2:

AATAATGATGTTAGGCACTTTAGGTACGCGGGATGAGCTCGGATACAT
CTAGATATGGTATATTAACTTAGATG

Exon 18 Target 2:

(3) D-18 2-1:

GGCAGCTTACTTAAACTTAATCACAGCCTTTAATGTAATACCTGTGAC
CGGATTAAGCTAAGTTAATATACCATATC

(4) D-18 2-2:

AATAATGATGTTAGGCACTTTAGGTACAATACCTGTGACCGGATTAA
GCTAGATATGGTATATTAACTTAGCTT

Exon 19 Target 1:

(1) D-19 1-1:

GGCAGCTTACTTAAACTTAATCACAGCCTTTAATGTCCTGGGACCCTC
GACGCAATCCTAAGTTAATATACCATATC

(2) D-19 1-2:

AATAATGATGTTAGGCACTTTAGGTACCCTGGGACCCTCGACGCAATC
CTAGATATGGTATATTAACTTAGGAT

Exon 19 Target 2:

(3) D-19 2-1:

GGCAGCTTACTTAAACTTAATCACAGCCTTTAATGTACGGCCACGCCC
ACGGCAATGCTAAGTTAATATACCATATC

(4) D-19 2-2:

AATAATGATGTTAGGCACTTTTAGGTACACGGCCACGCCCACGGCAATGCTAGATATGGTATATTAACTTAGCAT

Exon 18-20 Target:

(1) D-18-20 -1:

GGCAGCTTACTTAAACTTAATCACAGCCTTTAATGTATTAAGCGAGGCATGGAAGATGTAAGTTAATATACCATATC

(2) D-18-20 -2:

AATAATGATGTTAGGCACTTTTAGGTACATTAAGCGAGGCATGGAAGATGTAGATATGGTATATTAACTTACTAC

Exon 23 Target:

(1) D-23-1:

GGCAGCTTACTTAAACTTAATCACAGCCTTTAATGTGATCTCCACAACCGAAAGATCATAAGTTAATATACCATATC

(2) D-23-2:

AATAATGATGTTAGGCACTTTTAGGTACGATCTCCACAACCGAAAGATCATAGATATGGTATATTAACTTAGATATGAT

Exon 22-24 Target:

(1) D-22-24 -1:

GGCAGCTTACTTAAACTTAATCACAGCCTTTAATGTGGAAACTACGGAGAAACGAAACTAAGTTAATATACCATATC

(2) D-22-24 -2:

AATAATGATGTTAGGCACTTTTAGGTACGGAAACTACGGAGAAACGAAACTAGATATGGTATATTAACTTAGTTT

Bibliography

Allen MJ, Shan X, Caruccio P, Froggett SJ, Moffat KG, Murphey RK (1999) Targeted Expression of Truncated Glued Disrupts Giant Fiber Synapse Formation in Drosophila. *J. Neurosci.*, **19**, 9374-9384

Anastassiou D, Liu H, Varadan V (2006) Variable window binding for mutually exclusive alternative splicing. *Genome Biol.*, **7**, R2

Andrews GL, Tanglao S, Farmer WT, Morin S, Brotman S, Berberglu MA, Price H, Fernandez GC, Mastick GS, Charron F, Kidd T (2008) Dscam guides embryonic axons by Netrin-dependent and -independent functions. *Development*, **135**, 3839-3848

Arnold DB (2007) Polarized targeting of ion channels in neurons. *Eur. J. Physio.*, **453**, 763-769

Baas PW, Deitch JS, Black MM, Banker GA (1988) Polarity Orientation of Microtubules in Hippocampal Neurons: Uniformity in the Axon and Nonuniformity in the Dendrite. *Proceedings of the National Academy of Sciences*, **85**, 8335-8339

Brand A, Perrimon N (1993) Targeted gene expression as a means of altering cell fates and generating dominant phenotypes. *Development*, **118**, 401-415

Brites D, McTaggart S, Morris K, Anderson J, Thomas K, Colson I, Fabbro T, Little TJ, Ebert D, Du Pasquier L (2008) The dscam homologue of the crustacean Daphnia is diversified by alternative splicing like in insects. *Mol Biol Evol.*, **25**, 1429-1439

Burack MA, Silverman MA, Banker G (2000) The Role of Selective Transport in Neuronal Protein Sorting. *Neuron*, **26**, 465-472

Cajal SR (1989) Recollections of My Life. *Cambridge: The MIT Press*, 1–638

Campbell RE, Tour O, Palmer AE, Steinbach PA, Baird GS, Zacharias DA, Tsien RY (2002) A monomeric red fluorescent protein. *Proceedings of the National Academy of Sciences*, **99**, 7877-7882

Chen BE, Kondo M, Garnier A, Watson FL, Puettmann-Holgado R, Lamar DR, Schmucker D (2006) The molecular diversity of Dscam is functionally required for neuronal wiring specificity in Drosophila. *Cell*, **125**, 607-620

Chen CH, Huang H, Ward CM, Su JT, Schaeffer LV, Guo M, Hay BA (2007) A

synthetic maternal-effect selfish genetic element drives population replacement in Drosophila. *Science*, **316**, 597-600

Clark I, Jan L, Jan Y (1997) Reciprocal localization of Nod and kinesin fusion proteins indicates microtubule polarity in the Drosophila oocyte, epithelium, neuron and muscle. *Development*, **124**, 461-470

Clark SW, Rose MD (2005) Alanine Scanning of Arp1 Delineates a Putative Binding Site for Jnm1/Dynamitin and Nip100/p150Glued. *Mol. Biol. Cell*, **16**, 3999-4012

Craig AM, Banker G (1994) Neuronal Polarity. *Ann. Rev. Neurosci.*, **17**, 267-310

Didelot G, Molinari F, Tchenio P, Comas D, Milhiet E, Munnich A, Colleaux L, Preat T (2006) Tequila, a Neurotrypsin Ortholog, Regulates Long-Term Memory Formation in Drosophila. *Science*, **313**, 851-853

Dietzl G, Chen D, Schnorrer F, Su K-C, Barinova Y, Fellner M, Gasser B, Kinsey K, Oppel S, Scheiblauer S, Couto A, Marra V, Keleman K, Dickson BJ (2007) A genome-wide transgenic RNAi library for conditional gene inactivation in Drosophila. *Nature*, **448**, 151-156

Dotti CG, Simons K (1990) Polarized sorting of viral glycoproteins to the axon and dendrites of hippocampal neurons in culture. *Cell*, **62**, 63-72

Endoh T (2004) Characterization of modulatory effects of postsynaptic metabotropic glutamate receptors on calcium currents in rat nucleus tractus solitarius. *Brain Research*, **1024**, 212-224

Francesconi A, Duvoisin RM (2002) Alternative Splicing Unmasks Dendritic and Axonal Targeting Signals in Metabotropic Glutamate Receptor 1. *J. Neurosci.*, **22**, 2196-2205

Garrido JJ, Fernandes F, Giraud P, Mouret I, Pasqualini E, Fache M-P, Jullien F, Dargent BD (2001) Identification of an axonal determinant in the C-terminus of the sodium channel Nav1.2. *EMBO J.*, **20**, 5950-5961

Goldstein LSB, Gunawardena S (2000) Flying Through the Drosophila Cytoskeletal Genome. *J. Cell Biol.*, **150**, 63F-68

Goldstein LSB, Yang Z (2000) Microtubule-Based Transport Systems in Neurons: The Roles of Kinesins and Dyneins. *Annual Review of Neuroscience*, **23**, 39-71

Gong WJ, Golic KG (2003) Ends-out, or replacement, gene targeting in Drosophila. *Proc Natl Acad Sci U S A*, **100**, 2556-2561

Graveley BR, Kaur A, Gunning D, Zipursky SL, Rowen L, Clemens JC (2004) The organization and evolution of the dipteran and hymenopteran Down syndrome cell adhesion molecule (Dscam) genes. *RNA*, **10,** 1499-1506

Gu C, Jan YN and Jan LY (2003) A Conserved Domain in Axonal Targeting of Kv1 (Shaker) Voltage-Gated Potassium Channels. *Science*, **301**, 646-649

Hodgkinson JL, Peters C, Kuznetsov SA, Steffen W (2005) Three-dimensional reconstruction of the dynactin complex by single-particle image analysis. *Proceedings of the National Academy of Sciences*, **102**, 3667-3672

Hoffman DA, Magee JC, Colbert CM, Johnston D (1997) K+ channel regulation of signal propagation in dendrites of hippocampal pyramidal neurons. *Nature*, **387**, 869-875

Horton AC, Ehlers MD (2003) Neuronal Polarity and Trafficking. *Neuron*, **40**, 277-295.

Ibáñez CF (2007) Message in a bottle: long-range retrograde signaling in the nervous system. *Trends in Cell Bio.*, **17**, 519-528

King SJ, Schroer TA (2000) Dynactin increases the processivity of the cytoplasmic dynein motor. **2**, 20-24

Kosik K, Finch E (1987) MAP2 and tau segregate into dendritic and axonal domains after the elaboration of morphologically distinct neurites: an immunocytochemical study of cultured rat cerebrum. *J. Neurosci.*, **7**, 3142-3153

Hughes ME, Bortnick R, Tsubouchi A, Baumer P, Kondo M, Uemura T, Schmucker D (2007) Homophilic Dscam interactions control complex dendrite morphogenesis. *Neuron*, **54**, 417-427

Koonce MP, Samso M (2004) Of rings and levers: the dynein motor comes of age. *Trends in Cell Biology*, **14**, 612-619

Kurusu M, Awasaki T, Masuda-Nakagawa LM, Kawauchi H, Ito K, Furukubo-Tokunaga K (2002) Embryonic and larval development of the Drosophila mushroom bodies: concentric layer subdivisions and the role of fasciclin II. *Development*, **129**, 409-419

Lee T, Lee A, Luo L (1999) Development of the Drosophila mushroom bodies: sequential generation of three distinct types of neurons from a neuroblast. *Development*, **126**, 4065-4076

Lee T, Luo L (1999) Mosaic Analysis with a Repressible Cell Marker for Studies of Gene

Function in Neuronal Morphogenesis. *Neuron*, **22**, 451-461

Lee T, Marticke S, Sung C, Robinow S, Luo L (2000) Cell-Autonomous Requirement of the USP/EcR-B Ecdysone Receptor for Mushroom Body Neuronal Remodeling in Drosophila. *Neuron*, **28**, 807-818

Lee T, Winter C, Marticke SS, Lee A, Luo L (2000) Essential Roles of Drosophila RhoA in the Regulation of Neuroblast Proliferation and Dendritic but Not Axonal Morphogenesis. *Neuron*, **25**, 307-316

Lewis EB, Bacher F (1968) Method of feeding ethylmethane sulfonate (EMS) to Drosophila males. *Drosoph. Inf. Serv*, **43**, 193

Lim ST, Antonucci DE, Scannevin RH, Trimmer JS (2000) A Novel Targeting Signal for Proximal Clustering of the Kv2.1 K+ Channel in Hippocampal Neurons. *Neuron,* **25**, 385-397

Liu Z, Steward R, Luo L (2000) Drosophila Lis1 is required for neuroblast proliferation, dendritic elaboration and axonal transport. *Nature Cell Biology,* **2**, 776-783

Low S, Chapin S, Weimbs T, Komuves L, Bennett M, Mostov K (1996) Differential localization of syntaxin isoforms in polarized Madin-Darby canine kidney cells. *Mol. Biol. Cell,* **7**, 2007-2018

Ma Y, Creanga A, Lum L, Beachy PA (2006) Prevalence of off-target effects in Drosophila RNA interference screens. *Nature,* **443**, 359-363

Marszalek JR, Weiner JA, Farlow SJ, Chun J, Goldstein LSB (1999) Novel Dendritic Kinesin Sorting Identified by Different Process Targeting of Two Related Kinesins: KIF21A and KIF21B. *J Cell Biol.*, **145**, 469-479

Matter K, Mellman I (1994) Mechamisms of cell polarity: sorting and transport in epithelial cells. *Curr Opin Cell Bio.*, 6, 545-554

Matter K, Yamamoto E, Mellman I (1994) Structural requirements and sequence motifs for polarized sorting and endocytosis of LDL and Fc receptors in MDCK cells. *J. Cell Biol.*, **126**, 991-1004

Matthews BJ, Kim ME, Flanagan JJ, Hattori D, Clemens JC, Zipursky SL, Grueber WB (2007) Dendrite Self-Avoidance Is Controlled by Dscam. *Cell,* **129**, 593-604

McDonald HB, Stewart RJ, Goldstein LSB (1990) The kinesin-like ncd protein of Drosophila is a minus end-directed microtubule motor. *Cell,* **63**, 1159-1165

McGrail M, Gepner J, Silvanovich A, Ludmann S, Serr M, et al. (1995) Regulation of cytoplasmic dynein function in vivo by the Drosophila Glued complex. *J Cell Biol.*, **131**, 411-425.

McGuire SE, Le PT, Osborn AJ, Matsumoto K, Davis RL (2003) Spatiotemporal Rescue of Memory Dysfunction in Drosophila. *Science*, **302**, 1765-1768

McGuire SE, Mao Z, Davis RL (2004) Spatiotemporal Gene Expression Targeting with the TARGET and Gene-Switch Systems in Drosophila. *Sci STKE*, **220**, pl6

Monaghan MM, Trimmer JS, Rhodes KJ (2001) Experimental Localization of Kv1 Family Voltage-Gated K+ Channel {alpha} and {beta} Subunits in Rat Hippocampal Formation. *J Neurosci.*, **21**, 5973-5983

Nakada C, Ritchie K, Oba Y, Nakamura M, Hotta Y, Iino R, Kasai RS, Yamaguchi K, Fujiwara T, Kusumi A (2003) Accumulation of anchored proteins forms membrane diffusion barriers during neuronal polarization. *Nat Cell Bio.*, **5**, 626-632

Nakanishi S (1992) Molecular diversity of glutamate receptors and implications for brain function. *Science*, **258**, 597-603

Neves G, Zucker J, Daly M, Chess A (2004) Stochastic yet biased expression of multiple Dscam splice variants by individual cells. *Nat Genet.*, **36**, 240-246

Odorizzi G, Trowbridge IS (1997) Structural Requirements for Basolateral Sorting of the Human Transferrin Receptor in the Biosynthetic and Endocytic Pathways of Madin-Darby Canine Kidney Cells. *J Cell Biol.*, **137**, 1255-1264

Pilling AD, Horiuchi D, Lively CM, Saxton WM (2006) Kinesin-1 and Dynein Are the Primary Motors for Fast Transport of Mitochondria in Drosophila Motor Axons. *Mol Bio Cell*, **17**, 2057-2068

Puls I, Jonnakuty C, LaMonte BH, Holzbaur ELF, Tokito M, Mann E, Floeter MK, Bidus K, Drayna D, Oh SJ, Brown RH, Ludlow CL, Fischbeck KH (2003) Mutant dynactin in motor neuron disease. *Nature Genetics*, **33**, 455-456

Reiner O, Carrozzo R, Shen Y, Wehnert M, Faustinella F, Dobyns WB, Caskey CT, Ledbetter DH (1993) Isolation of a Miller-Dicker lissencephaly gene containing G protein [beta]-subunit-like repeats. *Nature*, **364**, 717-721

Reuter JE, Nardine TM, Penton A, Billuart P, Scott EK, Usui T, Uemura T, Luo L (2003) A mosaic genetic screen for genes necessary for Drosophila mushroom body neuronal

morphogenesis. *Development*, **130**, 1203-1213

Rivera JF, Ahmad S, Quick MW, Liman ER, Arnold DB (2003) An evolutionarily conserved dileucine motif in Shal K+ channels mediates dendritic targeting. *Nature Neurosci.*, **6**, 243-250

Rolls M, Satoh D, Clyne P, Henner A, Uemura T, Doe C (2007) Polarity and intracellular compartmentalization of Drosophila neurons. *Neural Dev.*, **2**, 7

Saito N, Okada Y, Noda Y, Kinoshita Y, Kondo S, Hirokawa N (1997) KIFC2 Is a Novel Neuron-Specific C-Terminal Type Kinesin Superfamily Motor for Dendritic Transport of Multivesicular Body-Like Organelles. *Neuron*, **18**, 425-438

Sampo B, Kaech S, Kunz S, Banker G (2003) Two Distinct Mechanisms Target Membrane Proteins to the Axonal Surface. *Neuron*, **37**, 611-624

Sanchez-Soriano N, Bottenberg W, Fiala A, Haessler U, Kerassoviti A, Knust E, Lohr R, Prokop A (2005) Are dendrites in Drosophila homologous to vertebrate dendrites? *Dev Bio.*, **288**, 126-138

Satpute-Krishnan P, DeGiorgis JA, Conley MP, Jang M, Bearer EL (2006) A peptide zipcode sufficient for anterograde transport within amyloid precursor protein. *Proc Nat Aca Sci.*, **103**, 16532-16537

Schmucker D, Clemens JC, Shu H, Worby CA, Xiao J, Muda M, Dixon JE, Zipursky SL (2000) Drosophila Dscam Is an Axon Guidance Receptor Exhibiting Extraordinary Molecular Diversity. *Cell*, **101**, 671-684

Schroer TA (2004) DYNACTIN. *Ann Rev Cell Dev Bio.*, **20**, 759-779

Setou M, Nakagawa T, Seog D-H, Hirokawa N (2000) Kinesin Superfamily Motor Protein KIF17 and mLin-10 in NMDA Receptor-Containing Vesicle Transport. *Science*, **288**, 1796-1802

Shi L, Yu H-H, Yang JS, Lee T (2007) Specific Drosophila Dscam Juxtamembrane Variants Control Dendritic Elaboration and Axonal Arborization. *J Neurosci.*, **27**, 6723-6728

Silverman MA, Peck R, Glover G, He C, Carlin C, et al. (2005) Motifs that mediate dendritic targeting in hippocampal neurons: A comparison with basolateral targeting signals. *Mol Cell Neurosci.*, **29**, 173-180

Soba P, Zhu S, Emoto K, Younger S, Yang S-J, Yu H-H, Lee T, Jan LY, Jan Y-N (2007) Drosophila Sensory Neurons Require Dscam for Dendritic Self-Avoidance and Proper Dendritic Field Organization. *Neuron*, **54**, 403-416

Stone MC, Roegiers F, Rolls MM (2008) Microtubules Have Opposite Orientation in Axons and Dendrites of Drosophila Neurons. *Mol Biol Cell*, **19**, 4122-4129

Stowell JN, Craig AM (1999) Axon/Dendrite Targeting of Metabotropic Glutamate Receptors by Their Cytoplasmic Carboxy-Terminal Domains. *Neuron*, **22**, 525-536

Stuart G, Spruston N, Sakmann B, Hausser M (1997) Action potential initiation and backpropagation in neurons of the mammalian CNS. *Trends in Neurosci.*, **20**, 125-131

Swan A, Nguyen T, Suter B (1999) Drosophila Lissencephaly-1 functions with Bic-D and dynein in oocyte determination and nuclear positioning. *Nature Cell Bio.*, **1**, 444-449

Tai AW, Chuang J-Z, Sung C-H (2001) Cytoplasmic Dynein Regulation by Subunit Heterogeneity and Its Role in Apical Transport. *J Cell Biol.*, **153**, 1499-1510

Vanden Broeck J (2001) Neuropeptides and their precursors in the fruitfly, Drosophila melanogaster. *Peptides*, **22**, 241-254

Wang J, Lee C-HJ, Lin S, Lee T (2006) Steroid hormone-dependent transformation of polyhomeotic mutant neurons in the Drosophila brain. *Development*, **133**, 1231-1240

Wang J, Ma X, Yang JS, Zheng X, Zugates CT, Lee C-HJ, Lee T (2004) Transmembrane/Juxtamembrane Domain-Dependent Dscam Distribution and Function during Mushroom Body Neuronal Morphogenesis. *Neuron*, **43**, 663-672

Wang J, Zugates CT, Liang IH, Lee C-HJ, Lee T (2002) Drosophila Dscam Is Required for Divergent Segregation of Sister Branches and Suppresses Ectopic Bifurcation of Axons. *Neuron*, **33**, 559-571

Watson FL, Puttmann-Holgado R, Thomas F, Lamar DL, Hughes M, Kondo M, Rebel VI, Schmucker D (2005) Extensive diversity of Ig-superfamily proteins in the immune system of insects. *Science*, **309**, 1874-1878

Wei A, Covarrubias M, Butler A, Baker K, Pak M, Salkoff L (1990) K+ current diversity is produced by an extended gene family conserved in Drosophila and mouse. *Science*, **248**, 599-603

West AE, Neve RL, Buckley KM (1997) Identification of a Somatodendritic Targeting Signal in the Cytoplasmic Domain of the Transferrin Receptor. *J Neurosci.*, **17**, 6038-6047

Whited JL, Cassell A, Brouillette M, Garrity PA (2004) Dynactin is required to maintain nuclear position within postmitotic Drosophila photoreceptor neurons. *Development*, **131**, 4677-4686

Wojtowicz WM, Flanagan JJ, Millard SS, Zipursky SL, Clemens JC (2004) Alternative splicing of Drosophila Dscam generates axon guidance receptors that exhibit isoform-specific homophilic binding. *Cell*, **118**, 619-633

Wojtowicz WM, Wu W, Andre I, Qian B, Baker D, Zipursky SL (2007) A vast repertoire of Dscam binding specificities arises from modular interactions of variable Ig domains. *Cell*, **130**, 1134-1145

Xu J, Zhu Y, Heinemann SF (2006) Identification of Sequence Motifs That Target Neuronal Nicotinic Receptors to Dendrites and Axons. *J Neurosci.*, **26**, 9780-9793

Yang JS-J, Bai J-M, Lee T (2008) Dynein-Dynactin Complex Is Essential for Dendritic Restriction of TM1-Containing Drosophila Dscam. *PLoS ONE*, **3**, e3504

Zhan XL, Clemens JC, Neves G, Hattori D, Flanagan JJ, Hummel T, Vasconcelos ML, Chess A, Zipursky SL (2004) Analysis of Dscam diversity in regulating axon guidance in Drosophila mushroom bodies. *Neuron*, **43**, 673-686

Zheng X, Wang J, Haerry TE, Wu AY-H, Martin J, O'Connor MB, Lee C-HJ, Lee T (2003) TGF-[beta] Signaling Activates Steroid Hormone Receptor Expression during Neuronal Remodeling in the Drosophila Brain. *Cell*, **112**, 303-315

Zheng Y, Wildonger J, Ye B, Zhang Y, Kita A, Younger SH, Zimmerman S, Jan LY, Jan YN (2008) Dynein is required for polarized dendritic transport and uniform microtubule orientation in axons. *Nature Cell Biology*, **10**, 1172-1180

Zhu H, Hummel T, Clemens JC, Berdnik D, Zipursky S L, Luo L (2006) Dendritic patterning by Dscam and synaptic partner matching in the Drosophila antennal lobe. *Nat. Neurosci.*, **9**, 349-355

Zhu S, Lin S, Kao C-F, Awasaki T, Chiang A-S, Lee T (2006) Gradients of the Drosophila Chinmo BTB-Zinc Finger Protein Govern Neuronal Temporal Identity. *Cell*, **127**, 409-422

Zhu S, Perez R, Pan M, Lee T (2005) Requirement of Cul3 for Axonal Arborization and Dendritic Elaboration in Drosophila Mushroom Body Neurons. *J. Neurosci.*, **25**, 4189-4197

Ye B, Zhang Y, Song W, Younger SH, Jan LY, Jan YN (2007) Growing Dendrites and Axons Differ in Their Reliance on the Secretory Pathway. *Cell*, **130**, 717-729